DEVELOPMENT OF SILVER NANOPARTICLE PROBES FOR DETECTION OF CORALYNE

A THESIS SUBMITTED TO
THE GRADUATE SCHOOL OF NATURAL AND APPLIED SCIENCES
OF
MIDDLE EAST TECHNICAL UNIVERSITY

BY

HATİCE MÜGE USTA

IN PARTIAL FULFILLMENT OF THE REQUIREMENTS
FOR
THE DEGREE OF MASTER OF SCIENCE
IN
CHEMISTRY

JULY 2020

Approval of the thesis:

DEVELOPMENT OF SILVER NANOPARTICLE PROBES FOR DETECTION OF CORALYNE

submitted by **HATİCE MÜGE USTA** in partial fulfillment of the requirements for the degree of **Master of Science** i**n Chemistry, Middle East Technical University** by,

Prof. Dr. Halil Kalıpçılar
Dean, Graduate School of **Natural and Applied Sciences** _____

Prof. Dr. Cihangir Tanyeli
Head of the Department, **Chemistry** _____

Assoc. Prof. Dr. Özgül Persil Çetinkol
Supervisor, **Chemistry, METU** _____

Examining Committee Members:

Prof. Dr. Levent Toppare
Chemistry, METU _____

Assoc. Prof. Dr. Özgül Persil Çetinkol
Chemistry, METU _____

Prof. Dr. Yasemin Arslan Udum
Advanced Technologies, Gazi University _____

Prof. Dr. Ceyhan Kayran İşçi
Chemistry, METU _____

Assist. Prof. Dr. Süreyya Özcan Kabasakal
Chemistry, METU _____

Date: 24.07.2020

I hereby declare that all information in this document has been obtained and presented in accordance with academic rules and ethical conduct. I also declare that, as required by these rules and conduct, I have fully cited and referenced all material and results that are not original to this work.

Name, Last name: Hatice Müge Usta

Signature:

ABSTRACT

DEVELOPMENT OF SILVER NANOPARTICLE PROBES FOR DETECTION OF CORALYNE

Usta, Hatice Müge
Master of Science, Chemistry
Supervisor: Assoc. Prof. Özgül Persil Çetinkol

July 2020, 94 pages

Silver nanoparticles (AgNPs) possess unique photochemical, optical and physical properties with superior localized surface plasmon resonance (LSPR) in the visible range. Consequently, the development of biosensors based on silver nanoparticles emerged in various fields in the last two decades, including medical, food and health care industries. Colorimetric detection platforms based especially on the aggregation of AgNPs have drawn great interest due to their simplicity, ease of synthesis and low cost. Likewise, the fluorometric detection platforms based on AgNPs, have emerged as useful tools, mostly due to their higher sensitivity.

In this thesis, two different platforms based on AgNPs for the detection of coralyne (COR) were developed. COR is a planar alkaloid with proven anti-proliferative activity in several cell lines and its detection using a simple, low cost technique is desired for its further utilization. The first platform was a colorimetric biosensor based on the LSPR of the AgNPs in the presence of COR and NaCl. First, the AgNPs and their aggregation behavior upon addition of COR were characterized by High Resolution Transmission Electron Microscopy (HRTEM), Fourier Transform Infrared Spectroscopy (FTIR), Dynamic Light Scattering (DLS) and Zeta potential experiments. The optimal salt concentration, pH, temperature and time for the

detection platform were determined by monitoring the change in SPR (A_{612}/A_{400}) using UV-Vis spectroscopy, and the lower limit of detection (LOD) was determined as 8.54 nM under the optimized conditions. Real sample experiments were also conducted for measuring the applicability of the probe in complex matrices. The second platform developed was a fluorometric probe based on dT_{32} modified AgNPs in the presence of coumarin (COU). dT_{32} modified AgNPs were also characterized by using HRTEM, FTIR, DLS and Zeta potential experiments. LOD was determined to be as 5.24 nM under the optimized dT_{32} concentration, temperature and time. The developed colorimetric and the fluorometric probes were also tested in urine as real sample via spiking experiments, and the overall recovery percentages were found to be between 92.32%-116.0% and 87%-105%, respectively.

Keywords: Coralyne, Silver Nanoparticles, Colorimetric Detection, Fluorometric Detection, Sensors

ÖZ

CORALYNE TESPİTİ İÇİN KOLORİMETRİK GÜMÜŞ NANOPARÇACIK PROBLARININ GELİŞTİRİLMESİ

Usta, Hatice Müge
Yüksek Lisans, Kimya
Tez Yöneticisi: Doç. Dr. Özgül Persil Çetinkol

Temmuz 2020, 94 sayfa

Gümüş nanoparçacıklar (AgNPs) görünür ışıkta üstün Lokalize Yüzey Plasmon Rezonansı (LSPR) ile sıradışı fotokimyasal, optik ve fiziksel özelliklere sahiplerdir. Bu nedenle gümüş nanoparçacıklara dayanan biyosensörlerin geliştirilmesi son yirmi yılda tıp, gıda ve sağlık endüstrileri de dahil olmak üzere çeşitli alanlarda öne çıkmıştır. Özellikle gümüş nanoparçacıkların toplanmasına (agregasyonuna) dayalı kolorimetrik tespit yöntemleri, basitlikleri, sentez kolaylığı ve düşük maliyetleri nedeniyle büyük ilgi görmektedirler. Benzer şekilde, gümüş nanoparçacıklara dayanan florometrik tespit platformları da çoğunlukla yüksek hassasiyetleri nedeniyle faydalı araçlar olarak ortaya çıkmışlardır.

Bu tez kapsamında, coralyne (COR) tespiti için gümüş nanoparçacıklara dayalı iki farklı platform geliştirilmiştir. COR birçok hücre dizisinde antiproliferatif aktivite gösterdiği kanıtlanmış düzlemsel bir alkaloittir ve basit, düşük maliyetli bir metot kullanarak tespitine ihtiyaç duyulmaktadır. İlk platform, COR ve NaCl varlığında gümüş nanoparçacıkların LSPR özelliğine dayanan bir kolorimetrik biyosensördür. Öncelikli olarak, gümüş nanoparçacıklar ve onların COR eklenmesiyle gerçekleşen toplanması, Yüksek Çözünürlüklü İletim Elektron Mikroskobu (HRTEM), Fourier

Dönüşümlü Kızılötesi Spektroskopisi (FTIR), Dinamik Işık Saçılım Spektrometresi ve Zeta Potansiyel ölçümleri ile karakterize edilmiştir. Optimal tuz derişimi, pH, sıcaklık ve süre, UV-Vis spektroskopisi ile SPR'deki değişiklik (A_{612}/A_{400}) izlenerek belirlenmiştir ve optimize edilmiş koşullar altında tespit limiti (LOD) de 8.54 nM olarak belirlenmiştir. Karmaşık matrislerde probun uygulanabilirliğini ölçmek için gerçek numune deneyleri de yapılmıştır. Geliştirilen ikinci platform, kumarin (COU) varlığında dT_{32} ile modifiye edilmiş gümüş nanoparçacıklara dayanan bir florometrik probdur. dT_{32}-AgNPs, HRTEM, FTIR, DLS ve Zeta Potansiyel ölçümleri ile karakterize edilmiştir. LOD, optimize edilmiş dT_{32} konsantrasyonu, sıcaklığı ve süresi altında 5.24 nM olarak belirlenmiştir. Geliştirilen her iki prob da spike deneyleri yoluyla idrarda test edilmiş ve geri kazanım yüzdeleri sırasıyla %92.32 ile %116.0 ve %87% ile %105 aralığındadır.

Anahtar Kelimeler: Coralyne, Gümüş Nanoparçacıklar, Kolorimetrik Tespit, Florometrik Tespit, Sensörler.

To my family…

ACKNOWLEDGMENTS

I would like to express my deepest gratitude to my supervisor Assoc. Prof. Özgül Persil Çetinkol for her guidance, patience and continuous support. It has been a great honor for me to be a part of her research group. I could not imagine having a better supervisor and a working environment.

My appreciation also extends to my laboratory colleagues. I would like to thank Dr. Mehrdad Forough for his support and immense knowledge throughout the research. I am thankful to all the members of Özgül Persil Çetinkol Research Group especially to Ecenaz Bilgen, Kübra Doğan and Zeynep Suvacı for their help and friendship.

I also would like to thank Assoc. Prof. Dr. İrem Erel and her group members for providing the opportunity for DLS and Zeta potential experiments.

I am grateful to the academic stuff of Department of Chemistry at METU for their support and guidance throughout my education.

I am thankful to my committee members; Prof. Dr. Ceyhan Kayran İşçi, Prof. Dr. Yasemin Arslan Udum, Prof. Dr. Levent Toppare and Assist. Prof. Dr. Süreyya Özcan Kabasakal for their time and effort.

Last but not least, I would like to thank my dear husband Engin Deniz Usta, my beloved parents and my lovely sister Selin Meltem Pazar for their endless love.

TABLE OF CONTENTS

LIST OF TABLES

TABLES

LIST OF FIGURES

FIGURES

LIST OF ABBREVIATIONS

AgNPs	Silver Nanoparticles
Aza3	7H-1,13-Dimethyldibenzoimidazolo [1,2-a:2′,1′-d] [1,3,5]-triazin-6-ium
Aza4	7H-Dibenzothiazolo[1,2-a:2′,1′-d] [1,3,5]-triazin-6-ium
Aza5	7H-3,11-Dimethoxydibenzothiazolo [1,2-a:2′,1′-d] [1,3,5]-triazin-6-ium
COR	Coralyne
COU	Coumarin
dA_{32}	5’- AAA AAA AAA AAA AAA AAA AAA AAA AAA AAA AA -3’
DLS	Dynamic Light Scattering
DMSO	Dimethyl Sulfoxide
DNA	Deoxyribonucleic Acid
DOX	Doxorubicin
dT_{16}	5’- TTT TTT TTT TTT TTT T -3’
dT_{32}	5’- TTT TTT TTT TTT TTT TTT TTT TTT TTT TTT TTT TT -3’
ELP	Ellipticine
EtBr	Ethidium Bromide
FRET	Fluorescence Resonance Energy Transfer
FTIR	Fourier Transform Infrared Spectroscopy
HOE	Hoechst
HRTEM	High Resolution Transmission Electron Microscopy
LDR	Linear Dynamic Range

LOD	Limit of Detection
LSPR	Localized Surface Plasmon Resonance
NET	Netropsin
OXP	Oxaliplatin
R	Recovery
RNA	Ribonucleic Acid
RSD	Relative Standard Deviation
SPR	Surface Plasmon Resonance
UV	Ultraviolet

CHAPTER 1

INTRODUCTION

1.1 A Brief Introduction to Nanotechnology

Nano is a Greek word meaning *dwarf* and used as an SI prefix to describe the billionth of a unit. [1] Nanotechnology is the science and engineering of materials that are billion times smaller than one-meter size. It has been first discussed by Richard Feynman when he presented the idea of rearranging individual atoms and molecules as desired in his talk in 1959 [2] although, the term 'nanotechnology' has introduced by Norio Taniguchi in his work on semiconductor processes in 1974 [3]. Yet, there were many works attributed to nanotechnology such as, the study of interfaces and colloids in 1900s, discovery of the concept of monolayer in 1932 and decoration of cups and glasses with nano-sized metals in fourth century BC [1] before the name was given.

Nanomaterials can be in various forms including nano tubes, shells, cages, fibers, plates, wires, rods and particles [4]–[6]. Several methods have been developed for the synthesis of nanomaterials to achieve different shapes and morphologies and in general there are two main approaches to the synthesis of nanostructures which are referred as top-down and bottom-up. Top-down approach is the destruction of bulk units to nano units while bottom-up approach is the building up nano units from atoms and clusters [4], [6].

Nanotechnology has been growing rapidly due to the accessibility of synthesis methods and characterization techniques [7]. Despite there are numerous classes of nanomaterials, nanoparticles are the major focus of nanotechnology [8] because they possess characteristic optical properties, can be easily modified, and their particle size can be altered readily [9].

1.2 Nanoparticles

Particles that are at most 100 nm in one dimension are defined as Nanoparticles and, they can be made up of metals, metal oxides, carbons or organic matter [8], [10]. What makes nanoparticles unique are their optical, structural and electrical properties that are different from their bulk properties [11]. Although bulk materials have certain physical properties regardless of their size, they show entirely different properties at nanoscales [10]. These phenomena can be explained by the large surface area to volume ratio of nanoparticles which increases the rate of fusion making nanoparticles chemically more reactive [8]. In addition, at nanoscales, the motion of electrons is confined which makes them react differently with light when compared with the large scales, thus changing optical properties [12]. Likewise, electronic motion is restricted because of this confinement that leads to inseparable conduction and valence band and changes electrical properties [13].

1.2.1 Metallic Nanoparticles

Among many types of nanoparticles, metal nanoparticles have drawn great attention due to the ease of functionalization or modification, uniform particle size and size distribution, and Localized Surface Plasmon Resonance (LSPR) characteristics [6], [9]. LSPR is generated as a result of the interaction between surface electrons in the conduction band and the incident light. This interaction causes coherent oscillation of the surface conduction electrons, and the frequency of these oscillations depends on the size, shape, particle distance and composition of the nanoparticles. LSPR is used in many applications ranging from electronics to biomedicine [14], [15].

1.2.1.1 Silver Nanoparticles

Silver nanoparticles (AgNPs) have high electrical and thermal conductivity, catalytical activity and chemical stability which make them useful in medicine,

electronics, antibacterial applications and biosensing [16], [17]. One of the best-known characteristics of the AgNPs is their LSPR properties. They have gained advantage over other noble metals in optical applications because they are relatively cheap, their plasmonic resonance is in the visible region of the electromagnetic spectrum and they have the sharpest and the strongest LSPR bands [18], [19].

1.3 Stabilization and Modification of Nanoparticles

Nanoparticles have high surface energy that can lead to agglomeration in the absence of the repulsive forces. Stabilization of the nanoparticles is needed to prevent this coagulation. It is achieved either by electrostatic stabilization in which surface of the particles stabilized with charged molecules or steric stabilization where particles bind to long alkyl chains, polymers or surfactants [6], [9]. While electrostatic stabilization is obtained during in-situ synthesis, steric stabilization usually requires additional post-modification steps [20].

Modification of nanoparticles is equally important as their synthesis and stabilization for the successful application and the improvement of practical use. Surface modifications allow nanoparticles to bind to the desired ligand, antibodies or drugs [9]. Physical adsorption or chemical reaction between the nanoparticle surface and the modifier are the two main approaches to modifications [20], [21].

1.3.1 Modification of Nanoparticles with DNA

Nanoparticles can be modified with oligonucleotides through specific or non-specific binding. Silver and Gold Nanoparticles are usually covalently modified with deoxyribonucleic acid (DNA) that have thiolate groups to achieve sequence specific recognition. On the other hand, simple adsorption of DNA to nanoparticle surface results in non-specific binding of the oligonucleotides [22].

1.4 Application of Nanoparticles

Nanoparticles are incorporated to variety of applications owing to their unique properties [6]. For instance, cosmetics industry uses zinc and titanium oxide nanoparticles to enhance the stability of UV protection in sunscreens since they reflect UV but transparent to visible light. In addition to cosmetics, nanoparticles found their way in electronics thanks to their high surface area. Batteries that are made up of metal hydride and nickel nanoparticles have less charging frequency and are long-lasting [8]. Having high surface area also makes nanoparticles applicable in catalysis applications. They are highly active, selective and have long lifetimes as catalysts [9]. Nanoparticles are great adsorbents and used in the treatment of water and air pollutants for environmental remediation [4]. Improvable biocompatibility of nanoparticles makes them great candidates for drug delivery [23]. Controlled delivery of drug to desired cells can be achieved by the use of nanoparticles which lowers the side effects and drug consumption [8].

One of the biggest application areas of the nanoparticles is the sensors. Rapid and reliable detection using simple and low-cost tools is needed for a number of ranging industries [24]. Nanoparticles are used as selective and sensitive sensors in integrated circuit, chemical and biological applications [25].

1.4.1.1 Nanoparticles as Sensors

Sensors are devices that are designed to bind a specific substance and translate this interaction into quantitative or qualitative signal [18]. Over the decade, the advancements in the field of nanosensors have increased rapidly due to their advantages over conventional detection methods in terms of selectivity, sensitivity and practicality [20]. One of the biggest advantages of nanosensors is their high surface area. Because sensing occurs on the surface of the nanoparticles, large surface area helps to increase the sensitivity [23].

Nanoparticles have size dependent optical properties that can be used in the LSPR based colorimetric sensors. LSPR based nanosensors are highly responsive to the presence of a target analyte. Change in the LSPR band upon the interaction of the sensor with the target analyte was shown to be useful in detection of several molecules [25]. Fluorometric detection platforms are also promising because of their higher sensitivity in general than the colorimetric probes. Many fluorescence nanomaterials, carbon-dots, quantum dots, conjugated polymers have been developed for detection with better sensitivity and selectivity. The main reason for using fluorescence nanomaterials and fluorophores with nanomaterials instead of conventional fluorophores is to increase optical response and sensing [26].

1.5 Coumarin

Coumarin (COU) is a naturally occurring compound that can be found in many natural plants (Figure 1). It has unique fluorescent properties, stability and high quantum yield. Coumarin and its derivatives have been used as fluorescent dyes in many applications [27]. It has been used in fluorometric detection of thiols, cations, anions, H_2O_2, O_2 and many biomolecules [28]–[30]. In addition, it has been shown that upon excitation at 350 nm coumarin reacts with thymidine via cycloaddition reaction and, so it has been used in DNA cross-linking studies [31].

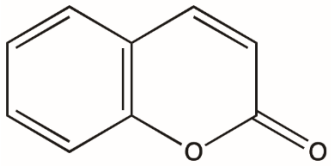

Figure 1. Coumarin structure.

1.6 Coralyne

Coralyne (COR, Figure 2) is a planar, synthetic protoberberine alkaloid that shows antitumor, antibacterial and anti-oxidant properties [32], [33].

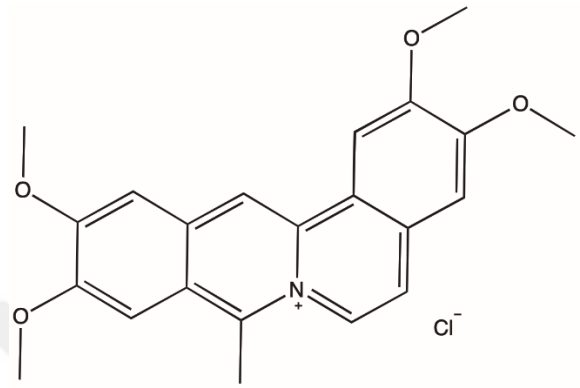

Figure 2. Coralyne Chloride structure.

COR have drawn attention for its biological and pharmacological potency. It is considered as a potential anticancer agent since it can bind to DNA via intercalation and lead to structural damage [34]. Photochemotherapy studies showed that UVA exposure enhances the anticancer property of COR [35]. In addition, COR can bind to RNA structures which makes it an ideal candidate in RNA-targeted drug design [36], [37]. COR can act also as a poison towards topo I and topo II enzymes [38]. Hemoglobin binding studies for a possible drug carrier showed that COR strongly binds also to hemoglobin [39].

1.7 Scope of the Thesis

The aim of this thesis is to develop sensitive, selective, rapid and cost-effective AgNP probes for detection of COR. Within the scope of this study, two different detection probes were developed. In the first part of the studies, a DNA-free colorimetric detection platform was developed using unmodified AgNPs for the detection of COR. LSPR of the unmodified AgNPs in the presence of COR under different conditions was investigated and the optimal conditions were found by using UV-vis spectroscopy. In the second part of the studies, another novel and facile technique for the detection of COR was developed using dT_{32}-modified AgNPs. Coumarin was used as the sensing element and the interaction of the target analyte with the modified system was evaluated and optimized using fluorescence spectroscopy. Overall, the two developed detection platforms were compared in terms of their analytical merits, selectivity, response time and ease of applicability.

CHAPTER 2

MATERIALS AND METHODS

2.1 Materials

Coralyne chloride ($C_{22}H_{22}ClNO_4$), coumarin ($C_9H_6O_2$), tri-sodium citrate dihydrate ($Na_3C_6H_5O_7.2H_2O$), ethidium bromide (EtBr, $C_{21}H_{20}BrN_3$), sodium chloride (NaCl), sodium hydroxide (NaOH), netropsin dihydrochloride (NET, $C_{18}H_{26}N_{10}O_3.2HCl$), 2-(2-ethoxyethoxy)ethanol ($C_6H_{14}O_3$), 2-aminobenzothiazole ($C_7H_6N_2S$), 1-methyl-1H-benzoimidazol-2-ylamine ($C_8H_9N_3$), dimethyl sulfoxide (DMSO, C_2H_6OS), dipotassium hydrogen phosphate (K_2HPO_4), potassium dihydrogen phosphate (KH_2PO_4) and potassium chloride (KCl) were purchased from Sigma Aldrich (USA). Silver nitrate ($AgNO_3$), sodium borohydride ($NaBH_4$), ellipticine (ELP, $C_{17}H_{14}N_2$), hydrochloric acid (HCl), methanol (CH_3OH) and acetonitrile (CH_3CN) were purchased from Merck KGaA (Germany). Oxaliplatin (OXP, $C_8H_{14}N_2O_4Pt$) was obtained from Sicor De Mexico, S.A. De C.V. (Mexico). Doxorubicin hydrochloride (DOX, $C_{27}H_{30}ClNO_{11}$) was obtained from Zhejiang Hisun Pharmaceutical CO., LTD (China). 2-Amino-6-methoxybenzothiazole ($C_8H_8N_2OS$) and diiodomethane (CH_2I_2) were obtained from TCI Chemicals (Japan) and Alfa Aesar (Germany), respectively. dT_{32} (5'- TTT TTT TTT TTT TTT TTT TTT TTT TTT TTT TT -3'), dA_{32} (5'- AAA AAA AAA AAA AAA AAA AAA AAA AAA AAA AA -3'), and dT_{16} (5'- TTT TTT TTT TTT TTT T -3') were purchased from Integrated DNA Technologies (Germany). 7H-3,11-Dimethoxydibenzothiazolo [1,2-a:2′,1′-d] [1,3,5]-triazin-6-ium (Aza5), 7H-Dibenzothiazolo[1,2-a:2′,1′-d] [1,3,5]-triazin-6-ium (Aza4) and 7H-1,13-Dimethyldibenzoimidazolo [1,2-a:2′,1′-d] [1,3,5]-triazin-6-ium (Aza3) were synthesized, purified and characterized according to the method that was reported by us and Hung et al. [40], [41]. Structure of small molecules are presented at Appendix A Figure 31.

Millipore water (Milli-Q, 18.2 MΩ cm^{-1}) was used throughout the experiments. Standard stock solutions of all small molecules were prepared by dissolving required amount of solid in DMSO or Millipore water. Concentrations of the stock solutions were calculated by using molar extinction coefficient (ε), path length (b) and absorbance (A) in UV-Visible spectroscopy (Beer-Lambert's Law, $A = \varepsilon \times b \times C$). Molar extinction coefficients of compounds are listed in Table 1. Fresh working solutions were diluted with Millipore water from these stock solutions. Stock solutions of oligonucleotides were prepared in 25 mM K-Phosphate buffer (pH = 7.0) containing 70 mM KCl. Stock solutions were heated to 95°C for 5 min and cooled down to room temperature for 24 h for the formation of proper DNA secondary structure. Concentrations of the stock solutions of the oligonucleotides were also calculated by using Beer-Lambert's Law. Molar extinction coefficients of the oligonucleotides are listed in Table 1. Fresh working solutions were diluted with Millipore water from these stock solutions.

Table 1. Extinction coefficients of small molecules and oligonucleotides [42]–[46].

Compound	Extinction Coefficient (M^{-1} cm^{-1})
COR	ε_{420} = 14 500
DOX	ε_{480} = 11 500
OXP	ε_{210} = 4513
ELP	ε_{295} = 60 000
NET	ε_{296} = 21 500
EtBr	ε_{478} = 5680
HOE	ε_{338} = 42 000
Aza3	ε_{343} = 45 700
Aza4	ε_{387} = 24 240
Aza5	ε_{407} = 25 000
dT_{32}	ε_{260} = 259 800
dT_{16}	ε_{260} = 130 200
dA_{32}	ε_{260} = 387 400

2.2 Methods

2.2.1 Equipment and Characterization

The absorption spectra were measured on a Cary 8454 UV–vis photodiode array spectrophotometer equipped with an Agilent 89090A peltier (Santa Clara, CA, USA). UV–vis spectra were collected using a 10 mm quartz cell between 250 and 950 nm. The fluorescence spectra were collected using a Cary Eclipse fluorescence spectrophotometer (Santa Clara, CA, USA) equipped with a Cary single cell peltier temperature controller (Agilent Technologies, USA). The emission spectra of the samples were recorded in the range of 430 to 700 nm by exciting at the wavelength of 420 nm and operating at 660 V. The excitation and emission slits width were both set at 5 nm. The quartz cells with 10 mm light path lengths (QS, Hellma) were used to record the absorption and emission measurements. A Mettler Toledo Seven Compact S210 pH meter (Greifensee, Switzerland) and a vortex mixer (Isolab, Germany) were used for pH adjustments and homogenization of mixtures, respectively. Hermle Z 326 K centrifuge (Hermle Labortechnik, Wehingen, Germany) was used to remove excess silver ions and purify the synthesized AgNPs.

AgNPs and its probes were characterized by using High Resolution Transmission Electron Microscopy, Fourier Transmission Infrared Spectroscopy, Dynamic Light Scattering and Zeta Potential measurements. JEOL JEM-2100 F (Akishima, Tokyo, Japan) with an acceleration voltage of 200 kV was used for capturing the HRTEM images. Prior to analysis, samples were sonicated 5 min and, placed onto commercial carbon-coated copper grids and, air dried for 24 h. Thermo Scientific Nicolet iS10 Fourier Transform Infrared spectrometer (Thermo Scientific, Waltham, MA, USA) was used for FTIR analysis in attenuated total reflection (ATR) mode. Total of 32 scans were carried out with resolution of 4 cm^{-1} in the range of 600-4000 cm^{-1}. The collected background was the surrounding air. Zetasizer Nano-ZS instrument (Malvern Instruments Ltd, Malvern, UK) was used for dynamic light scattering (DLS) and zeta(ζ)-potential measurements.

2.2.2 Synthesis of AgNPs

AgNPs were synthesized by using the previously reported one-pot synthesis by Flores et al. [47]. Concisely, to 400 mL 1.06 mM trisodium citrate solution, 15.0 mL of 5.0 mM silver nitrate solution was added under ice bath around 0°C. Next, 2500 µL of 100 mM sodium borohydride solution was added dropwise to the mixture over 5 min. Color change was observed from colorless to light yellow. The mixture was allowed to stir for 1 h 45 min in dark until color changes to shiny yellow. Then ice bath was removed and, the solution was kept at dark overnight. The as synthesized AgNPs were centrifuged at 6000 rpm for 15 min for purification, mainly to remove unreacted ions. The final concentration of the AgNPs was estimated to be 3.16×10^{-2} mg Ag/mL. For UV-Vis spectroscopy experiments AgNPs were diluted in 1:3 ratio with Millipore water (final concentration of 0.01 mg Ag/mL). For fluorescence spectroscopy experiments, AgNPs were used without further dilution.

2.2.3 Colorimetric Detection of Coralyne

For detection of COR, to 289.5 µL AgNPs solution (1 in 3 dilution), 1.5 µL of 10.0 mM NaCl was added, vortex-mixed and kept at room temperature for a few minutes prior to addition of COR. Different volumes of COR was added to the mixture from 10.0 µM stock solution to evaluate the response of the system to COR concentration. The concentration dependence of the system was monitored using UV-Vis spectroscopy while color change from yellow to pink was observed with naked-eye. The effect of temperature, pH and time on the system was observed in the presence of 300 nM COR and 500 µM NaCl. Selectivity of the system to COR or NaCl as the present salt was investigated by using different small molecules or salts, respectively, in the optimized concentrations (300 nM small molecule and 500 µM salt). For further investigation of the selectivity of the probe towards COR, response of the probe to other molecules such as sugars, amino acids, cations or anions were

monitored and compared. All the experiments were repeated three times and the mean value of results with the error bars were used in calculations.

2.2.4 Fluorometric Detection of Coralyne

For detection of COR, to 1502.5 µL of AgNPs solution (without dilution), 40.0 µL of 100.0 µM dT_{32} solution was added and solution was vortex-mixed and incubated for 15 min. Next, 7.5 µL of 1.0 mM COU was added to dT_{32}-AgNPs and incubated for 5 min. Prior to measurement, 950.0 µL Millipore water was added to mixture. Different volumes of COR were added to the mixture from 5.0 µM stock solution to evaluate the response of the system to COR concentration. The concentration dependence of the system was monitored using fluorescence spectroscopy. The effect of temperature and time on the system was observed in the presence of 100 nM COR and 3.0 µM COU. Selectivity of the system to COR or dT_{32} sequence was investigated by using different small molecules or oligonucleotides, respectively, under the optimized concentrations (100 nM small molecule and 1.5 µM oligonucleotide). All experiments were repeated three times and the mean value of results with error bars were used in calculations.

CHAPTER 3

RESULTS AND DISCUSSION

Part of this thesis study was published as ‘‘A DNA-free Colorimetric Probe Based on Citrate-capped Silver Nanoparticles for Sensitive and Rapid Detection of Coralyne’’ by H. M. Usta, M. Forough and O. Persil Çetinkol in *Sensors and Actuators: B Chemical*, 298, 126823, 2019 [48].

3.1 Colorimetric Detection of Coralyne

The response of AgNPs to COR in the presence of NaCl was monitored by UV-Vis spectroscopy. AgNPs show a LSPR absorption peak at 400 nm that gives a yellow color to the solution (Figure 3, spectrum a; Figure 4, vial a). Addition of NaCl to AgNPs did not affect this LSPR band absorption of the AgNPs. (Figure 3, spectrum b) However, the addition of COR (final concentration of 300 nM) caused a decrease in the intensity of the LSPR band of the AgNPs and, the appearance of a new peak at with a maximum wavelength at around 612 nm (Figure 3, spectrum c). Color change was also observed from yellow to pink only after the addition of COR due to the aggregation of AgNPs upon complex formation (Figure 4, vial c). There was no color change after the addition of NaCl to AgNPs (Figure 4, vial b). In addition, there was no color change with the addition of COR to AgNPs in the absence of NaCl for 6 hours, however a slight color change was observed after 24 h.

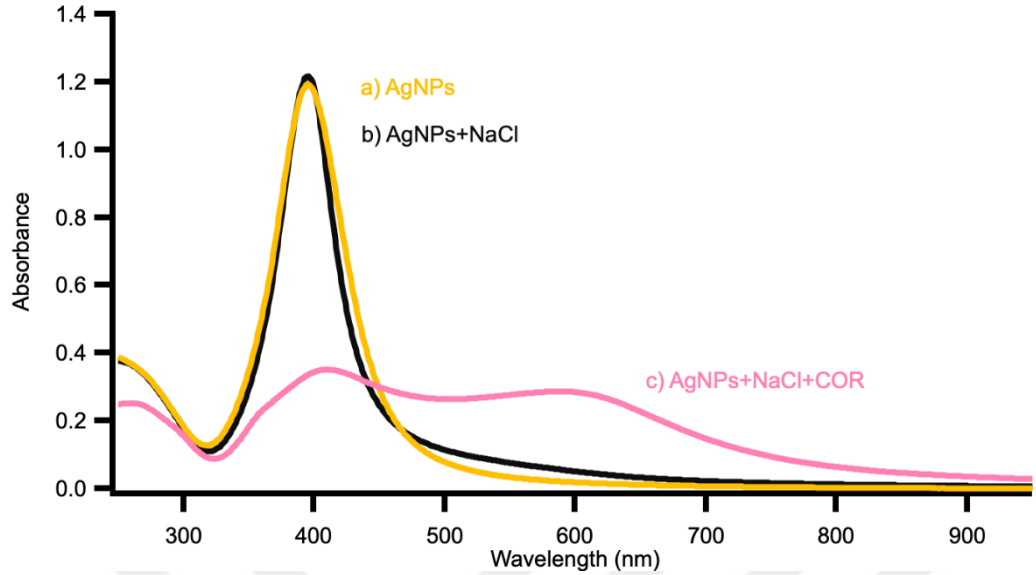

Figure 3. UV-Vis spectra of a) AgNPs, b) AgNPs + 500 µM NaCl and c) AgNPs + 500 µM NaCl + 300 nM COR.

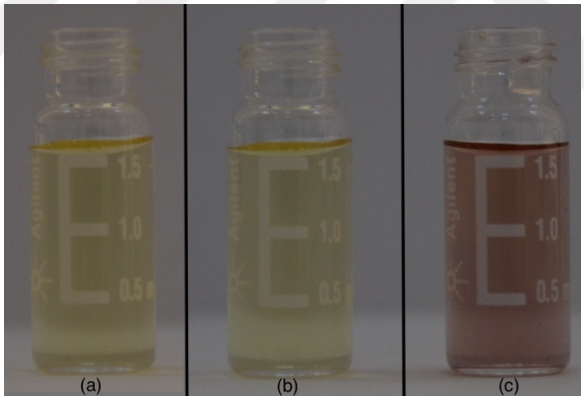

Figure 4. Photographs of a) AgNPs, b) AgNPs + 500 µM NaCl and c) AgNPs + 500 µM NaCl + 300 nM COR.

3.1.1 UV-Visible Spectroscopy Experiments

3.1.1.1 Salt Effect

Ionic strength had a significant impact on the detection of COR with the proposed method. In the absence of NaCl, aggregation of AgNPs was not observed with increasing COR concentration. For determination of the optimal salt concentration that induces the aggregation of AgNPs, different concentrations of NaCl were added to AgNPs + 300 nM COR between 0 to 3.3 mM. Experiments were repeated three times and the average A_{612}/A_{400} vs. NaCl concentration graph was plotted with error bars (Figure 5). UV-Vis spectra of AgNPs + COR with different concentrations of NaCl and plot of A_{612}/A_{400} vs. NaCl concentration of each replicate are listed in Appendix B (Figure 32-37).

A_{612}/A_{400} ratio increased with addition of NaCl up to 500 µM NaCl concentration and remained steady afterwards. Optimum and highest value of absorption ratio was obtained when NaCl concentration was 500 µM, thus all experiments were carried in the presence of 500 µM NaCl.

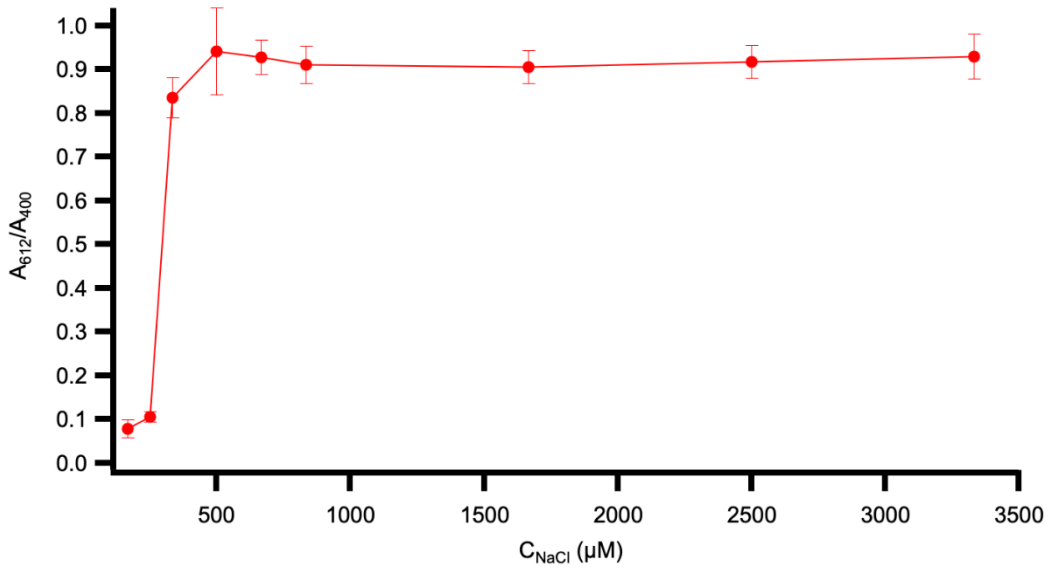

Figure 5. Plot of A_{612}/A_{400} vs. NaCl concentration in the presence of 300 nM COR.

The effect of other inorganic electrolytes on the response of AgNPs towards COR was also investigated by adding different electrolytes into AgNPs. UV-Vis spectrum of each electrolyte sample in the presence of 300 nM COR was collected and all the collected spectra are listed in Appendix B (Figure 38). Bar graph of A_{612}/A_{400} for different electrolyte samples was plotted in Figure 6. In the presence of NaI, NaBr, $NaNO_3$, $NaCH_3COO$, NaH_2PO_4 and Na_2HPO_4 aggregation rate of AgNPs were negligible. There was neither a spectral difference nor a color change in KCl and NaCl samples. However, the absorption ratio was smaller when LiCl is used instead. As the ionic strength increased, ($SrCl_2$, $MgCl_2$, $MnCl_2$: divalent; $AlCl_3$: trivalent), a dramatic change was observed on the response of the probe such that the AgNPs were able to aggregate even without the addition of COR.

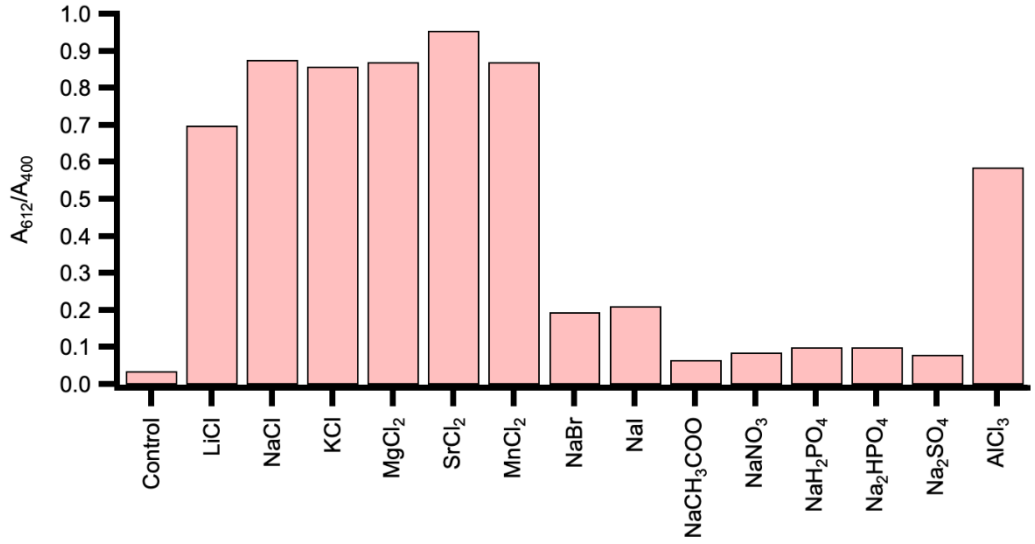

Figure 6. Bar graph of A_{612}/A_{400} vs. different electrolytes under optimized conditions (300 nM COR and 500 µM NaCl).

3.1.1.2 Temperature Effect

The influence of temperature on the response of the probe was investigated by changing the temperature of AgNPs + NaCl + COR between 5 and 55°C. UV-Vis spectrum was taken at each temperature. Experiments were repeated three times and the average graph of A_{612}/A_{400} vs. temperature was plotted in Figure 7. UV-Vis spectra of AgNPs + NaCl + COR at different temperatures and the plot of A_{612}/A_{400} vs. temperature for each replicate are listed in Appendix B (Figure 39-44). Since the temperature change did not affect the response of the probe towards COR; all the experiments were conducted at room temperature.

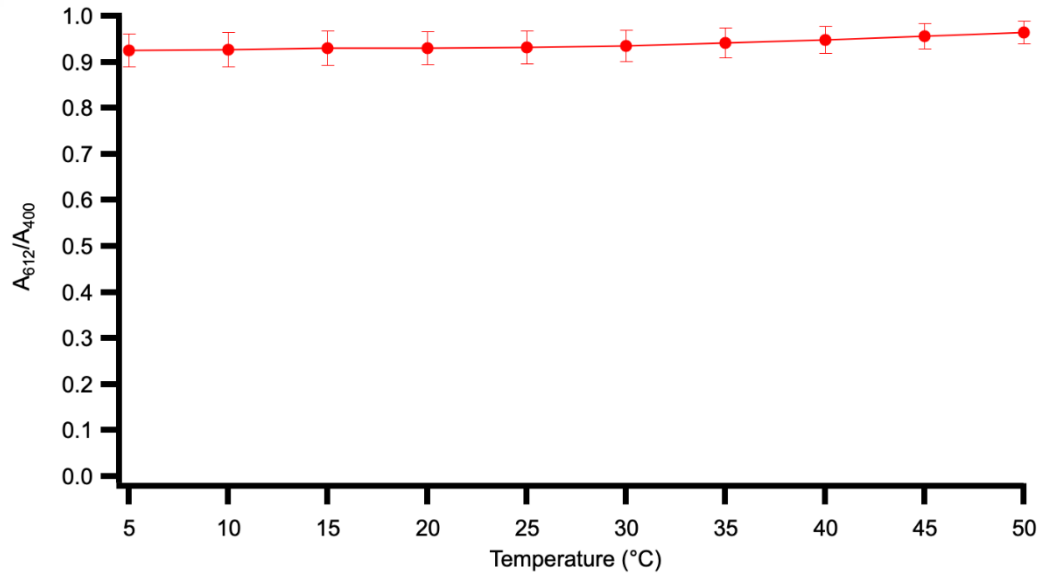

Figure 7. Plot of A_{612}/A_{400} vs. temperature under optimized conditions (300 nM COR and 500 µM NaCl).

3.1.1.3 Time Effect

Effect of the time on the response of probe towards COR was investigated at optimized concentrations (500 µM NaCl and 300 nM COR). UV-Vis spectra were taken after addition of COR to AgNPs + NaCl between 0 to 60 min. Experiments were repeated three times and, the average graph of A_{612}/A_{400} vs. time was plotted in Figure 8. UV-Vis spectra and plot of A_{612}/A_{400} vs. time for each replicate are listed in Appendix B (Figure 45-50). When the change in the ratio of absorbance was examined with respect to time, it was observed that the absorbance ratio reached its highest value at 5 minutes and remained steady afterwards. Therefore, 5 minutes was selected as the optimum response time for all the experiments.

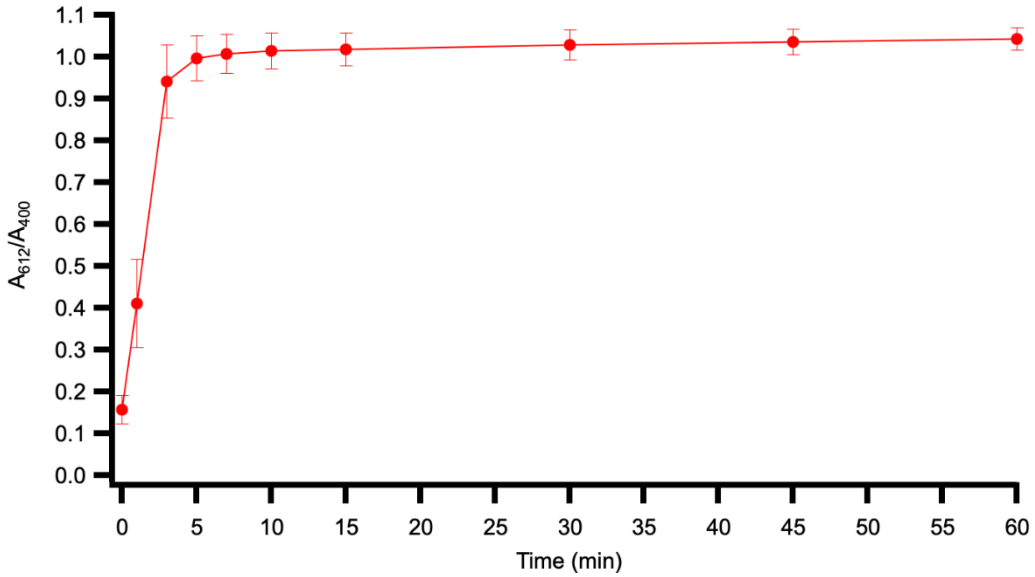

Figure 8. Plot of A_{612}/A_{400} vs. time under optimized conditions (300 nM COR and 500 µM NaCl).

3.1.1.4 pH Effect

In order to investigate the effect of pH on negatively charged AgNPs and positively charged COR, the pH of the analyte solution was changed between 3 and 11. UV-Vis spectra of AgNPs + NaCl + COR taken at different pH values are listed in Appendix B (Figure 51). The plot of of A_{612}/A_{400} vs. pH given in Figure 9 revealed that the highest absorption ratio was obtained at neutral pH; therefore, all the experiments were conducted at neutral pH.

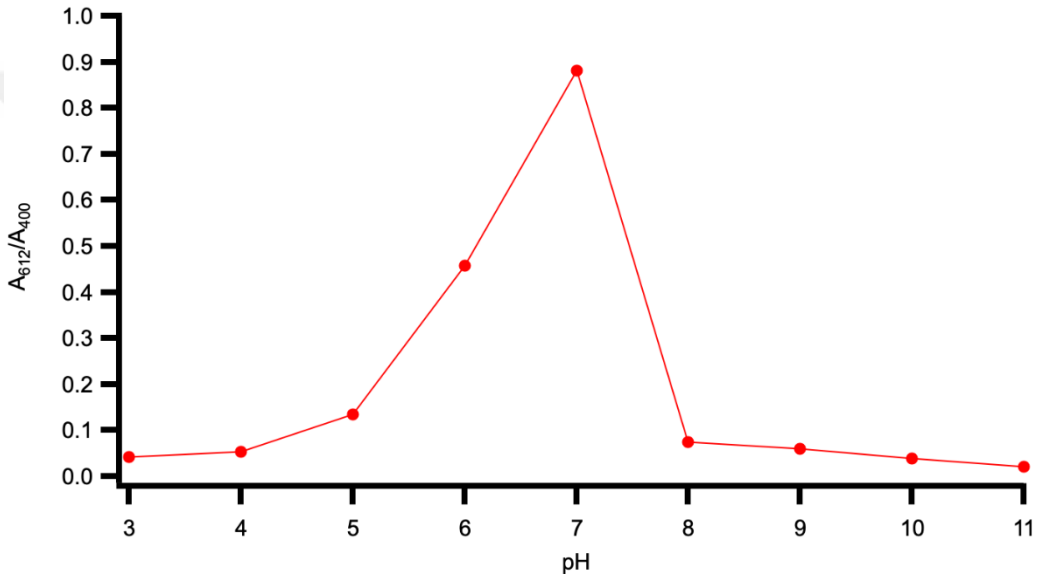

Figure 9. Plot of A_{612}/A_{400} vs. pH under optimized conditions (300 nM COR and 500 µM NaCl).

3.1.2 Characterization of the Probe

To provide a possible mechanism and get detailed information about the morphology change of AgNPs before and after the addition of COR, HRTEM micrographs were taken. AgNPs and AgNPs + NaCl (Figure 10, 1 and 2, respectively) images showed that AgNPs were spherical, monodisperse and had an average of 10 nm particle size. There was no significant change after the addition of NaCl to AgNPs. However, after the addition of COR, the formation of large flocs that are between 50 and 80 nm was observed (Figure 10, 3 and 4; different scales). HRTEM micrographs provide strong evidence for a mechanism based on the aggregation of AgNPs after the addition of COR. Several micrographs with different scales are listed in Appendix B (Figure 52-54).

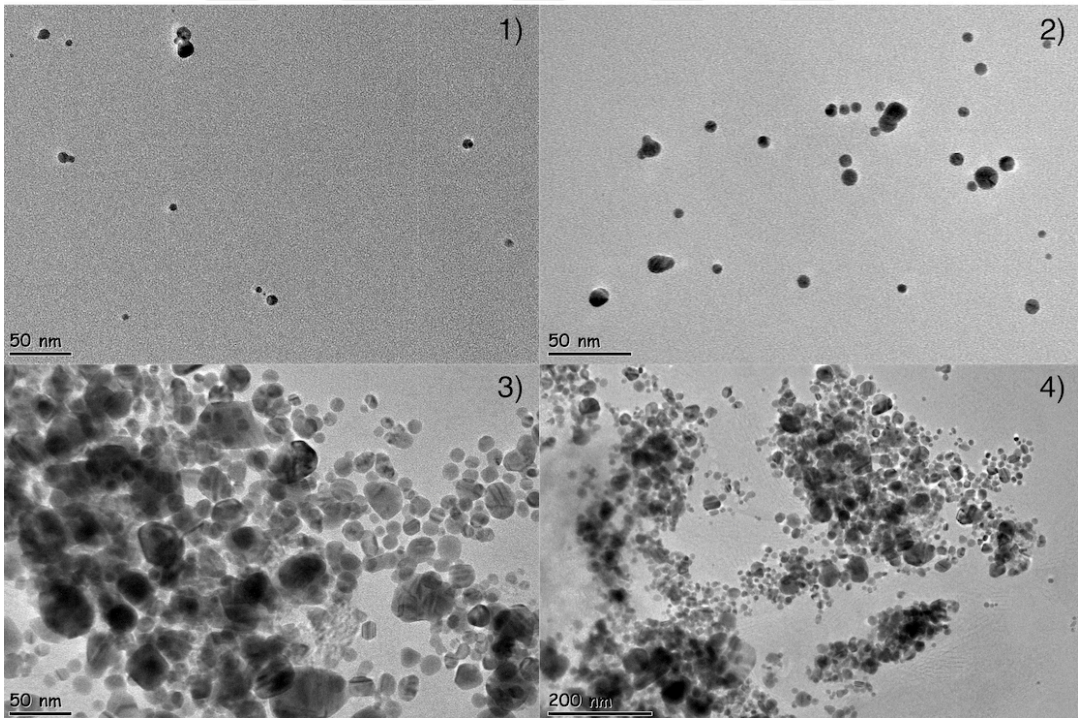

Figure 10. TEM images of 1) AgNPs, 2) AgNPs + NaCl, 3) AgNPs + NaCl + COR (scale: 50 nm) and 4) AgNPs + NaCl + COR (scale: 200 nm).

DLS and Zeta potential experiments provided further insight to the working principle of our probe by providing the change in the size and the charge of AgNPs before and after addition of COR (Figure 11). Before the addition of COR (Figure 11A), particle size of AgNPs were under 10 nm with an average hydrodynamic diameter of 1.84 ± 0.27 nm. However, the size of the AgNPs was determined to be between 60 and 198 nm with an average diameter of 84.54 ± 4.62 nm 5 minutes after the addition of COR (Figure 11B). Results were in good agreement with HRTEM results and indicated the aggregation of AgNPs after the addition of COR. In addition, zeta potential experiments revealed that in the absence of COR, AgNPs had a mean surface potential value of -43.71 ± 1.67 mV, which indicated that AgNPs were highly negatively charged. However, after the addition of COR, mean zeta potential value increased to -23.70 ± 2.93 mV which indicated the loss of negative charge upon formation of aggregates.

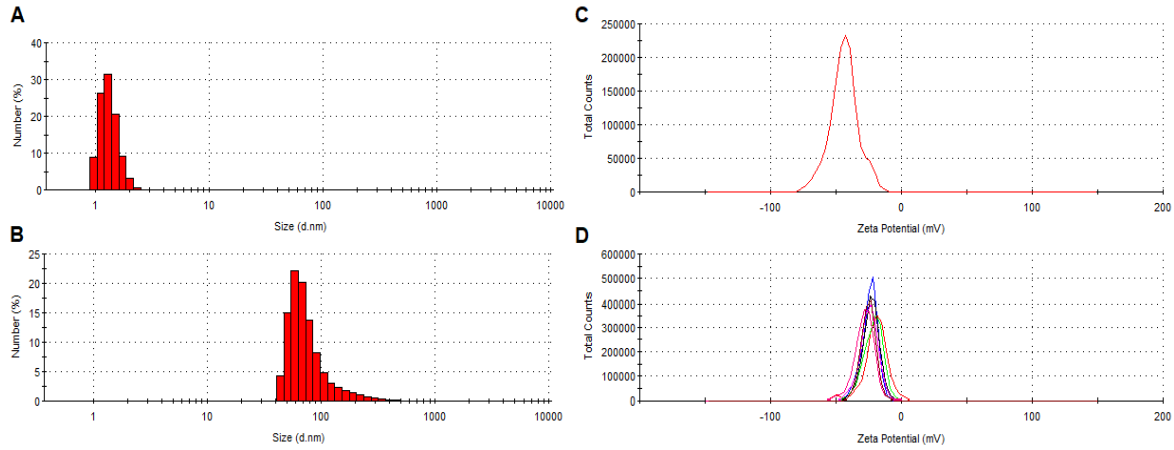

Figure 11. Particle size and zeta potential (mV) distributions of AgNPs (A and C) and AgNPs + NaCl + COR (B and D), respectively.

FTIR spectra of AgNPs in the absence and presence of COR and COR alone were also acquired (Figure 12). The disappearance of IR bands at 1520 and 1350 cm^{-1} which are attributed to C=O asymmetric stretching in COO^- and symmetric stretch of carboxylate ion, respectively, after the addition of COR confirmed the removal of citrate molecules from the surface of AgNPs.

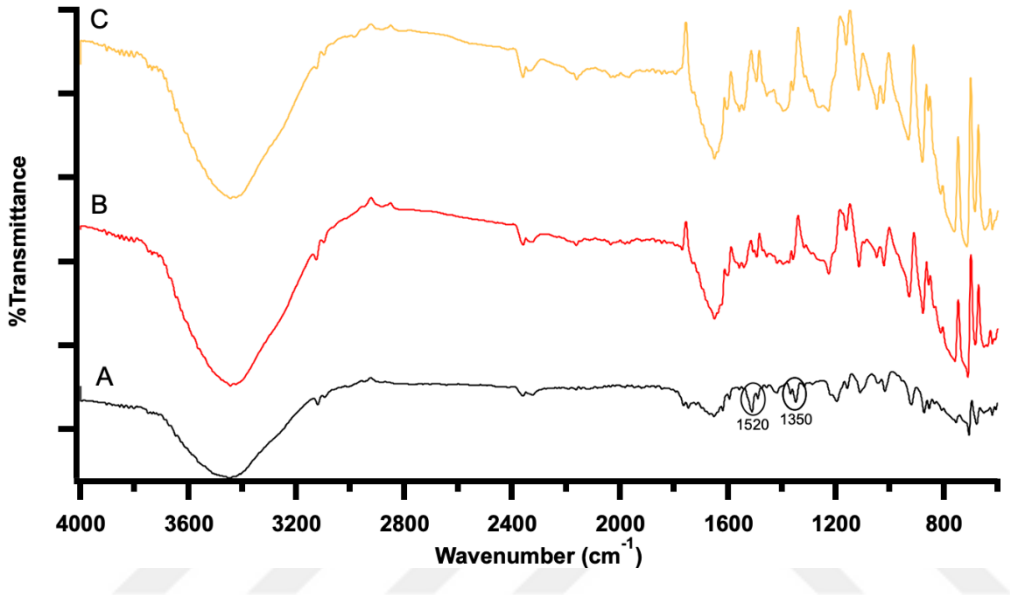

Figure 12. FTIR spectra of (C) COR and (B) AgNPs + NaCl + COR and (A) AgNPs + NaCl.

3.1.3 The Sensing Mechanism

The experimental results presented above points towards a sensing mechanism for the probe that depends on the aggregation of AgNPs upon COR addition. Possible explanation for the aggregation of AgNPs in the presence of COR can be the adsorption of positively charged COR on the surface of nanoparticles by displacing and/or neutralizing the negatively charged citrate ions. The negatively charged citrate ions prevent the aggregation of AgNPs due to the repulsion between the negatively charged particles, the addition of the positively COR, was unsurprisingly decreasing the repulsion between the AgNPs by displacing and/or neutralizing the negative charges and resulting in the aggregation of AgNPs. The presence of NaCl

as an electrolyte accelerated and enhanced the aggregation because of crucial effect of ionic strength in the loss of colloidal stability [49]. DLS, Zeta potential and FTIR experiments all support this proposed mechanism (Figure 13). It is believed that observation of color change and a red shift of LSPR band in UV-Vis spectrum was due to the aggregation of AgNPs in the presence of COR.

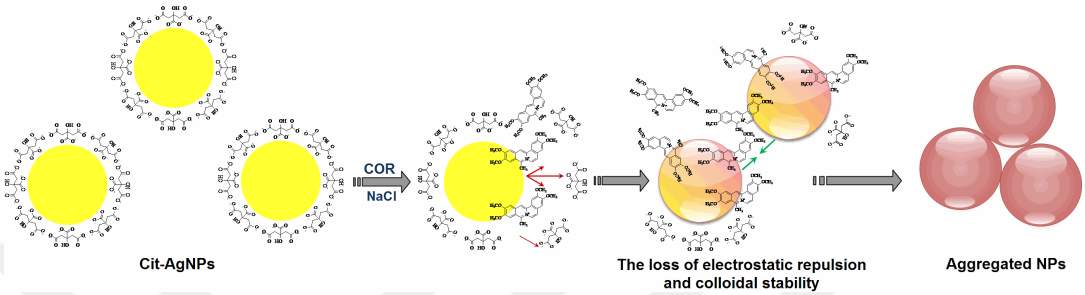

Figure 13. Schematic representation of proposed mechanism, taken from Usta et. al. (2019) [48].

3.1.4 The Sensitivity of the Probe

Sensitivity of the probe towards COR concentration was investigated by titration experiments. The sample of AgNPs in the presence of 500 µM NaCl was titrated with 10.0 µM COR solution (0.0 to 200.0 µL). After each titration, the change in the absorbance spectrum was monitored by using UV-Vis spectroscopy (Figure 14). Through titration, LSPR band at 400 nm was gradually decreased and, the formation of a new peak at 612 nm was observed.

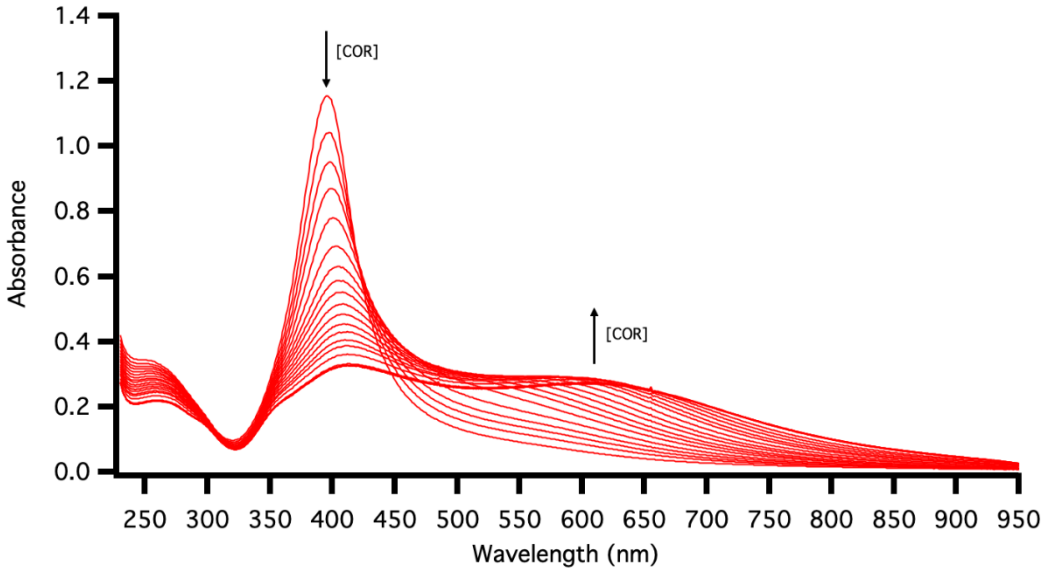

Figure 14. UV-Vis spectra of the titration of 10.0 µM COR into the AgNPs in the presence of 500 µM NaCl.

Calibration curve was constructed by plotting the absorption ratio (A_{612}/A_{400}) vs. COR concentration (Figure 15). Experiments were repeated three times and, average of the replicates were used in the calculation of linearity parameters (Table 2). UV-Vis spectra and calibration curves of each replicate are listed in Appendix B (Figure 55-60).

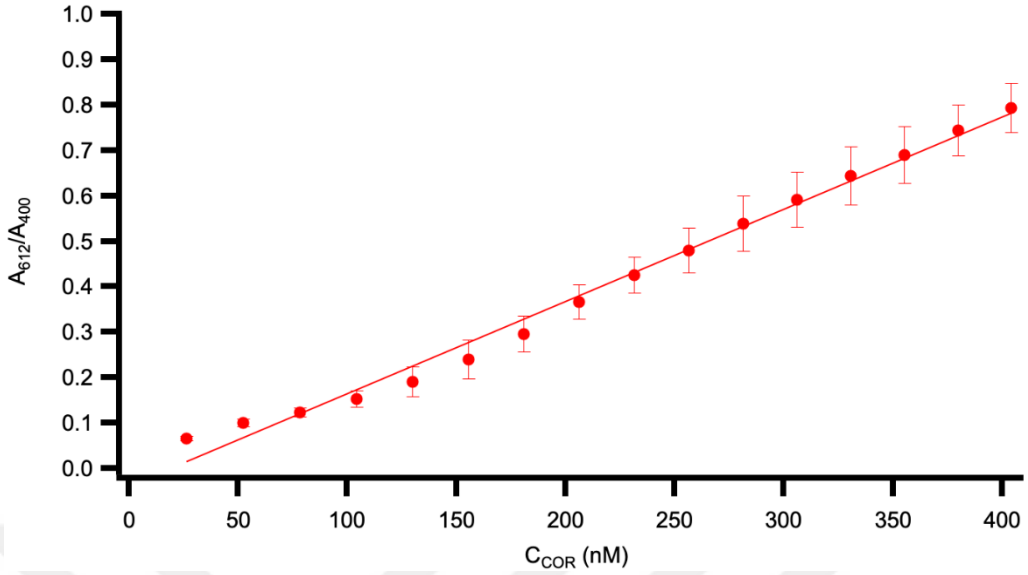

Figure 15. Calibration curve obtained through the titration of 10.0 µM COR into the AgNPs solution with 500 µM NaCl.

Table 2. Analytical merits of the colorimetric detection method for COR.

Calibration curve equation	R[a]	LOD [b]	LDR [c]
$A_{612}/A_{400} = 0.002C - 0.0392$[d]	0.9907	8.54 nM	26-404 nM

a. Correlation coefficient.
b. Limit of detection (nM); (LOD was calculated from the concentration at which the absorbance change is 3 times of standard deviation of the blank).
c. Liner dynamic range (nM).
d. A_{612}/A_{400} (A_{612} and A_{400} are the absorbance of AgNPs at 612 nm and 400 nm, represent the aggregated and dispersed AgNPs, respectively); C is the concentration of COR (nM) and absorption ratio (y) represents the intercept of the slope.

3.1.5 The Selectivity of the Probe

Selectivity of probe towards COR was investigated in the presence of several other ligands that have similar structures to COR. To determine the selectivity, samples including other small molecules at 300 nM concentration instead of COR were prepared, and their UV-Vis spectra were taken. Experiments were repeated three times and, average bar graph of A_{612}/A_{400} for different ligands with errors bars was

plotted (Figure 16). UV-Vis spectra and bar graph of for AgNPs + NaCl samples with different ligands are listed in Appendix B (Figure 61-66).

Besides COR, there was no significant change on the absorption ratio of A_{612}/A_{400} with the addition of ligands suggesting that the system was selective to COR.

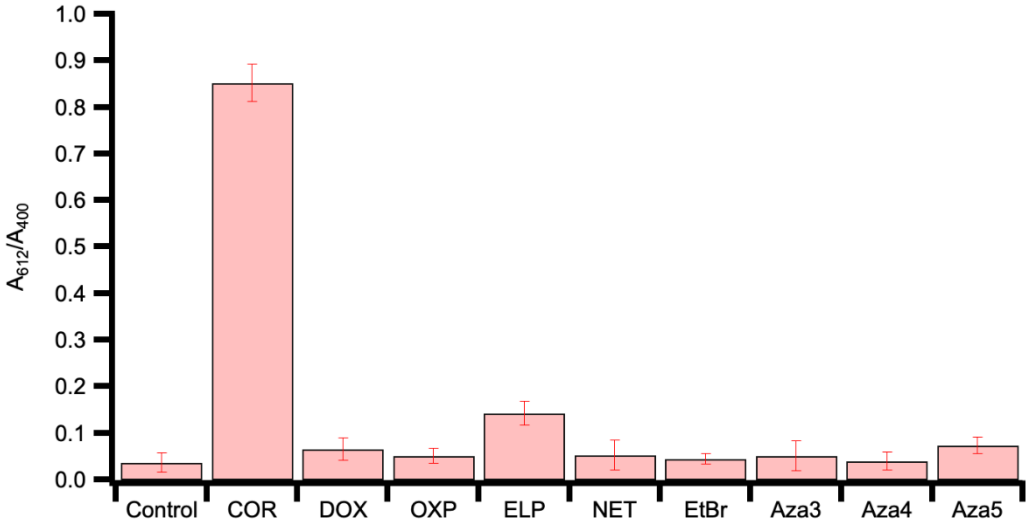

Figure 16. Bar graph of A_{612}/A_{400} for samples with different ligands under the optimized concentrations (500 µM NaCl 300 nM ligand).

In addition, the selectivity of the system was also tested a higher concentration of the other ligands (900 nM) by adding them to AgNPs + NaCl. UV-Vis spectra of AgNPs + NaCl with different ligands are listed in Appendix B (Figure 67). Bar graph of A_{612}/A_{400} for samples with different ligands at 900 nM and COR at 300 nM was plotted (Figure 17). The change in absorption ratio was insignificant among the ligands except COR. Results showed that even in the presence of higher concentrations of different ligands probe was selective to COR.

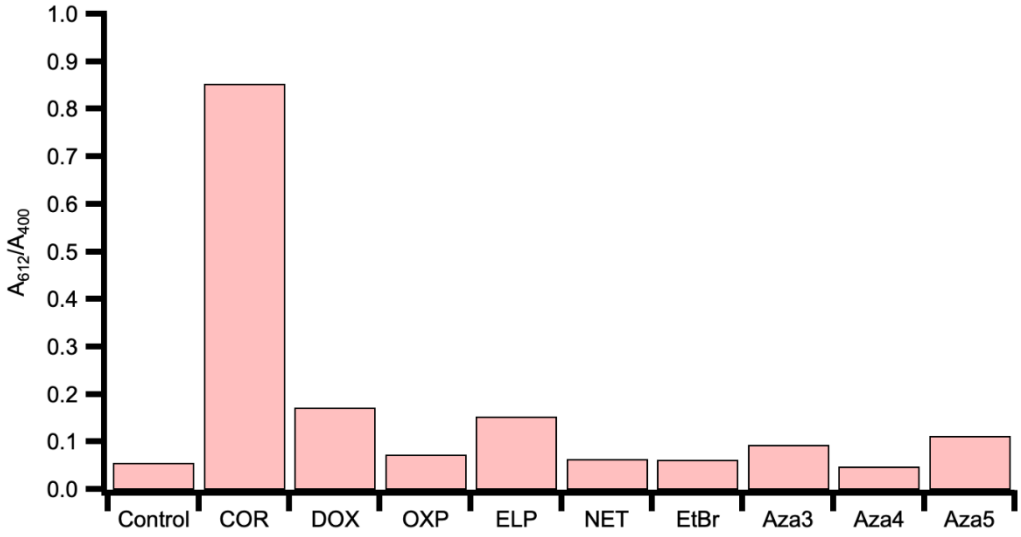

Figure 17. Bar graph of A_{612}/A_{400} for different ligands (final concentration of the ligands were 900 nM for different ligands and 300 nM for COR) in the presence of 500 µM NaCl.

For further investigation of selectivity of probe towards COR, a mixture containing AgNPs + 500 µM NaCl + 300 nM of different ligands (DOX, OXP, ELP, NET, EtBr, Aza3, Aza4 and Aza5) were prepared. UV-Vis spectra of the mixture taken before and after the addition of COR are listed in Appendix B (Figure 68). Bar graph of A_{612}/A_{400} for the mixed environment in the presence and absence of COR was plotted in Figure 18. There was not a significant change in the absorption ratio prior to the addition of COR into the mixture. After COR was added, the aggregation of AgNPs was observed. The results obtained confirmed that the system is highly selective towards COR even in a mixed matrix.

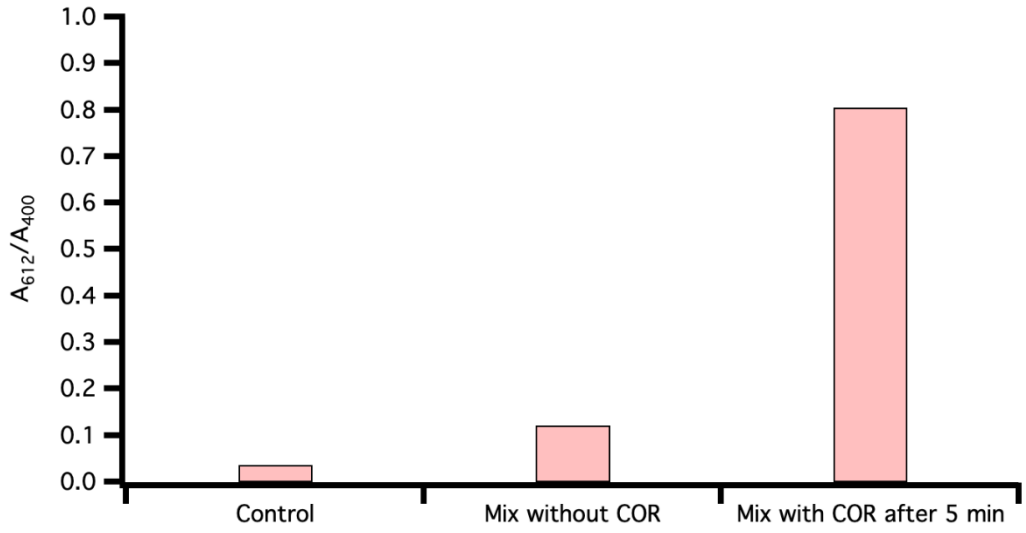

Figure 18. Bar graph of A_{612}/A_{400} for the mixed environment in the presence and absence of COR.

Finally, the response of the probe towards the diverse common substances were investigated by adding 300 nM of the common substances (except Fe^{3+} and tyrosine; 30 nM) into AgNPs + 500 µM NaCl. UV-Vis spectra of each sample were acquired, and the acquired spectra are listed in Appendix B (Figure 69). Bar graph of A_{612}/A_{400} for common substances was plotted in Figure 19.

Adding these organic/inorganic substances at a final concentration of around 100-1000-fold higher than COR concentration did not show any significant effect on the absorption ratio and color of the solution (except the addition of cysteine). Cysteine showed a slight color change and gave a different spectral response than COR. This response of the cysteine may be due to the high binding affinity of cysteine towards metallic nanoparticles [50]. Still, since there was no overlap of spectral response region of the cysteine and COR samples, the signal caused by cysteine can be ignored.

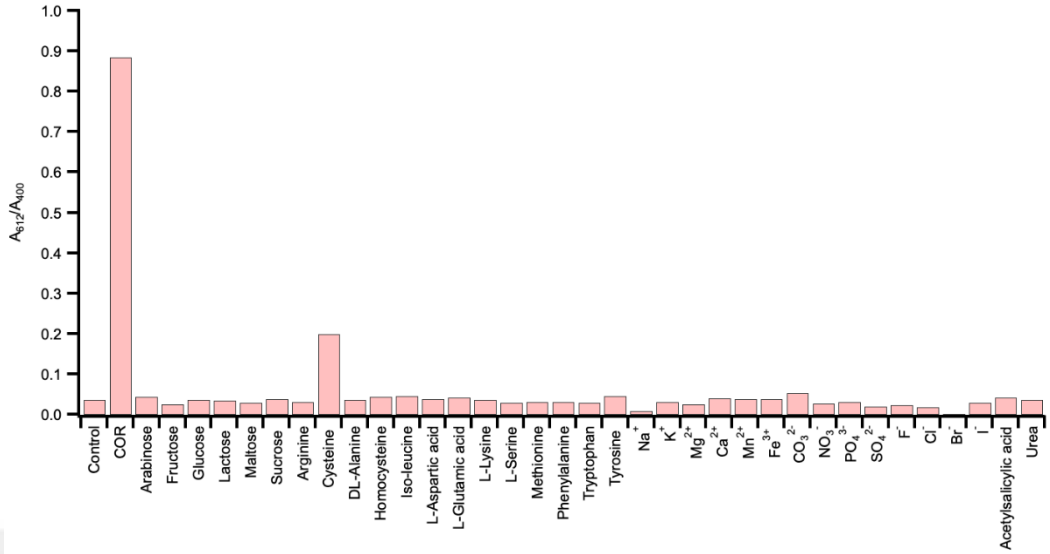

Figure 19. Bar graph of A_{612}/A_{400} for common substances (final concentration of 300 nM, except Fe^{3+} and Tyrosine that are 30 nM) in the presence of 500 µM NaCl.

3.1.6 Application of the Method

The applicability and feasibility of the probe in real samples was evaluated by using spiking experiments. COR was spiked at five different concentrations into three different human urine samples and or a tap water sample, and the concentration of COR in each sample was determined by using the previously constructed calibration curve after measuring the UV-Vis absorbance. UV-Vis spectra of samples are listed in Appendix B (Figure 70-81). Results are listed in Table 3. The obtained recoveries of COR were in the range of 92.32-116.0% for urine samples and 98.48-106.02% for tap water samples. The calculated values were within the acceptable range that is recommended by FDA [51], showing that the probe had reasonable precision and accuracy.

Table 3. Analytical results for the determination of COR in real samples using colorimetric detection method.

Sample	Spiked concentration (nM; n = 3[a])	Mean found concentration (nM)	RSD (%)[b]	Recovery (%)[c]	Accuracy (RE %)[d]
Urine sample 1	52	60.32	4.78	116.00	16.0
	100	102.53	5.02	102.53	2.53
	150	143.83	4.66	95.89	-4.11
	300	313.59	0.21	104.53	4.53
	404	418.11	4.37	103.49	3.49
Urine sample 2	52	48.01	5.81	92.32	-7.67
	100	97.41	1.71	97.41	-2.59
	150	144.30	0.78	96.20	-3.80
	300	299.91	2.71	99.97	-0.03
	404	414.75	2.54	102.68	2.66
Urine sample 3	52	59.08	9.43	113.62	13.61
	100	97.18	3.44	97.18	-2.82
	150	146.08	3.67	97.39	-2.61
	300	307.55	1.80	102.52	2.52
	404	409.75	3.43	101.42	1.42
Tap water	52	55.13	1.86	106.02	10.26
	150	147.63	3.57	98.43	-1.58
	404	412.44	0.93	102.09	3.11

[a] Number of replicates.
[b] RSD: Relative standard deviation.
[c] Recovery (%) = 100 × found value/nominal value.
[d] RE%=100 × ((found value – nominal value)/nominal value).

3.2 Fluorometric Detection of Coralyne

Even though the colorimetric probe we developed was one of the most sensitive detection platforms reported so far for COR with LOD of 8.54 nM, we decided to explore the possibility of developing a more sensitive fluorometric probe. The developed probe was based on the response of AgNPs with dT_{32} modification to COR in the presence of Coumarin (COU).

Here, the response of dT_{32}-AgNPs to COR in the presence of COU was monitored by fluorescence spectroscopy. AgNPs and dT_{32}-AgNPs are not fluorescent and do not display any fluorescence peak upon excitation at 420 nm (Figure 20, spectra a and b, respectively). On the other hand, COU that is used as the sensing element in our probe, is a natural compound and high quantum yields even at low concentrations (3.0 μM, Figure 21, a). After addition of COU to dT_{32}-AgNPs, an intense fluorescence peak with maximum intensity at 500 nm was observed upon excitation at 420 nm (Figure 20, spectrum c). However, the addition of COR (final concentration of 100 nM) resulted in a decrease in the intensity (Figure 20, d). The fluorescence change was also observable with the naked eye under UV-light with a wavelength of 365 nm after the addition of COR into dT_{32}-AgNPs + COU solution (Figure 21, vial c and d). The probe was developed based on these observed fluorescence changes.

Different dT_{32}-AgNPs + COU + COR probe systems were prepared by adding several concentrations of COU (1.0–5.0 μM) and dT_{32} (0.3-5.0 μM) for optimization of the system and to evaluate the dependence and response of the probe. 3.0 μM COU and 1.5 μM dT_{32} were found to be the optimum concentrations.

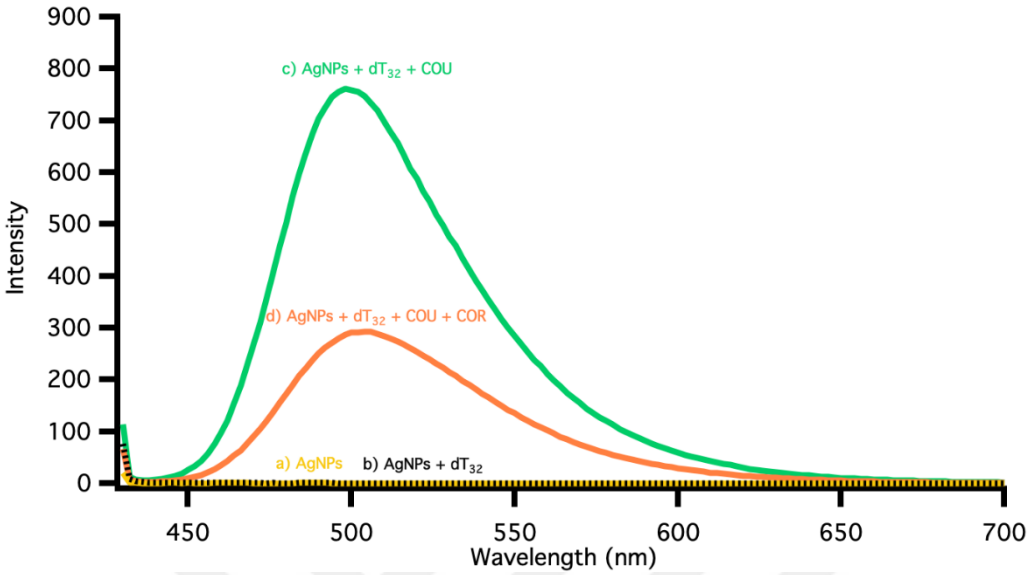

Figure 20. Fluorescence spectra of a) AgNPs, b) AgNPs + 1.5 µM dT_{32}, c) AgNPs + 1.5 µM dT_{32} + 3.0 µM COU and d) AgNPs + 1.5 µM dT_{32} + 3.0 µM COU + 100 nM COR.

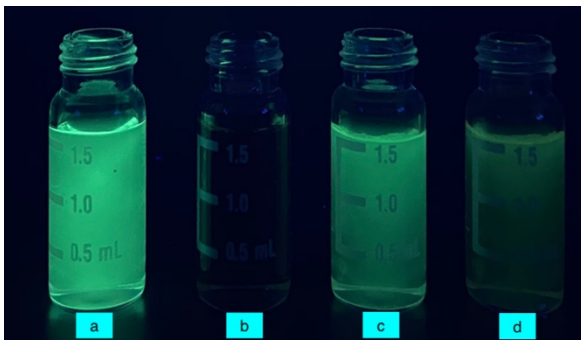

Figure 21. Photographs of a) 3.0 µM COU, b) AgNPs + 1.5 µM dT_{32}, c) AgNPs + 1.5 µM dT_{32} + 3.0 µM COU and d) AgNPs + 1.5 µM dT_{32} + 3.0 µM COU + 100 nM COR.

3.2.1 Fluorescence Spectroscopy Experiments

3.2.1.1 Temperature Effect

The influence of temperature on the response of the probe was investigated by changing the temperature of dT_{32}-AgNPs + COU + COR between 10 and 55°C. The change in fluorescence intensity at 500 nm was monitored at each temperature. Experiments were repeated three times and the average graph of F_0-F vs. temperature was plotted in Figure 22. Plots of F_0-F vs. temperature for each replicate are listed in Appendix C (Figure 82-84). Here, F_0 is the intensity of dT_{32}-AgNPs in the presence of 3.0 µM COU and F is the intensity after the addition of COR to dT_{32}-AgNPs + COU. As displayed in Figure 22, the temperature change did not significantly affect the response of the probe towards COR; thus, all the experiments were conducted at room temperature.

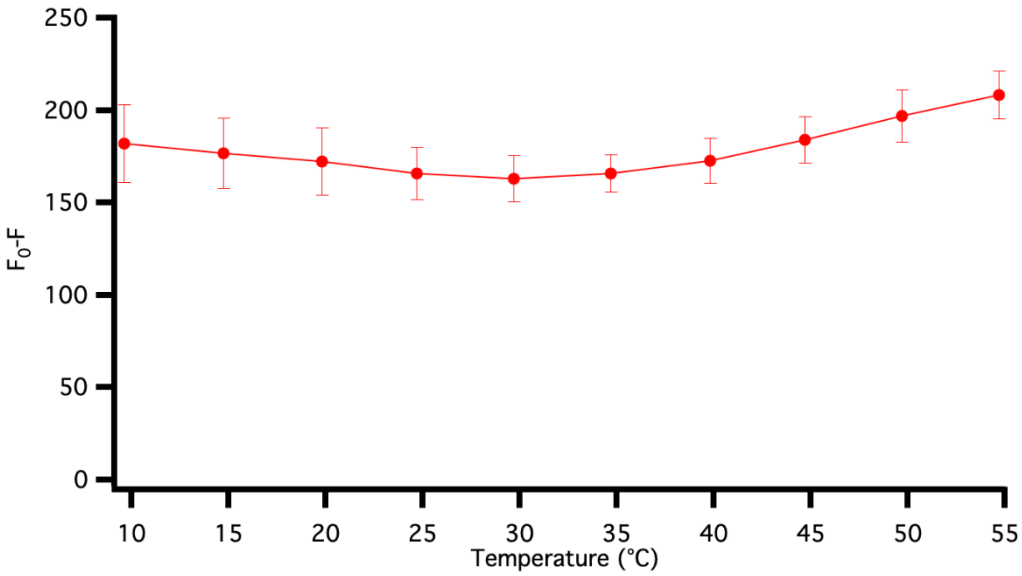

Figure 22. Plot of F_0-F vs. temperature under the optimized conditions (1.5 µM dT_{32}, 3.0 µM COU and 100 nM COR).

3.2.1.2 Time Effect

Effect of time on the response of probe towards COR was investigated at optimized concentrations (1.5 µM, 3.0 µM COU and 100 nM COR). Fluorescence intensity at 500 nm was monitored after the addition of COR to dT_{32}-AgNPs + COU solution between 0 to 60 min. Experiments were repeated three times and, the average graph of F_0-F vs. time was plotted with error bars in Figure 23. Plots of F_0-F vs. time for each replicate are listed in Appendix C (Figure 85-87). The intensity changes at 500 nm remained steady after 5 minutes of addition. Therefore, 5 minutes was selected as the optimum response time for all the experiments.

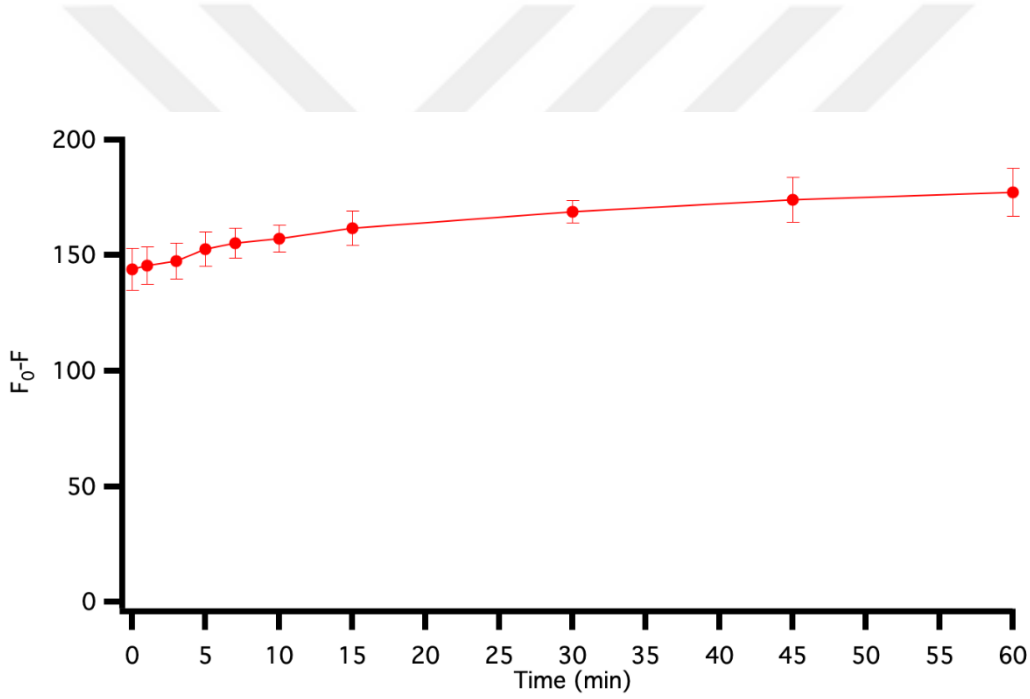

Figure 23. Plot of F_0-F vs. time under the optimized conditions (1.5 µM dT_{32}, 3.0 µM COU and 100 nM COR).

3.2.1.3 Oligonucleotide Effect

The effect of oligonucleotide length and structure on the sensing probe was investigated by replacing dT_{32} with dT_{16}, dA_{32}, duplex or triplex structures. Fluorescence spectra were taken after preparing AgNPs + COU + COR in the

presence of different oligonucleotides. Experiments were repeated three times and, average bar graph of F_0-F for different oligonucleotides with errors bars was plotted (Figure 24). Bar graphs of F_0-F for different oligonucleotides of each replicate are listed in Appendix C (Figure 88-90).

COU peak with maximum intensity at 500 nm was not affected from the presence of dA_{32}, double or triple stranded oligonucleotides. However, dT_{16} probe showed a similar response to the dT_{32} probe upon addition of COR. That is probably due to the lower binding affinity of dT_{32} to the surface of metallic nanoparticles than the adenine rich sequences [52].

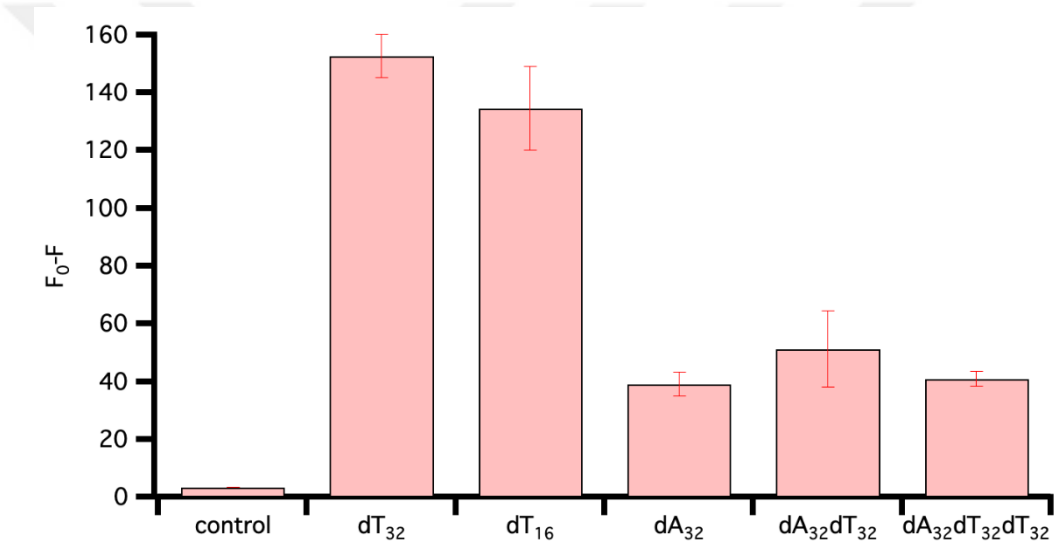

Figure 24. Bar graph of F_0-F for different oligonucleotides under optimized conditions (1.5 µM oligonucleotide, 3.0 µM COU and 100 nM COR).

3.2.2 Characterization of dT_{32}-modified Probe

To provide a possible mechanism and get detailed information about the morphology of AgNPs before and after the modification with dT_{32}, after the addition of COU and after the addition COR, HRTEM micrographs were taken. AgNPs and dT_{32}-AgNPs (Figure 25, A-C and D-F, respectively) images showed that AgNPs were spherical, monodisperse and had an average of 10 nm particle size. There was no significant

morphology change on the AgNPs after the modification with dT_{32}. Subsequently, neither the addition of COU, nor the addition of COR affected the size and morphology of dT_{32}-AgNPs (Figure 25, G-I and J-L, respectively). HRTEM micrographs provided that the mechanism of probe was not based on the aggregation of AgNPs.

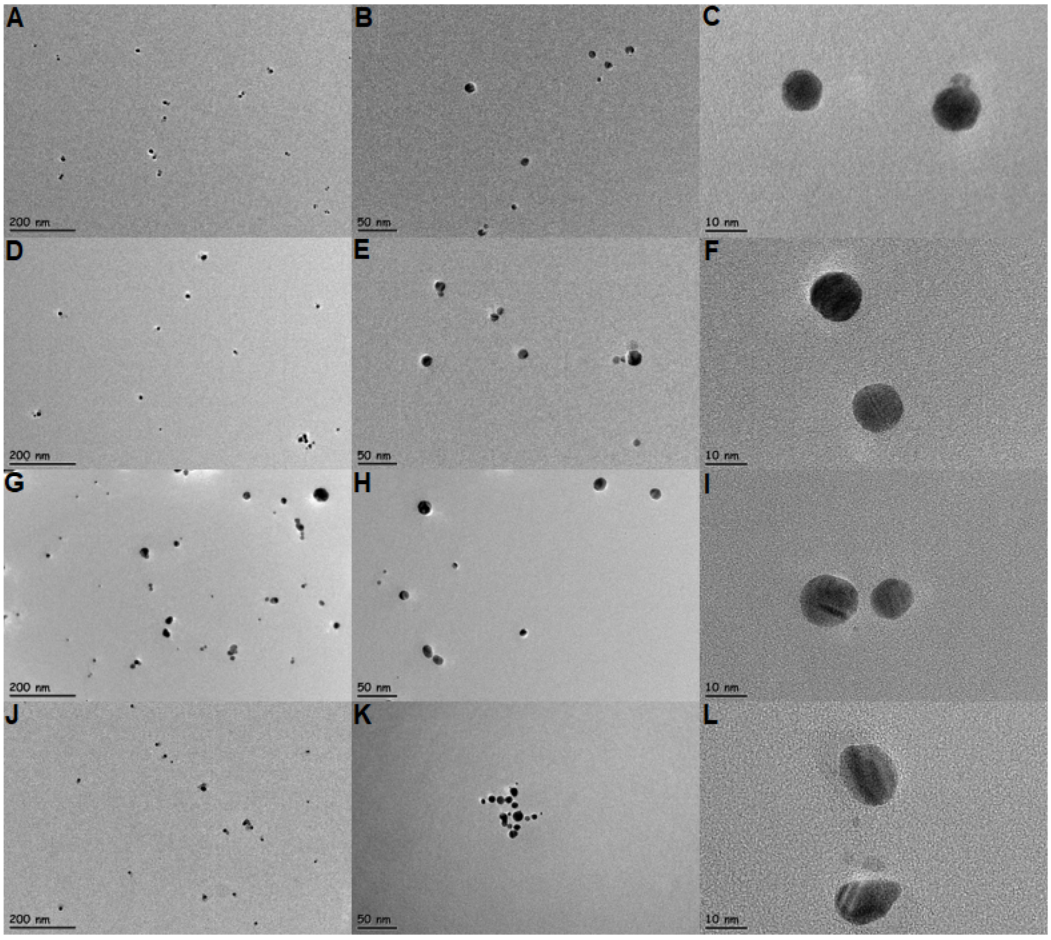

Figure 25. TEM images of (A-C) AgNPs, (D-F) dT_{32}-AgNPs, (G-I) dT_{32}-AgNPs + COU and (J-L) dT_{32}-AgNPs + COU + COR at different scales.

DLS and Zeta potential experiments were performed for further characterization. DLS and Zeta potential experiments showed that the nanoparticles size and charge did not change significantly with dT_{32} modification with and after the addition of COU and COR. Before the modification, particle size and charge of AgNPs were

5.55 ± 3.36 nm and -45.6 ± 3.35 mV, respectively (Figure 26, A, B). dT_{32} modification did not affect the size and charge of the AgNPs and the size and charge of the dT_{32}-AgNPs were 7.62 ± 2.64 nm and -38.9 ± 2.24 mV, respectively (Figure 26, C, D). Addition of COU and COR showed similar particle size and charge (Figure 26, E, F and G, H, respectively). Agreeing with HRTEM images, DLS and Zeta potential experiments provided insights towards a mechanism that is not based on the aggregation of AgNPs.

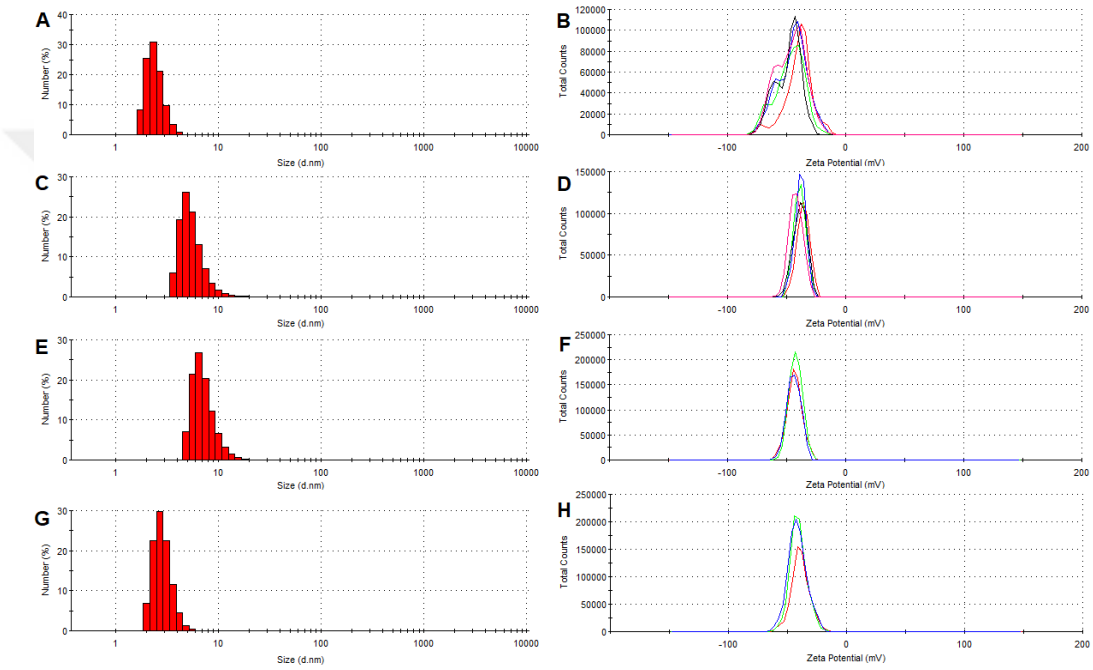

Figure 26. Particle size and zeta potential (mV) distributions of AgNPs (A and B), dT_{32}-AgNPs (C and D), dT_{32}-AgNPs + COU (E and F) and dT_{32}-AgNPs + COU + COR (G and F), respectively.

3.2.3 Mechanism

Possible explanation for the sensing mechanism of the probe was proposed below in the light of all the experiments and literature review (Figure 27). COU is a florescent molecule with an emission maximum of 500 nm. Its fluorescence is quenched in the presence of AgNPs due to the fluorescence resonance energy transfer (FRET). Thymine deoxynucleosides have an affinity towards AgNPs at physiological pH

conditions [53]. Adsorption of dT_{32} sequence on the surface of AgNPs hinders the FRET mechanism between COU and AgNPs (FRET OFF) and the fluorescence intensity decreases. However, the addition of COR alters the interactions ofdT_{32} sequences with AgNPs due to non-specific interactions. The altered interactions between dT_{32} and AgNPs led AgNPs to be less DNA-protected, allowing the FRET transfer between COU and AgNPs, resulting in the observation of the quenching mechanism (FRET ON). The addition of COR affects the intensity of the fluorescence peak and a linear decrease in the intensity was observed with increasing COR concentration.

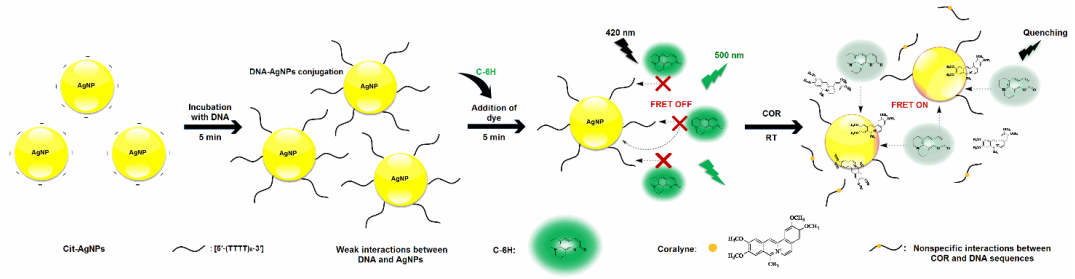

Figure 27. Schematic representation of proposed mechanism.

3.2.4 The Sensitivity of the dT_{32}-modified Probe

Sensitivity of the probe towards COR was investigated via titration experiments. AgNPs + 1.5 µM dT_{32} + 3.0 µM COU was titrated with 5.0 µM COR solution (0 to 150.0 µL). Upon each addition, the change in the fluorescence intensity was monitored by using fluorescence spectroscopy (Figure 28). The intensity of the peak between 450 nm and 600 nm was decreased gradually upon addition of COR.

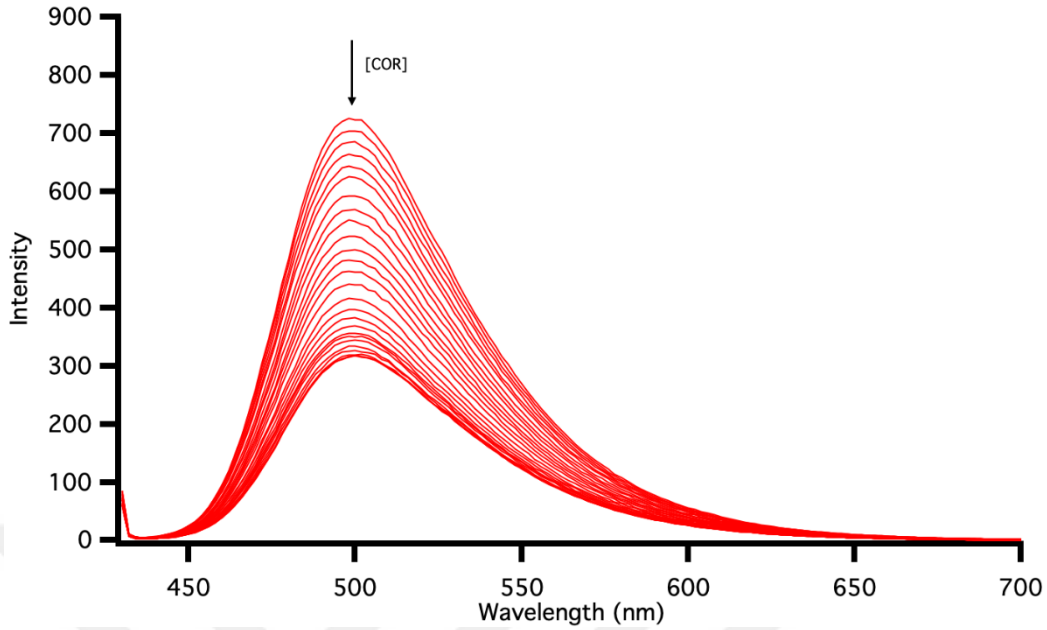

Figure 28. Fluorescence spectra obtained through the titration of 5.0 µM COR into the dT_{32}-AgNPs in the presence of 3.0 µM COU.

Calibration curve was plotted as intensity change (F_0-F) vs. COR concentration (Figure 29). Experiments were repeated three times and, the average values were used in the calculation of the linearity parameters (Table 4). Fluorescence spectra and the calibration curve of each replicate are listed in Appendix C (Figure 91-96).

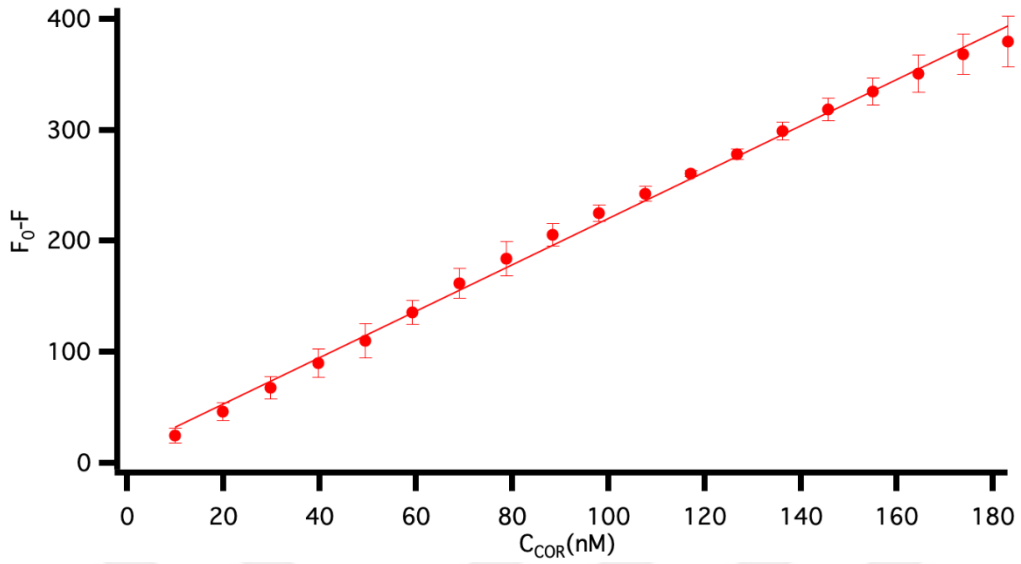

Figure 29. Calibration curve obtained via the titration of 5.0 µM COR into the dT_{32}-AgNPs in the presence of 3.0 µM COU.

Table 4. Analytical merits of the fluorometric detection method for COR

Calibration curve equation	R[a]	LOD [b]	LDR [c]
F_0-F = 2.0903C−11.286[d]	0.9982	5.24 nM	10-184 nM

a. Correlation coefficient.
b. Limit of detection (nM); (LOD was calculated from the concentration at which the intensity change is 3 times of standard deviation of the blank).
c. Liner dynamic range (nM).
d. F_0-F (F_0-F is the fluorescence intensity difference between dT_{32}-AgNPs + COU and dT_{32}-AgNPs + COU + COR, respectively); C is the concentration of COR (nM) and intensity change (y) represents the intercept of the slope.

3.2.5 The Selectivity of the dT_{32}-modified Probe

Selectivity of probe towards COR was investigated by testing it in the presence of several other ligands (DOX, OXP, ELP, NET, HOE, EtBr, Aza3, Aza4 and Aza5) that have similar structures to COR. 100 nM of each small molecule was added to dT_{32}-AgNPs + 3.0 µM COU and the fluorescence response of the system was monitored. Experiments were performed in triplicates and, the average bar graph of

F_0-F for different ligands was plotted in Figure 30. Bar graphs of F_0-F for different ligands of each replicate are listed in Appendix C (Figure 97-99).

Besides the COR addition, there wasn't a significant change on the intensity difference upon addition of the other ligands suggesting that the system is selective to COR.

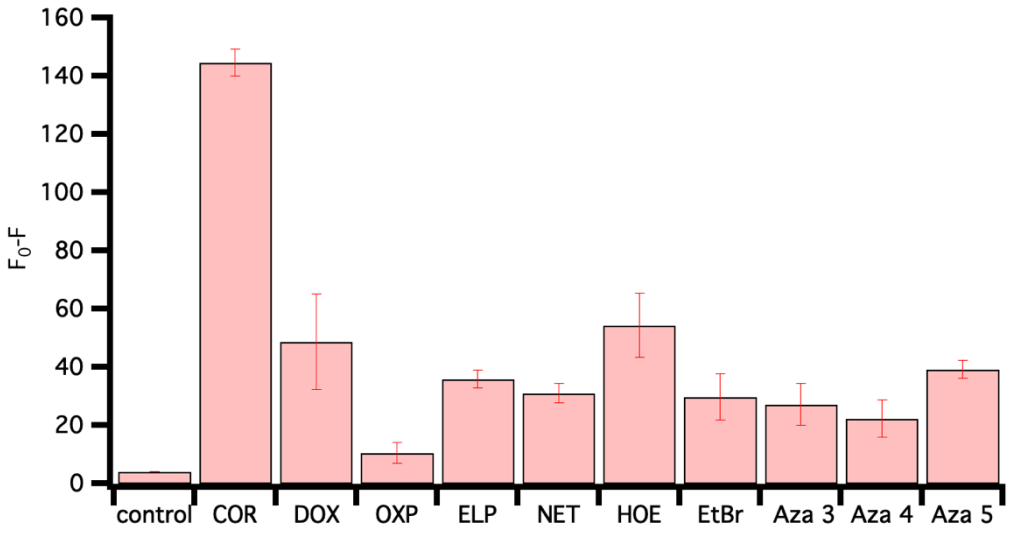

Figure 30. Bar graph of F_0-F for different ligands and COR under the optimized conditions (1.5 µM dT_{32}, 3.0 µM COU and 100 nM ligand).

3.2.6 Application of the Method

The applicability and feasibility of the probe in real samples was evaluated by using COR spiked three different human urine samples. The Fluorescence spectra of samples are listed in Appendix C (Figure 100-108) and the overall results are listed in Table 5. The obtained recoveries of COR were in the range of 87.28-104.52%. The calculated values were within the acceptable range that is recommended by FDA [51], showing that the probe had reasonable precision and accuracy.

Table 5. Analytical results for the determination of COR in real samples using the dT_{32}-modified fluorescence probe.

Sample source	Spiked concentration (nM; n = 3[a])	Mean found concentration (nM)	RSD (%)[b]	Recovery (%)[c]	Accuracy (RE %)[d]
Sample 1	50	45.86	10.48	91.71	-8.29
	98	93.70	5.82	95.62	-4.38
	183	170.34	3.08	93.08	-6.92
Sample 2	50	43.64	3.51	87.28	-12.72
	98	94.09	8.86	96.01	-3.99
	183	171.85	3.12	93.91	-6.09
Sample 3	50	51.84	12.81	103.68	3.68
	98	102.43	13.05	104.52	4.52
	183	169.26	3.59	92.49	-7.51

[a] Number of replicates.
[b] RSD: Relative standard deviation.
[c] Recovery (%) = 100 × found value/nominal value.
[d] RE%=100 × ((found value – nominal value)/nominal value).

CHAPTER 4

CONCLUSION

Here, we developed two different probes for the detection of COR by using AgNPs. Firstly, unmodified AgNPs was used for the detection of COR as a colorimetric detection method. LSPR band of the AgNPs in the presence of NaCl changed with the addition of COR due to aggregation of AgNPs. As COR concentration increased, aggregation rate of AgNPs was increasing. The effect of electrolytes on the rate of aggregation of AgNPs was investigated and the optimal concentration of NaCl was found to be as 500 μM. The effect of time, temperature and pH was investigated by variation experiments and optimal conditions were found as 5 minutes, room temperature and neutral pH, respectively. AgNPs before and after the addition of COR were characterized by HRTEM, FTIR, DLS and Zeta potential experiments and the results of all characterization experiments supported the aggregation of AgNPs upon addition of COR. Accordingly, a possible mechanism based on the aggregation behavior of AgNPs was proposed. The analytical merits, LOD and LDR, of the probe were determined to be 8.54 nM and 26-404 nM, respectively. The selectivity of the probe towards COR was also investigated among several other ligands that are similar to COR and common organic/inorganic substances. Selectivity results showed that the proposed probe was highly selective to COR even in the presence of higher concentrations of different ligands. The applicability and feasibility of the probe in real samples were evaluated by using COR spiked human urine and tap water samples. Real sample results proved that the probe was reliable with reasonable precision and accuracy.

Secondly, dT_{32} modified AgNPs were used for the detection of COR as a fluorometric detection method. The intensity of the fluorescence peak centered around 500 nm was decreased after the addition of COR to dT_{32}-AgNPs + COU sample. The effect of time and temperature was investigated by variation

experiments and optimal conditions were found to be as 5 minutes and room temperature, respectively. dT_{32}-AgNPs before and after the addition of COR were characterized by HRTEM, DLS and Zeta potential experiments and a possible mechanism based on the switching of FRET phenomena was proposed. The LOD and LDR were calculated as 5.24 nm and 10-184 nM, respectively. Selectivity of the probe towards COR was established via testing several ligands that are similar to COR. Results showed that the proposed probe is selective to single stranded dT sequences. The applicability and feasibility of the probe in real samples were evaluated by using COR spiked urine samples. Real sample results proved that the probe had reasonable precision and accuracy.

So far, optical detection of COR based on silver nanostructures were very few [32], [53], [54]. Most of these techniques require long analysis time and costly pre-modification that shows there is still a need for a simple and cost-effective detection platform for COR. In this thesis, two different optical probes that are convenient, selective and sensitive have been developed. Colorimetric probe does not require post-modifications that makes it cost effective than the fluorometric probe that requires dT_{32} modification. In addition, monitoring the color change by eye can be the easiest way of qualitative COR screening. However, the results confirmed that the fluorometric platform exhibited more sensitive results in terms of LOD that is 5.24 nM. In other words, the fluorometric probe is nearly 2-fold more sensitive to COR than the colorimetric probe. Overall, the lower limit of detection (LOD) with high sensitivity and satisfactory selectivity among a wide range of organic and inorganic compounds under the optimal conditions were obtained for both probes. LDR of unmodified AgNPs probe was found as 26-404 nM while that of dT_{32} modified AgNPs was 10-184 nM. Both probes have quick response times (5 min both), give optimal results at room temperature, does not require prelab work and are easy to use. These probes can provide reliable and rapid quantification of COR in various matrices.

REFERENCES

[1] D. Nunes *et al.*, *Metal Oxide Nanostructures: Synthesis, Properties and Applications*. Elsevier B.V., 2019.

[2] R. P. Feynman, "There's plenty of room at the bottom," *J. Microelectromechanical Syst.*, vol. 1, no. 1, pp. 60–65, 1992, doi: 10.1109/84.128057.

[3] R. M. Bakker *et al.*, "On the basic concept of nanotechnology," in *Proceedings of the International Conference on Production Engineering*, 1974, pp. 5–10.

[4] M. M. Khin, A. S. Nair, V. J. Babu, R. Murugan, and S. Ramakrishna, "A review on nanomaterials for environmental remediation," *Energy Environ. Sci.*, vol. 5, no. 8, pp. 8075–8109, 2012, doi: 10.1039/c2ee21818f.

[5] J. Jeevanandam, A. Barhoum, Y. S. Chan, A. Dufresne, and M. K. Danquah, "Review on nanoparticles and nanostructured materials: History, sources, toxicity and regulations," *Beilstein J. Nanotechnol.*, vol. 9, no. 1, pp. 1050–1074, 2018, doi: 10.3762/bjnano.9.98.

[6] I. Khan, K. Saeed, and I. Khan, "Nanoparticles: Properties, applications and toxicities," *Arab. J. Chem.*, vol. 12, no. 7, pp. 908–931, 2019, doi: 10.1016/j.arabjc.2017.05.011.

[7] Y. Gogotsi, Ed., *Nanomaterials Handbook*, 2nd ed. CRC Press, 2017.

[8] A. M. Ealia and M. P. Saravanakumar, "A review on the classification, characterisation, synthesis of nanoparticles and their application," *IOP Conf. Ser. Mater. Sci. Eng.*, vol. 263, no. 3, 2017, doi: 10.1088/1757-899X/263/3/032019.

[9] H. Kumar K, N. Venkatesh, H. Bhowmik, and A. Kuila, "Metallic nanoparticle: A review," *Biomed. J. Sci. Tech. Res.*, vol. 4, no. 2, pp. 3765–3775, 2018, doi: 10.26717/bjstr.2018.04.001011.

[10] K. N. Thakkar, S. S. Mhatre, and R. Y. Parikh, “Biological synthesis of metallic nanoparticles,” *Nanomedicine Nanotechnology, Biol. Med.*, vol. 6, no. 2, pp. 257–262, 2010, doi: 10.1016/j.nano.2009.07.002.

[11] M. Bonazzi, *Communicating Nanotechnology: Why, to Whom, Saying What and How? -An Action-packed Roadmap Towards a Brand New Dialogue*. 2010.

[12] “What’s So Special About the Nanoscale?” [Online]. Available: https://www.nano.gov/nanotech-101/special.

[13] G. M. Nazeruddin, S. R. Prasad, Y. I. Shaikh, and N. R. Prasad, “A brief review: Science at nanoscale,” *Int. J. Nanomater. Nanostructures*, vol. 1, no. 1, pp. 16–32, 2015.

[14] K. A. Willets and R. P. Van Duyne, “Localized surface plasmon resonance spectroscopy and sensing,” *Annu. Rev. Phys. Chem.*, vol. 58, no. 1, pp. 267–297, 2007, doi: 10.1146/annurev.physchem.58.032806.104607.

[15] E. Petryayeva and U. J. Krull, “Localized surface plasmon resonance: Nanostructures, bioassays and biosensing-A review,” *Anal. Chim. Acta*, vol. 706, no. 1, pp. 8–24, 2011, doi: 10.1016/j.aca.2011.08.020.

[16] L. Wei, J. Lu, H. Xu, A. Patel, Z.-S. Chen, and G. Chen, “Silver nanoparticles: Synthesis, properties, and therapeutic applications,” *Drug Discov. Today*, vol. 20, no. 5, pp. 595–601, 2015, doi: 10.1016/j.drudis.2014.11.014.

[17] Q. H. Tran, V. Q. Nguyen, and A. Le, “Silver Nanoparticles : Synthesis, properties, toxicology, applications and perspectives,” *Adv. Nat. Sci. Nanosci. Nanotechnol.*, vol. 4, pp. 1–20, 2013, doi: 10.1088/2043-6262/4/3/033001.

[18] B. Sepúlveda, P. C. Angelomé, L. M. Lechuga, and L. M. Liz-Marzán, “LSPR-based nanobiosensors,” *Nano Today*, vol. 4, no. 3, pp. 244–251, 2009, doi: 10.1016/j.nantod.2009.04.001.

[19] K. Y. Kim, Ed., *Plasmonics: Principles and Applications*. InTechOpen, 2012.

[20] L. Guerrini, R. A. Alvarez-Puebla, and N. Pazos-Perez, "Surface modifications of nanoparticles for stability in biological fluids," *Materials (Basel).*, vol. 11, no. 7, pp. 1–28, 2018, doi: 10.3390/ma11071154.

[21] B. Reddy, Ed., *Advances in Nanocomposites: Synthesis, Characterization and Industrial Applications*. InTechOpen, 2001.

[22] H. An and B. Jin, "Prospects of nanoparticle-DNA binding and its implications in medical biotechnology," *Biotechnol. Adv.*, vol. 30, no. 6, pp. 1721–1732, 2012, doi: 10.1016/j.biotechadv.2012.03.007.

[23] S. R. Mudshinge, A. B. Deore, S. Patil, and C. M. Bhalgat, "Nanoparticles: Emerging carriers for drug delivery," *Saudi Pharm. J.*, vol. 19, no. 3, pp. 129–141, 2011, doi: 10.1016/j.jsps.2011.04.001.

[24] G. A. Evtugyn, R. V. Shamagsumova, and T. Hianik, "Biosensors for detection mycotoxins and pathogenic bacteria in food," *Nanobiosensors*, pp. 35–92, 2017, doi: 10.1016/B978-0-12-804301-1/00002-3.

[25] Y. Dahman, A. Radwan, B. Nesic, and J. Isbister, "Nanosensors," in *Nanotechnology and Functional Materials for Engineers*, 2017, pp. 67–91.

[26] Y. Jeong, Y. M. Kook, K. Lee, and W. G. Koh, "Metal enhanced fluorescence (MEF) for biosensors: General approaches and a review of recent developments," *Biosens. Bioelectron.*, vol. 111, pp. 102–116, 2018, doi: 10.1016/j.bios.2018.04.007.

[27] Y. Jung, J. Jung, Y. Huh, and D. Kim, "Benzo[g]coumarin-based fluorescent probes for bioimaging applications," *J. Anal. Methods Chem.*, 2018, doi: 10.1155/2018/5249765.

[28] W. Sun, J. Li, W. Li, L. Su, L. Du, and M. Li, "Design of OFF/ON fluorescent thiol probes based on coumarin fluorophore," *Sci. China Chem.*, vol. 55, pp. 1776–1780, 2012, doi: 10.1007/s11426-012-4601-2.

[29] M. X. Wang, X. M. Meng, M. Z. Zhu, and Q. X. Guo, "Novel fluorescent

chemosensor for Ag^+ based on coumarin fluorophore," *Chinese Chem. Lett.*, vol. 19, no. 8, pp. 977–980, 2008, doi: 10.1016/j.cclet.2008.05.010.

[30] M. Vedamalai and T. R. Kumar, "Coumarin-derivatives for detection of biological important species," *Int. J. Pure Appl. Math.*, vol. 119, no. 12, pp. 7123–7132, 2018.

[31] H. Sun, H. Fan, and X. Peng, "Quantitative DNA interstrand cross-link formation by coumarin and thymine: Structure determination, sequence effect, and fluorescence detection," *J. Org. Chem.*, vol. 79, no. 23, pp. 11359–11369, 2014, doi: 10.1021/jo5014756.

[32] C. Y. Lee, S. W. Lin, Y. H. Wu, and Y. Z. Hsieh, "Combining DNA-stabilized silver nanocluster synthesis with exonuclease III amplification allows label-free detection of coralyne," *Anal. Chim. Acta*, vol. 1042, pp. 86–92, 2018, doi: 10.1016/j.aca.2018.08.030.

[33] C. Jash and G. S. Kumar, "Binding of alkaloids berberine, palmatine and coralyne to lysozyme: A combined structural and thermodynamic study," *RSC Adv.*, vol. 4, pp. 12514–12525, 2014, doi: 10.1039/c3ra46053c.

[34] A. Y. Khan, M. Hossain, and G. Suresh Kumar, "Investigations on the Interaction of the phototoxic alkaloid coralyne with serum albumins," *Chemosphere*, vol. 87, no. 7, pp. 775–781, 2012, doi: 10.1016/j.chemosphere.2011.12.079.

[35] R. Bhattacharyya, B. Saha, M. Tyagi, S. K. Bandyopadhyay, B. S. Patro, and S. Chattopadhyay, "Differential modes of photosensitisation in cancer cells by berberine and coralyne," *Free Radic. Res.*, vol. 51, no. 7–8, pp. 723–738, 2017, doi: 10.1080/10715762.2017.1368506.

[36] R. Sinha and G. S. Kumar, "Interaction of isoquinoline alkaloids with an RNA triplex: Structural and thermodynamic studies of berberine, palmatine, and coralyne binding to Poly(U).Poly(A)*Poly(U)," *J. Phys. Chem. B*, vol. 113, no. 40, pp. 13410–13420, 2009, doi: 10.1021/jp9069515.

[37] M. M. Islam and G. Suresh Kumar, “RNA-binding potential of protoberberine alkaloids: spectroscopic and calorimetric studies on the binding of berberine, palmatine, and coralyne to protonated RNA structures,” *DNA Cell Biol.*, vol. 28, no. 12, pp. 637–650, 2009, doi: 10.1089/dna.2009.0930.

[38] K. Bhadra and G. S. Kumar, “Therapeutic potential of nucleic acid-binding isoquinoline alkaloids: Binding aspects and implications for drug design,” *Med. Res. Rev.*, vol. 31, no. 6, pp. 821–862, 2011, doi: 10.1002/med.20202.

[39] S. Hazra, M. Hossain, and G. Suresh Kumar, “Binding of isoquinoline alkaloids berberine, palmatine and coralyne to hemoglobin: Structural and thermodynamic characterization studies,” *Mol. Biosyst.*, vol. 9, no. 1, pp. 143–153, 2013, doi: 10.1039/c2mb25345c.

[40] K. S. Huang, M. J. Haddadin, M. M. Olmstead, and M. J. Kurth, “Synthesis and reactions of some heterocyclic azacyanines,” *J. Org. Chem.*, vol. 66, no. 4, pp. 1310–1315, 2001, doi: 10.1021/jo001484k.

[41] Ö. P. Çetinkol and N. V. Hud, “Molecular recognition of poly(A) by small ligands: An alternative method of analysis reveals nanomolar, cooperative and shape-selective binding,” *Nucleic Acids Res.*, vol. 37, no. 2, pp. 611–621, 2009, doi: 10.1093/nar/gkn977.

[42] K. Bhadra and G. S. Kumar, “Interaction of berberine, palmatine, coralyne, and sanguinarine to quadruplex DNA: A comparative spectroscopic and calorimetric study,” *Biochim. Biophys. Acta - Gen. Subj.*, vol. 1810, no. 4, pp. 485–496, 2011, doi: 10.1016/j.bbagen.2011.01.011.

[43] N. N. Degtyareva, B. D. Wallace, A. R. Bryant, K. M. Loo, and J. T. Petty, “Hydration changes accompanying the binding of minor groove ligands with DNA,” *Biophys. J.*, vol. 92, no. 3, pp. 959–965, 2007, doi: 10.1529/biophysj.106.097451.

[44] D. E. Graves and T. R. Krugh, “Single-cell partition analysis - A direct fluorescence technique for examiningligand-macromolecule interactions,”

Anal. Biochem., vol. 134, no. 1, pp. 73–81, 1983, doi: 10.1016/0003-2697(83)90265-8.

[45] H. Soori, A. Rabbani-Chadegani, and J. Davoodi, "Exploring binding affinity of oxaliplatin and carboplatin, to nucleoprotein structure of chromatin: Spectroscopic study and histone proteins as a target," *Eur. J. Med. Chem.*, vol. 89, pp. 844–850, 2015, doi: 10.1016/j.ejmech.2014.10.063.

[46] C. Bailly, P. Colson, J. P. Hénichart, and C. Houssier, "The different binding modes of hoechst 33258 to DNA studied by electric linear dichroism," *Nucleic Acids Res.*, vol. 21, no. 16, pp. 3705–3709, 1993, doi: 10.1093/nar/21.16.3705.

[47] C. Y. Flores *et al.*, "Spontaneous adsorption of silver nanoparticles on Ti/TiO_2 surfaces. Antibacterial effect on pseudomonas aeruginosa," *J. Colloid Interface Sci.*, vol. 350, no. 2, pp. 402–408, 2010, doi: 10.1016/j.jcis.2010.06.052.

[48] H. M. Usta, M. Forough, and Ö. Persil Çetinkol, "A DNA-free colorimetric probe based on citrate-capped silver nanoparticles for sensitive and rapid detection of coralyne," *Sensors Actuators, B Chem.*, vol. 298, 2019, doi: 10.1016/j.snb.2019.126823.

[49] J. C. Lees *et al.*, "Nanoparticle impacts show high-ionic-strength citrate avoids aggregation of silver nanoparticles," *ChemPhysChem*, vol. 14, no. 17, pp. 3895–3897, 2013, doi: 10.1002/cphc.201300796.

[50] A. Vallee, V. Humblot, and C. M. Pradier, "Peptide interactions with metal and oxide surfaces," *Acc. Chem. Res.*, vol. 43, no. 10, pp. 1297–1306, 2010, doi: 10.1021/ar100017n.

[51] H. Services, Ed., *Analytical Procedures and Methods Validation for Drugs and Biologics Guidance for Industry Analytical*. 2015.

[52] J. J. Storhoff, R. Elghanian, C. A. Mirkin, and R. L. Letsinger, "Sequence-

dependent stability of DNA-modified gold nanoparticles," *Langmuir*, vol. 18, no. 17, pp. 6666–6670, 2002, doi: 10.1021/la0202428.

[53] X. Xu, J. Wang, F. Yang, K. Jiao, and X. Yang, "Label-free colorimetric detection of small molecules utilizing DNA oligonucleotides and silver nanoparticles," *Small*, vol. 5, no. 23, pp. 2669–2672, 2009, doi: 10.1002/smll.200901164.

[54] K. S. Park and H. G. Park, "A DNA-templated silver nanocluster probe for label-free, turn-on fluorescence-based screening of homo-adenine binding molecules," *Biosens. Bioelectron.*, vol. 64, pp. 618–624, 2015, doi: 10.1016/j.bios.2014.10.003.

APPENDICES

A. Structures of Small Molecules

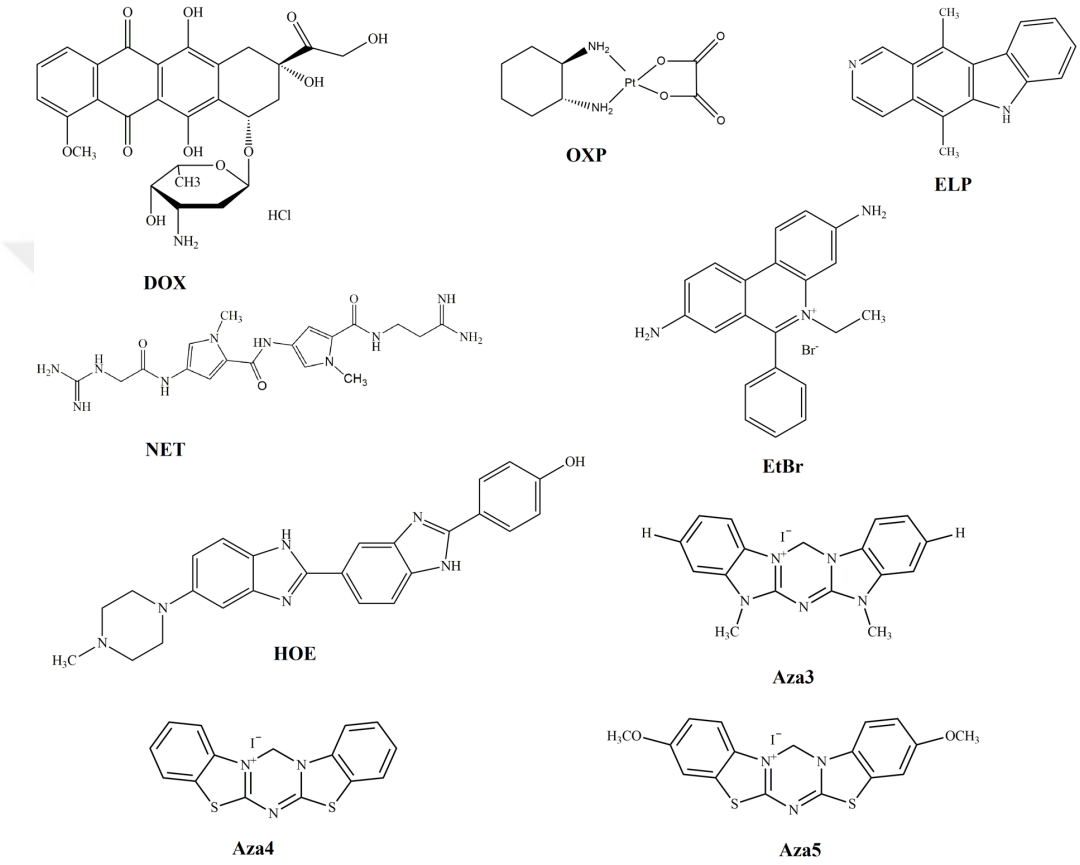

Figure 31. Structures of small molecules.

B. Colorimetric Detection of Coralyne

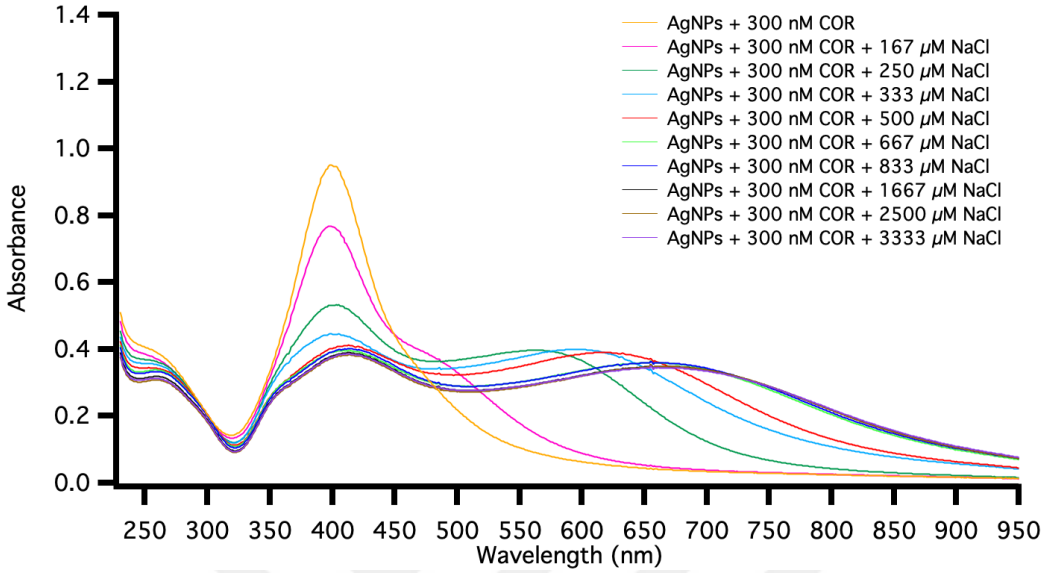

Figure 32. 1st replica - UV-Vis spectra of AgNPs with increasing NaCl concentrations in the presence of 300 nM COR.

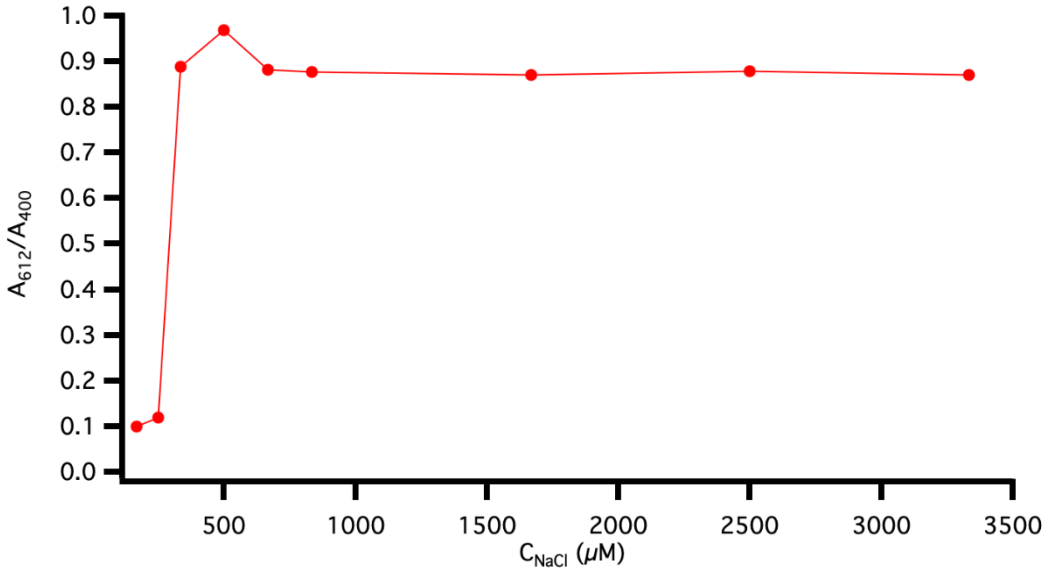

Figure 33. 1st replica - Plot of A_{612}/A_{400} vs. NaCl concentration in the presence of 300 nM COR.

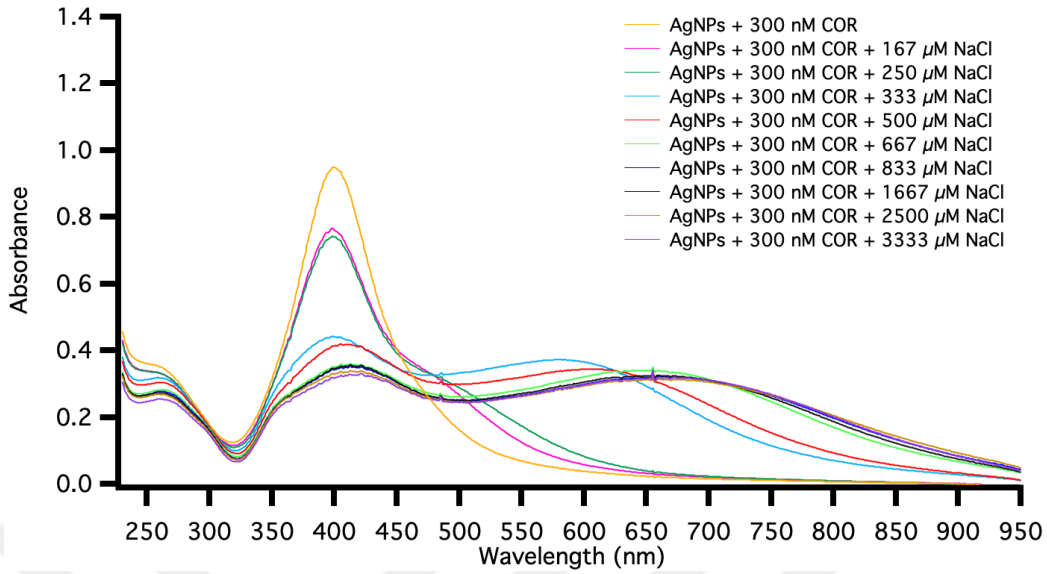

Figure 34. 2nd replica - UV-Vis spectra of AgNPs with increasing NaCl concentrations in the presence of 300 nM COR.

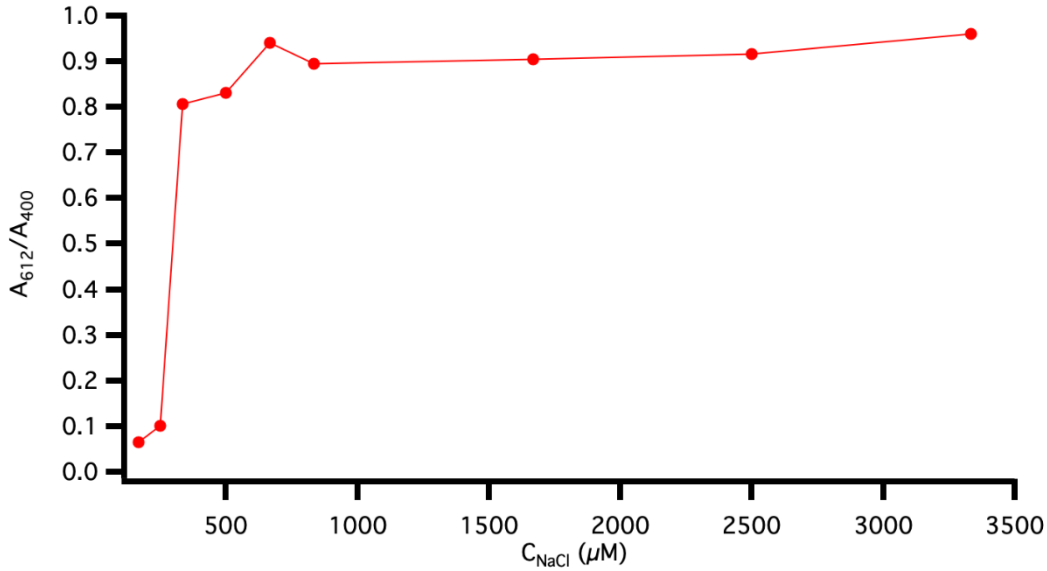

Figure 35. 2nd replica - Plot of A_{612}/A_{400} vs. NaCl concentration in the presence of 300 nM COR.

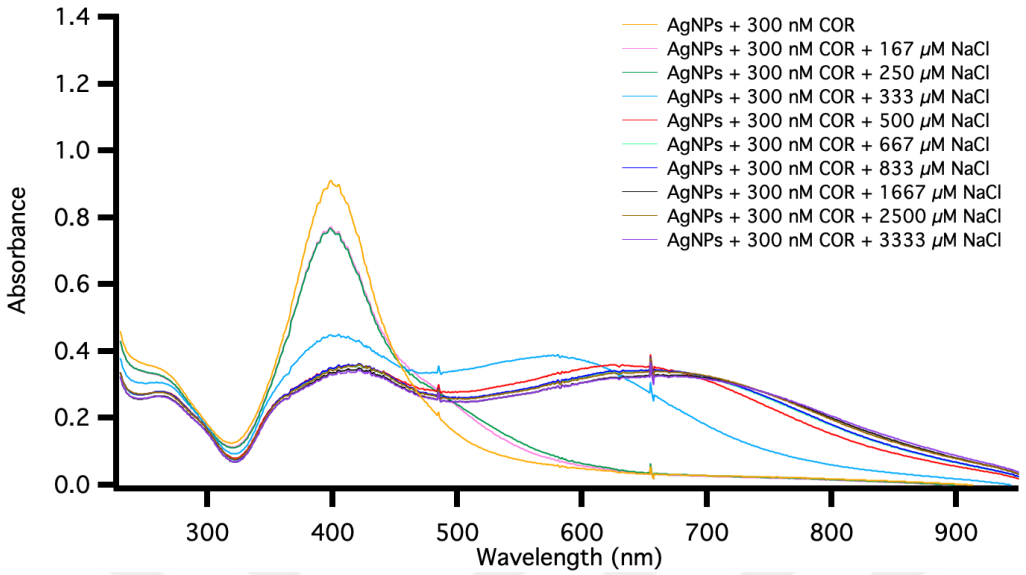

Figure 36. 3rd replica - UV-Vis spectra of AgNPs with increasing NaCl concentrations in the presence of 300 nM COR.

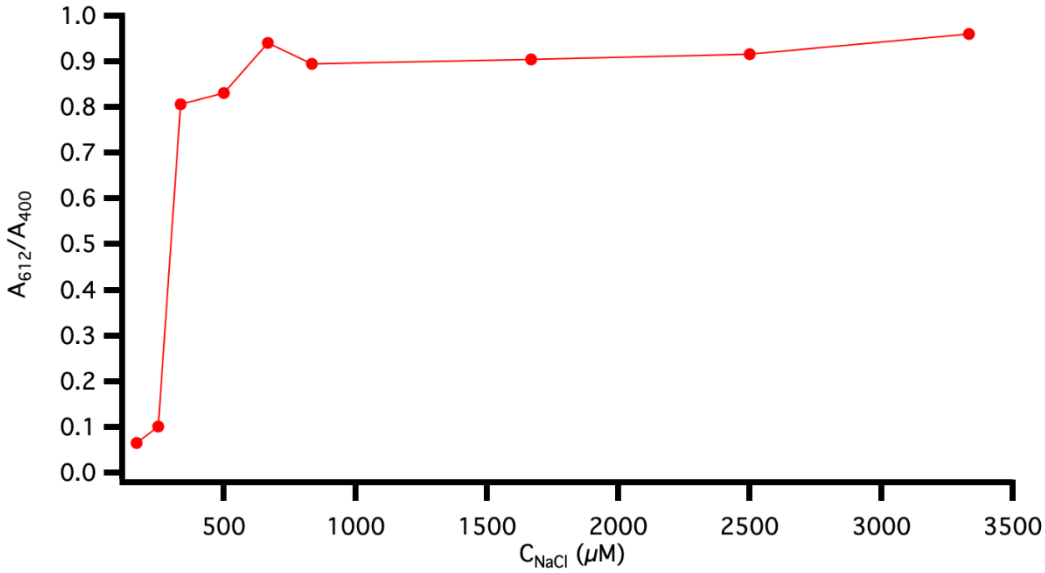

Figure 37. 3rd replica - Plot of A_{612}/A_{400} vs. NaCl concentration in the presence of 300 nM COR.

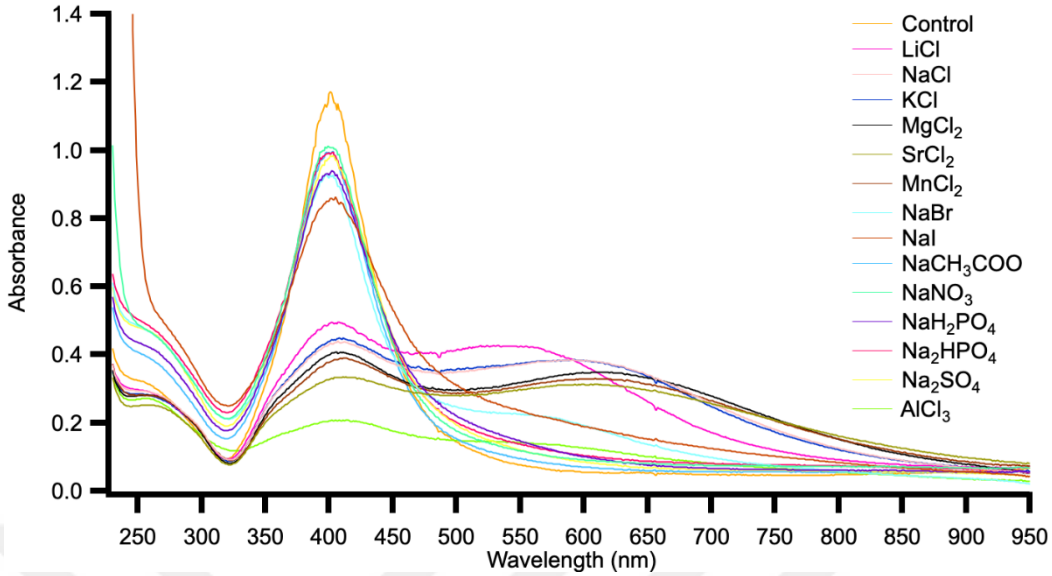

Figure 38. UV-Vis spectra of AgNPs + COR in the presence of different electrolytes under optimized concentrations (300 nM COR and 500 µM electrolyte).

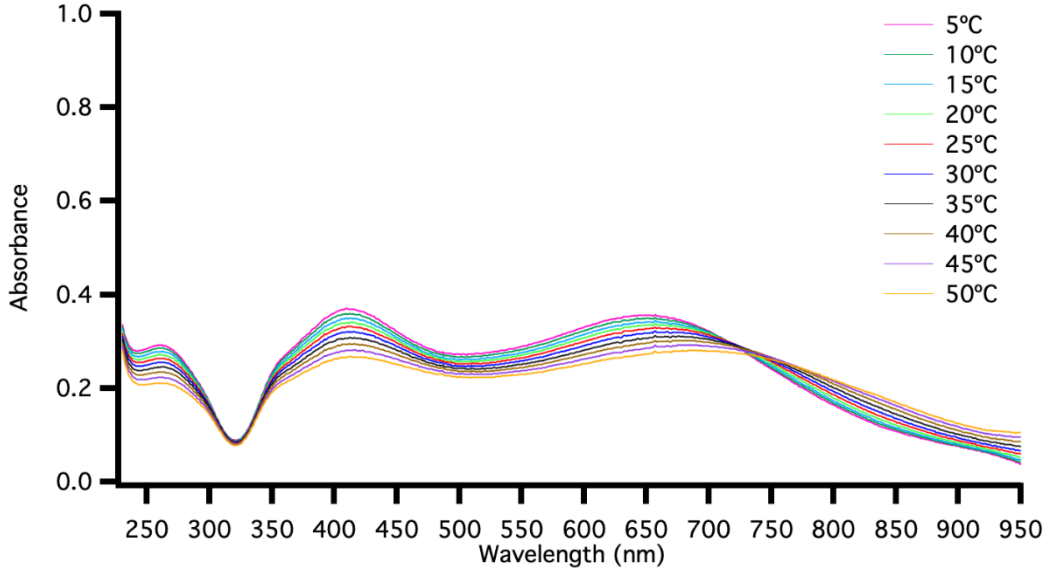

Figure 39. 1st replica - UV-Vis spectra of AgNPs + NaCl + COR acquired at different temperatures (300 nM COR and 500 µM NaCl).

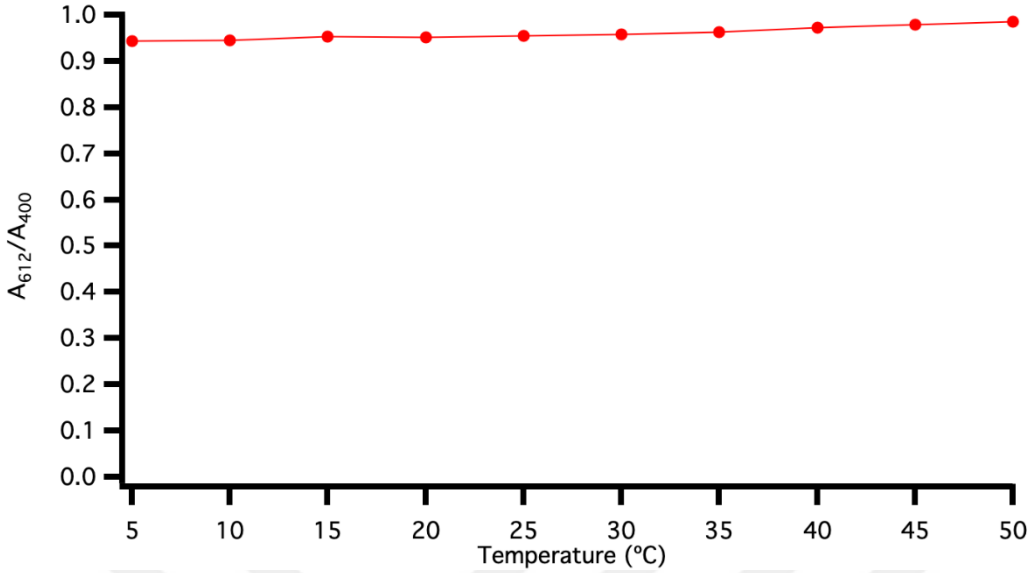

Figure 40. 1st replica - Plot of A_{612}/A_{400} vs. temperature (300 nM COR and 500 µM NaCl).

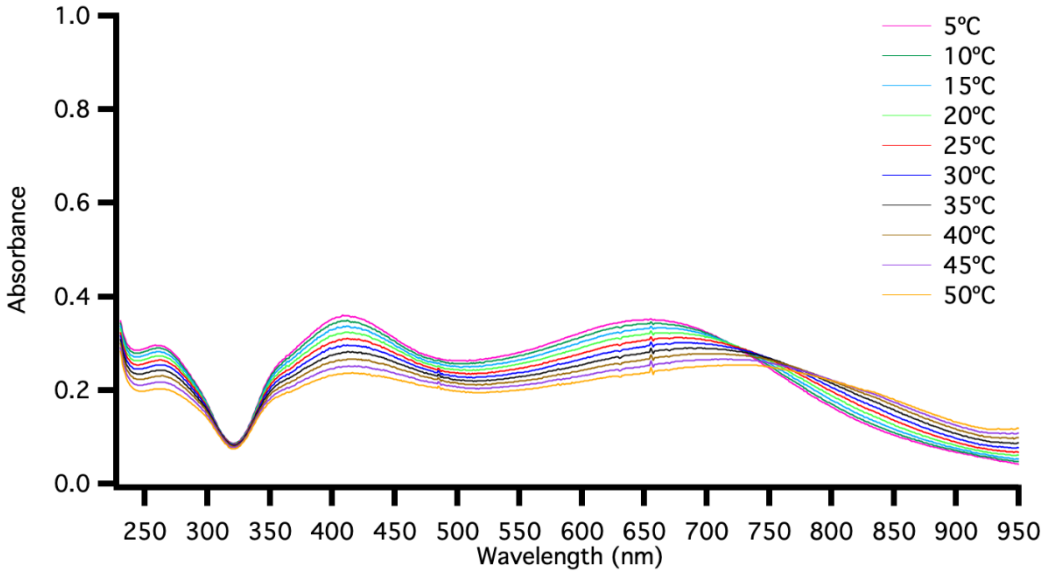

Figure 41. 2nd replica - UV-Vis spectra of AgNPs + NaCl + COR acquired at different temperatures (300 nM COR and 500 µM NaCl).

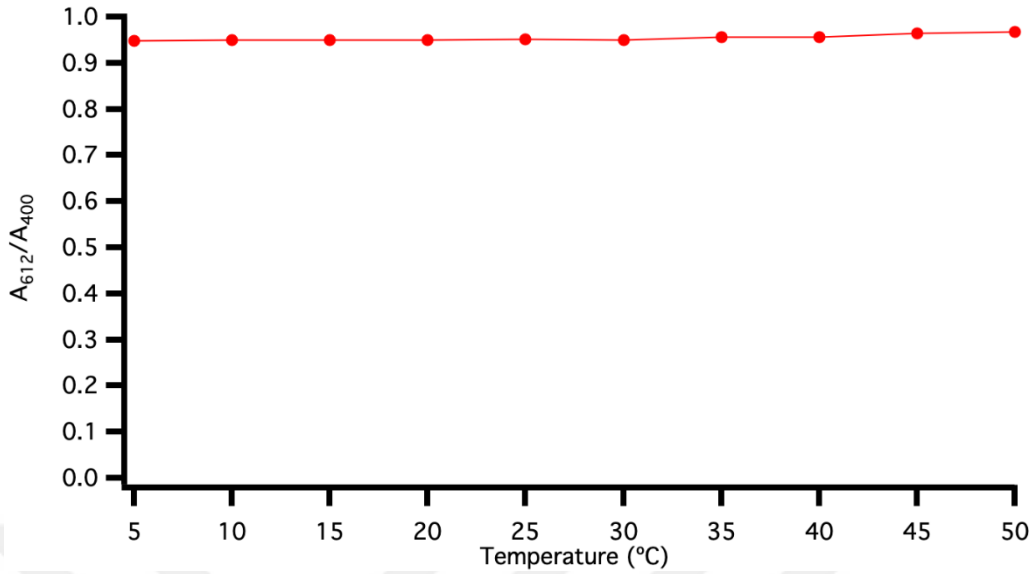

Figure 42. 2nd replica - Plot of A_{612}/A_{400} vs. temperature (300 nM COR and 500 µM NaCl.

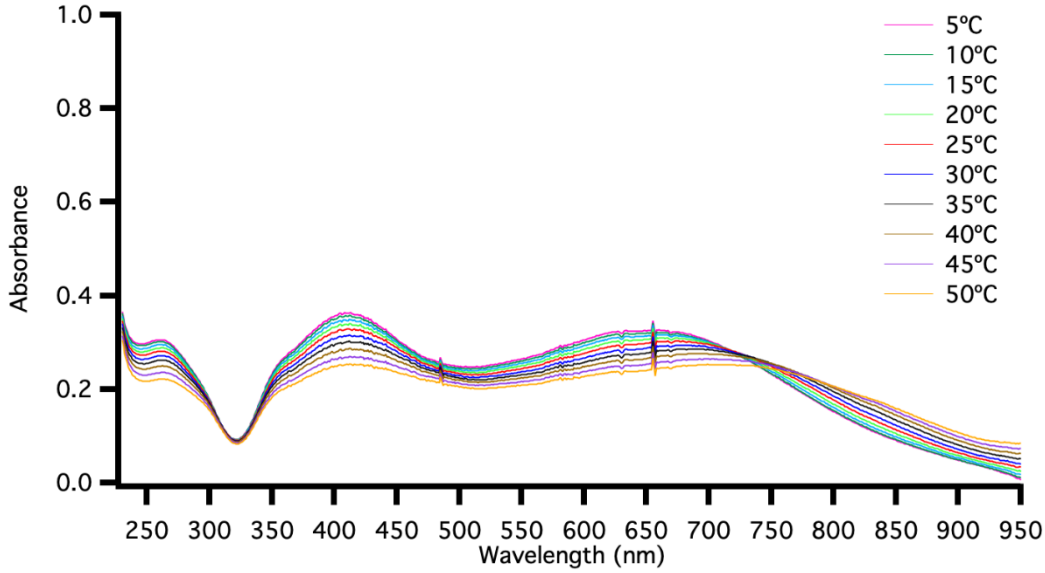

Figure 43. 3rd replica - UV-Vis spectra of AgNPs + NaCl + COR acquired at different temperatures (300 nM COR and 500 µM NaCl.

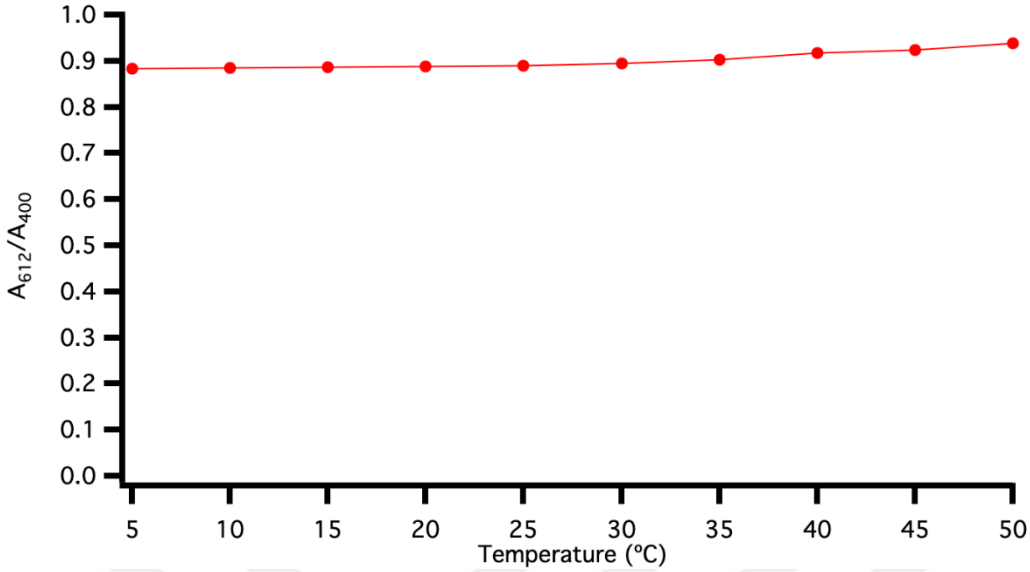

Figure 44. 3rd replica - Plot of A_{612}/A_{400} vs. temperature (300 nM COR and 500 µM NaCl).

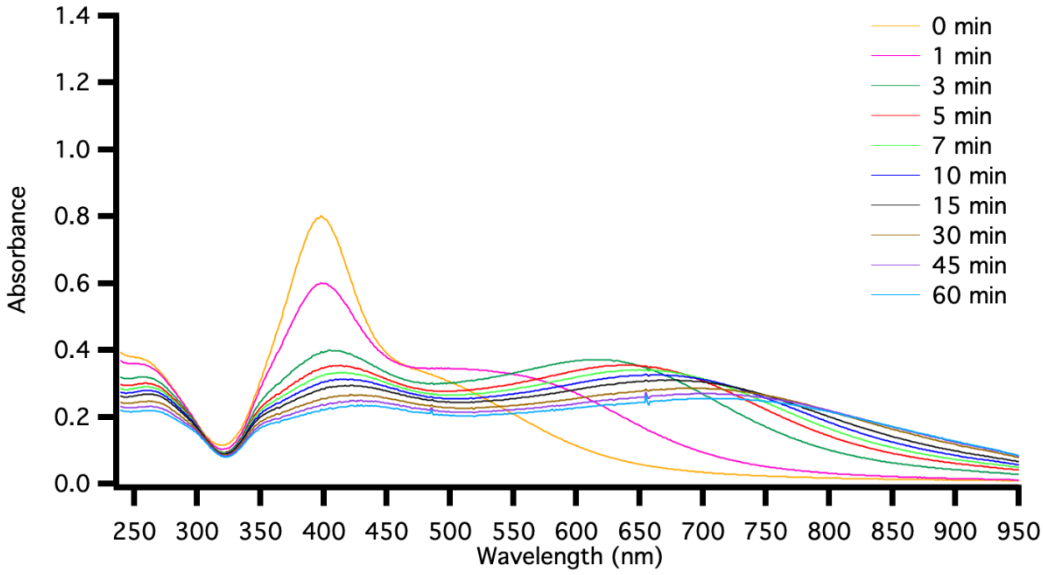

Figure 45. 1st replica - UV-Vis spectra of AgNPs + NaCl + COR acquired at different time points after the addition of COR (300 nM COR and 500 µM NaCl.

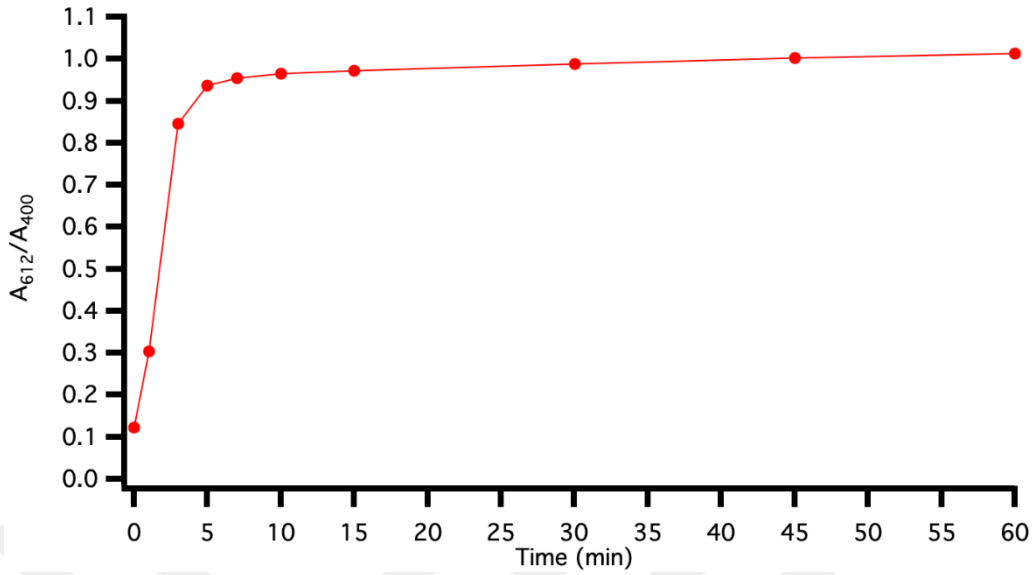

Figure 46. 1st replica - Plot of A_{612}/A_{400} vs. time (300 nM COR and 500 µM NaCl).

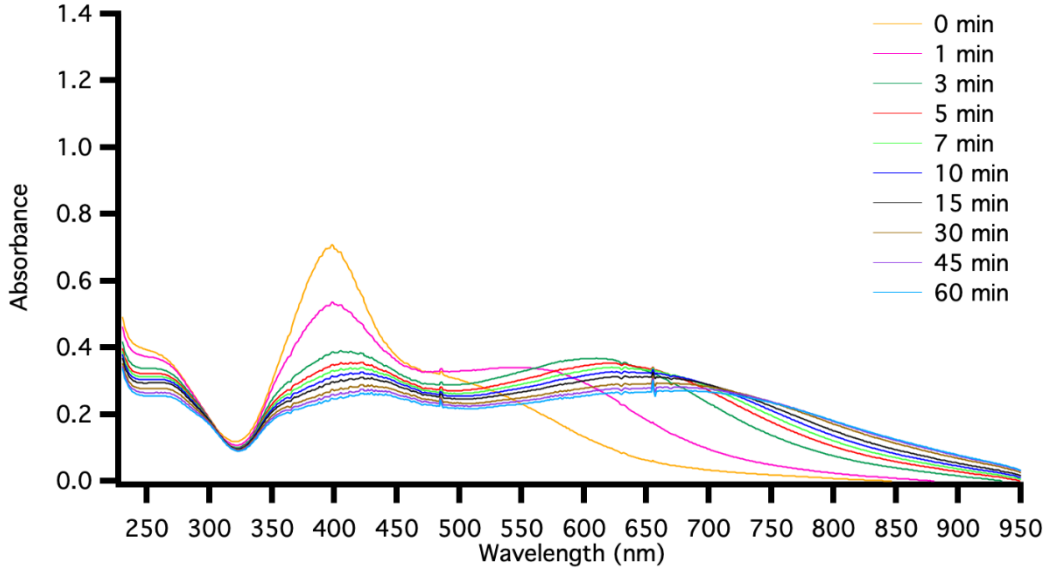

Figure 47. 2nd replica - UV-Vis spectra of AgNPs + NaCl + COR acquired at different time points after the addition of COR under optimized conditions (300 nM COR and 500 µM NaCl).

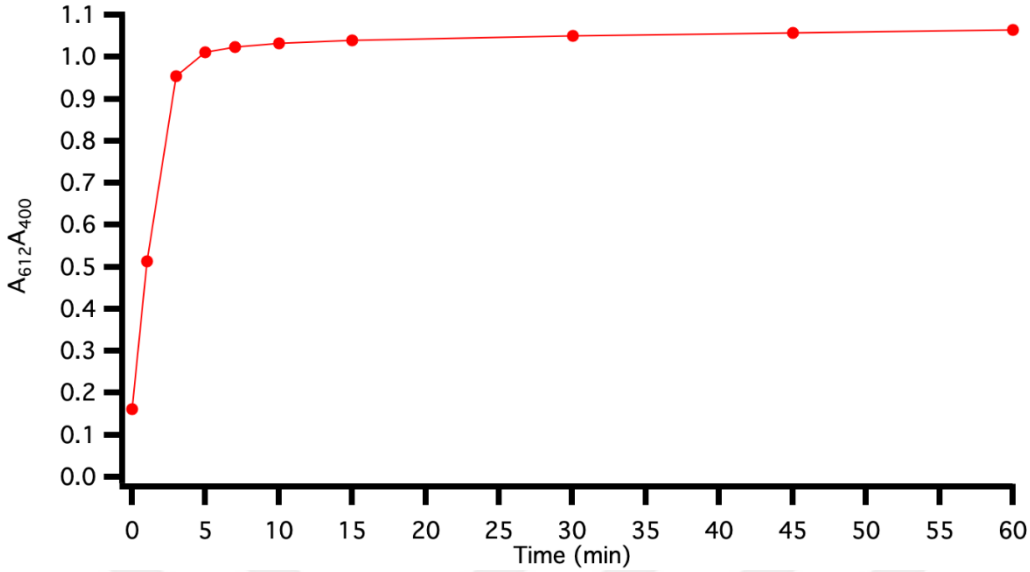

Figure 48. 2nd replica - Plot of A_{612}/A_{400} vs. time (300 nM COR and 500 µM NaCl).

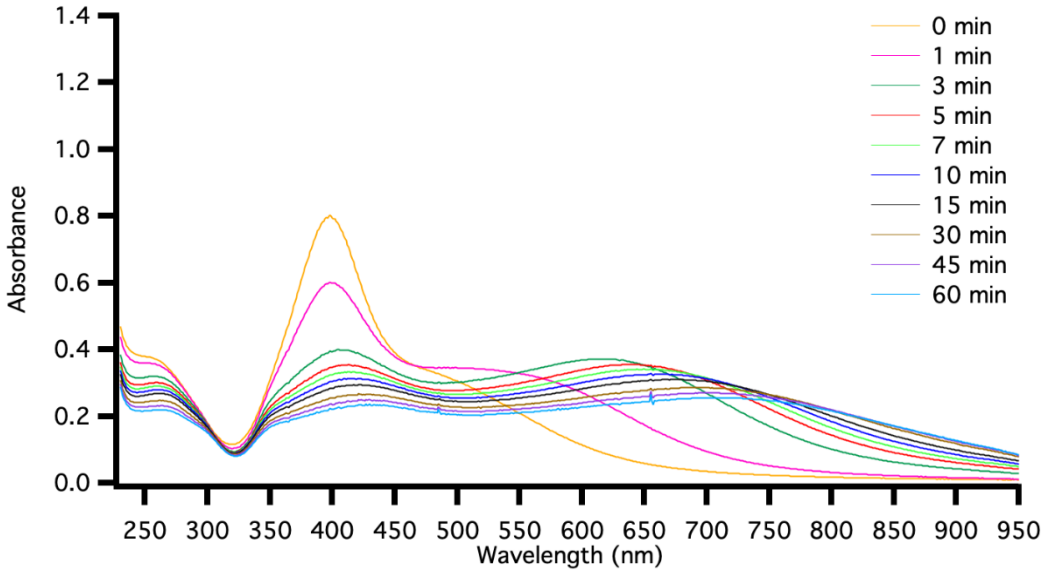

Figure 49. 3rd replica - UV-Vis spectra of AgNPs + NaCl + COR acquired at different time points after the addition of COR (300 nM COR and 500 µM NaCl).

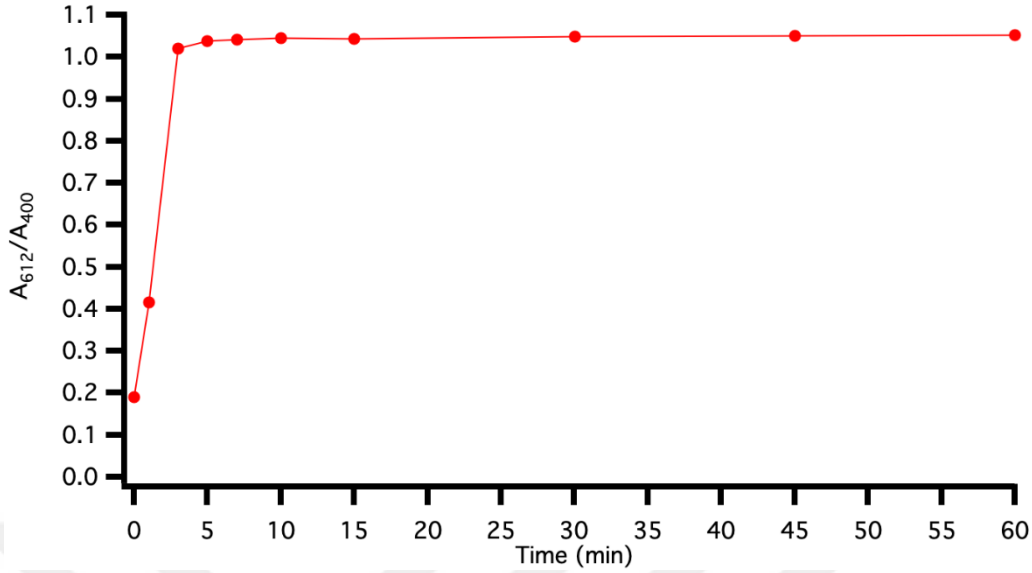

Figure 50. 3rd replica - Plot of A_{612}/A_{400} vs. time (300 nM COR and 500 µM NaCl).

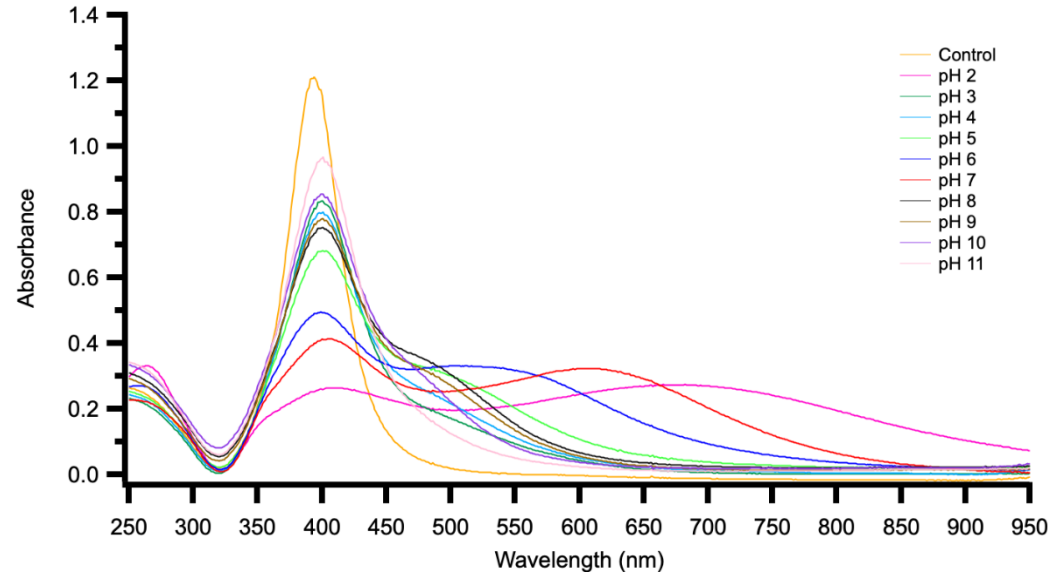

Figure 51. UV-Vis spectra of AgNPs + NaCl + COR samples with different pH values (300 nM COR and 500 µM NaCl).

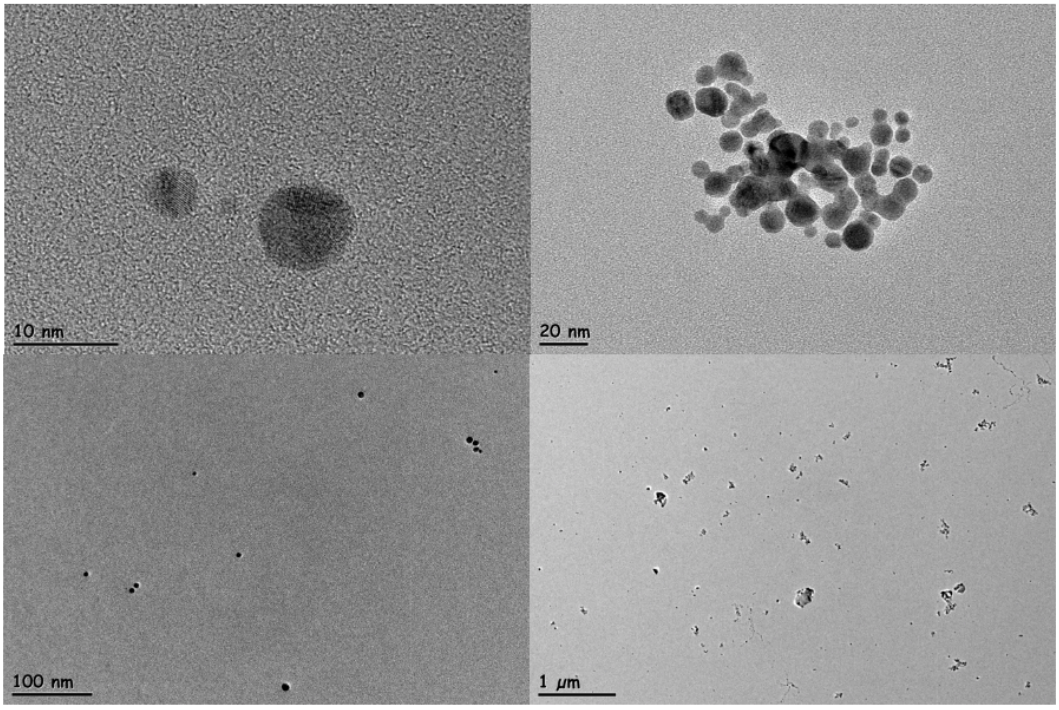

Figure 52. HRTEM images of AgNPs at different scales.

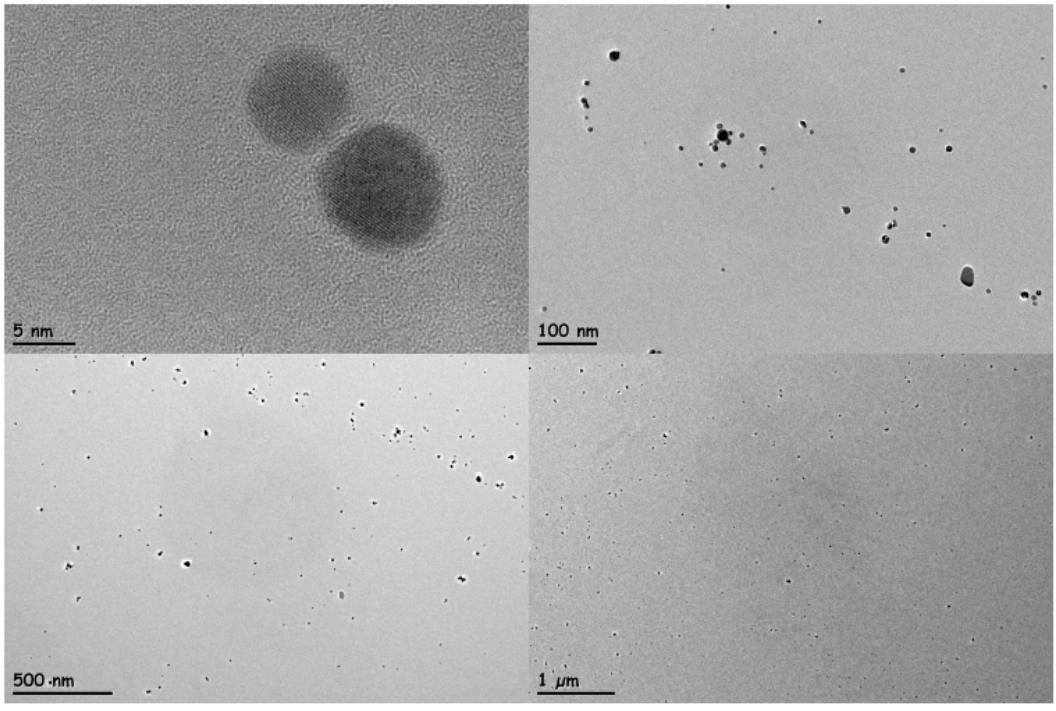

Figure 53. HRTEM images of AgNPs + NaCl at different scales.

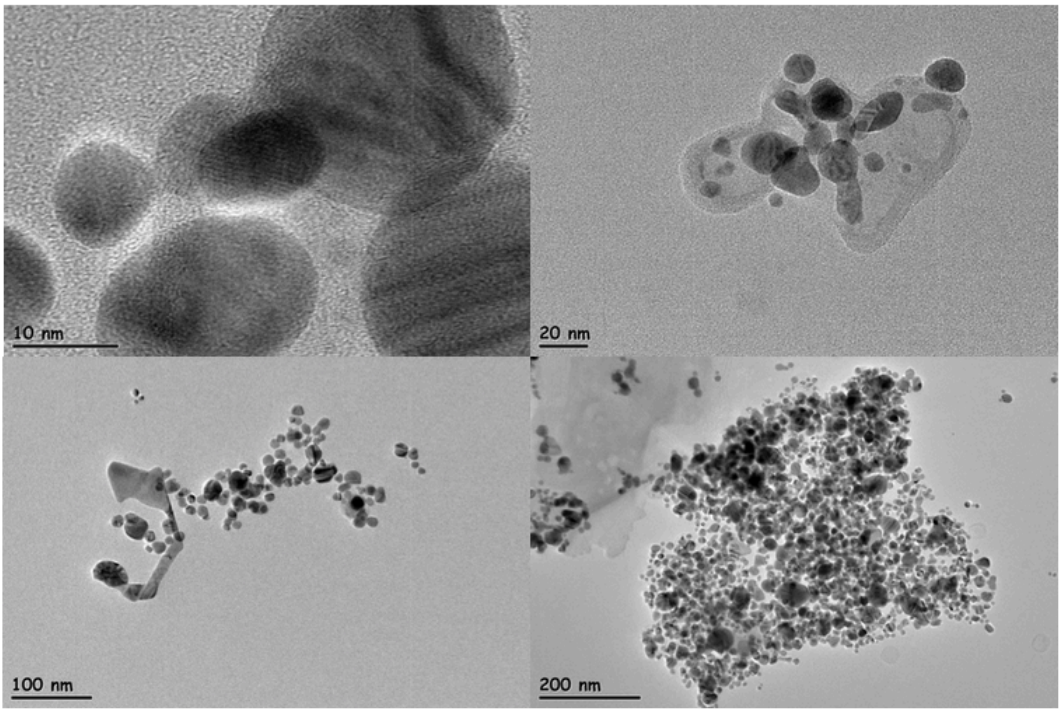

Figure 54. HRTEM images of AgNPs + NaCl + COR at different scales.

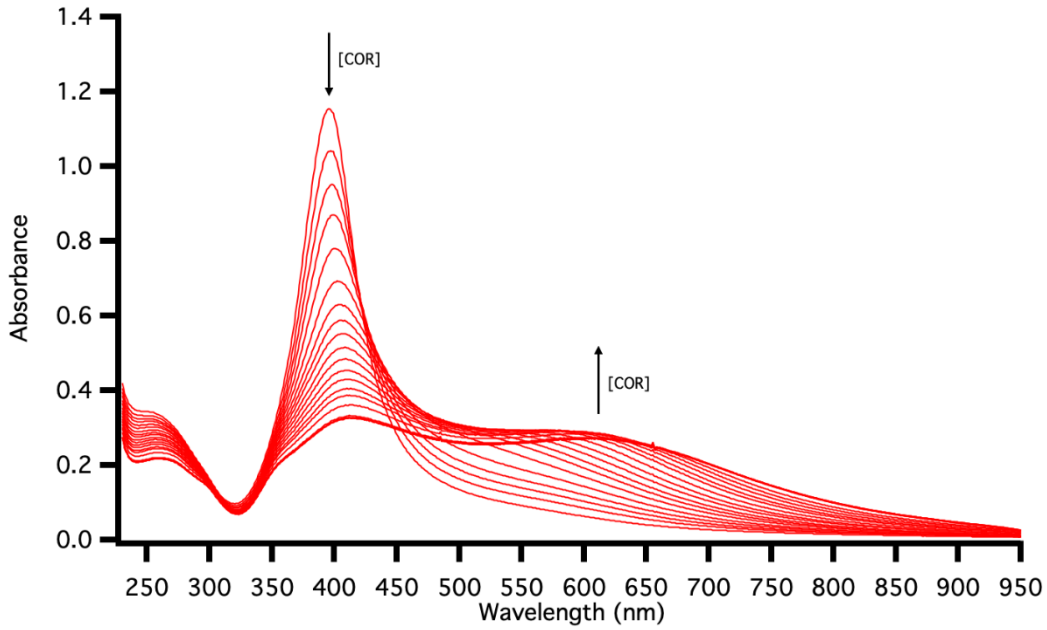

Figure 55. 1st replica - UV-Vis spectra of the titration of 10.0 µM COR into the AgNPs in the presence of 500 µM NaCl.

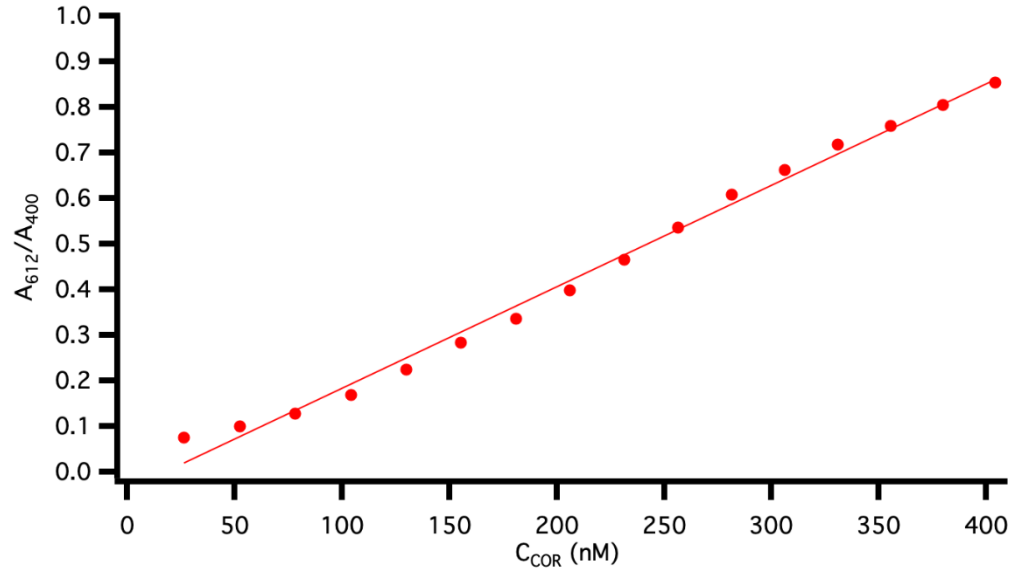

Figure 56. 1st replica - Calibration curve of the titration of 10.0 µM COR into the AgNPs in the presence of 500 µM NaCl.

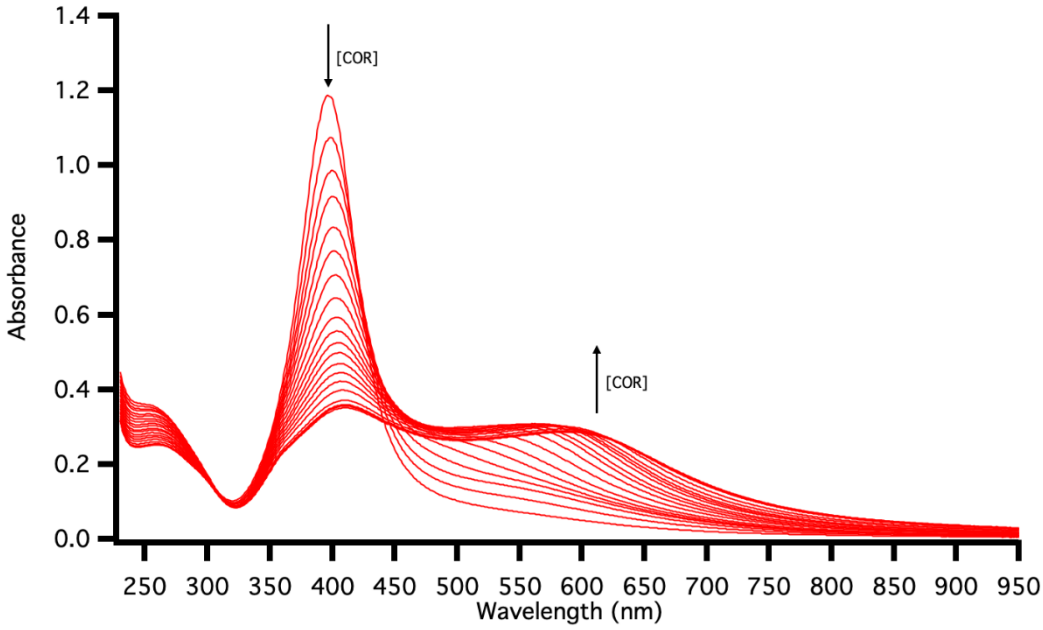

Figure 57. 2nd replica - UV-Vis spectra of the titration of 10.0 µM COR into the AgNPs in the presence of 500 µM NaCl.

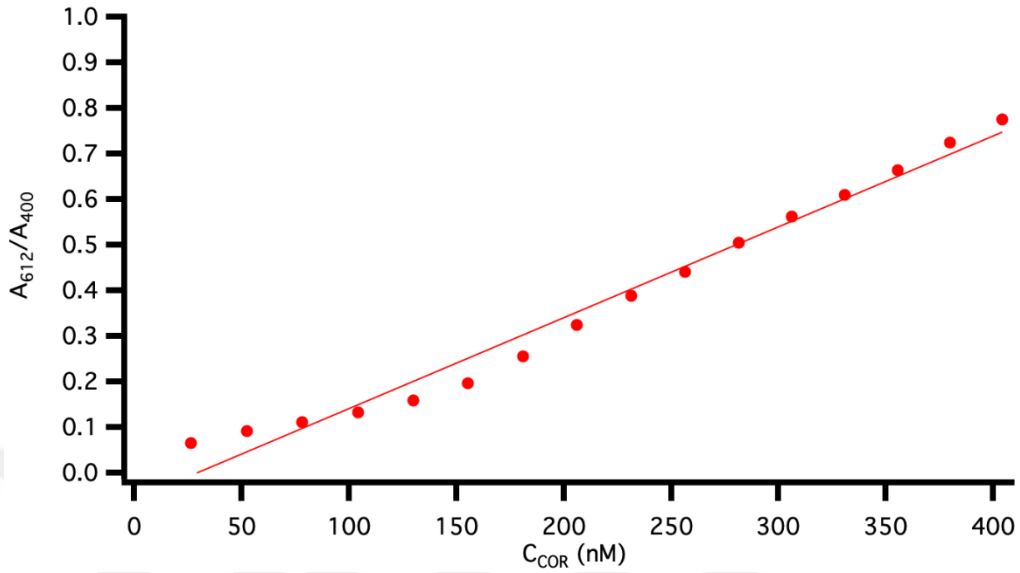

Figure 58. 2nd replica - Calibration curve of the titration of 10.0 µM COR into the AgNPs in the presence of 500 µM NaCl.

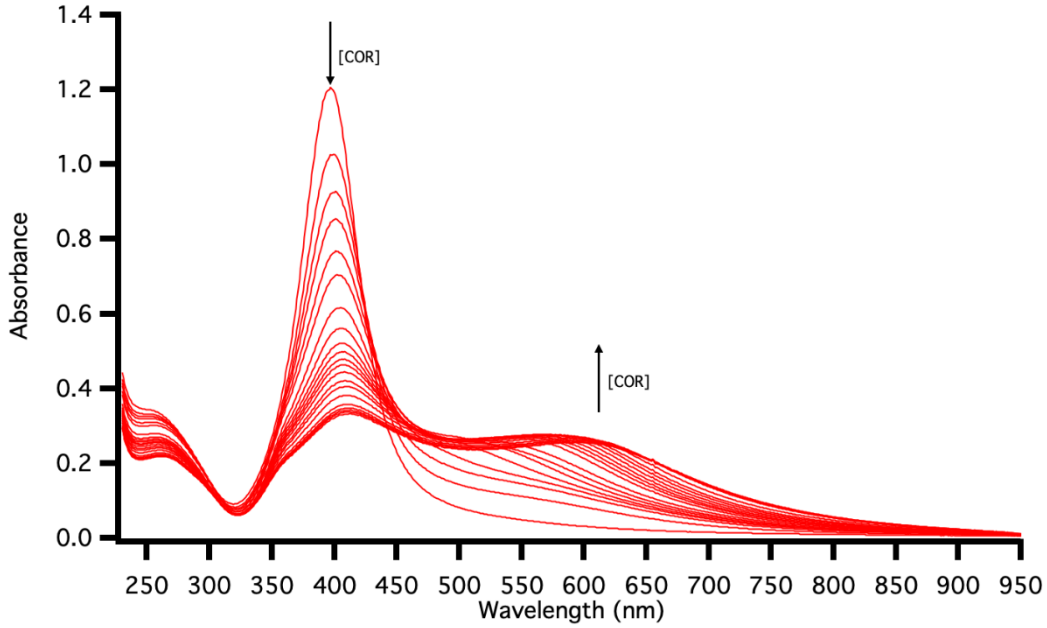

Figure 59. 3rd replica - UV-Vis spectra of the titration of 10.0 µM COR into the AgNPs in the presence of 500 µM NaCl.

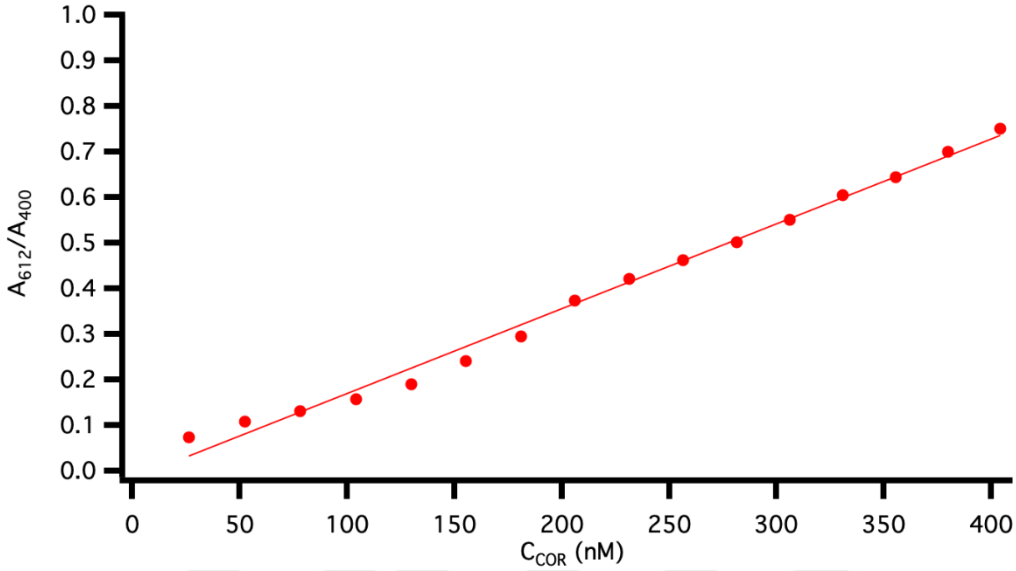

Figure 60. 3rd replica - Calibration curve of the titration of 10.0 µM COR into the AgNPs in the presence of 500 µM NaCl.

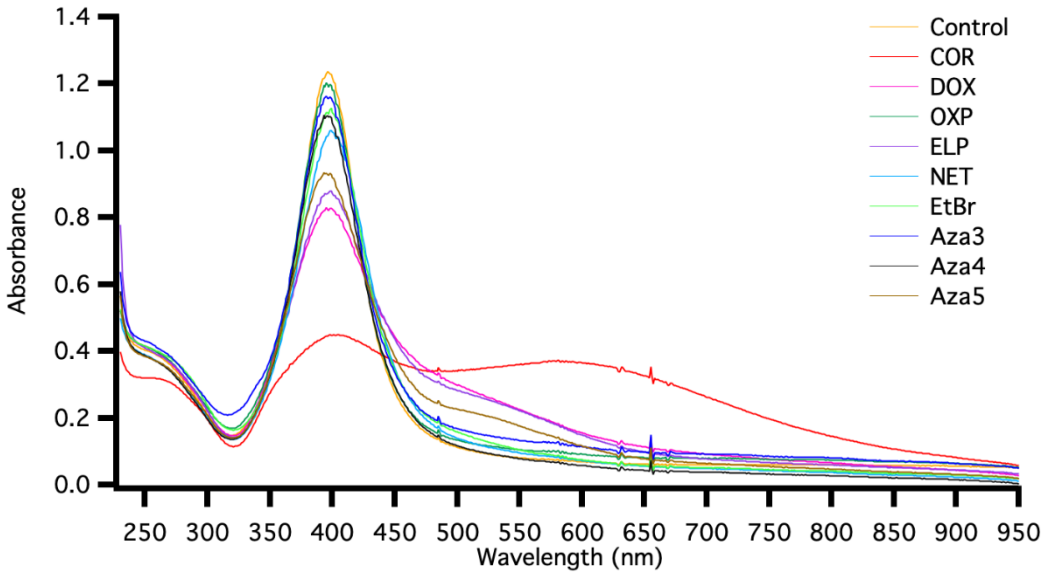

Figure 61. 1st replica - UV-Vis spectra of AgNPs + NaCl in the absence and presence different ligands under optimized conditions (500 µM NaCl and 300 nM ligand).

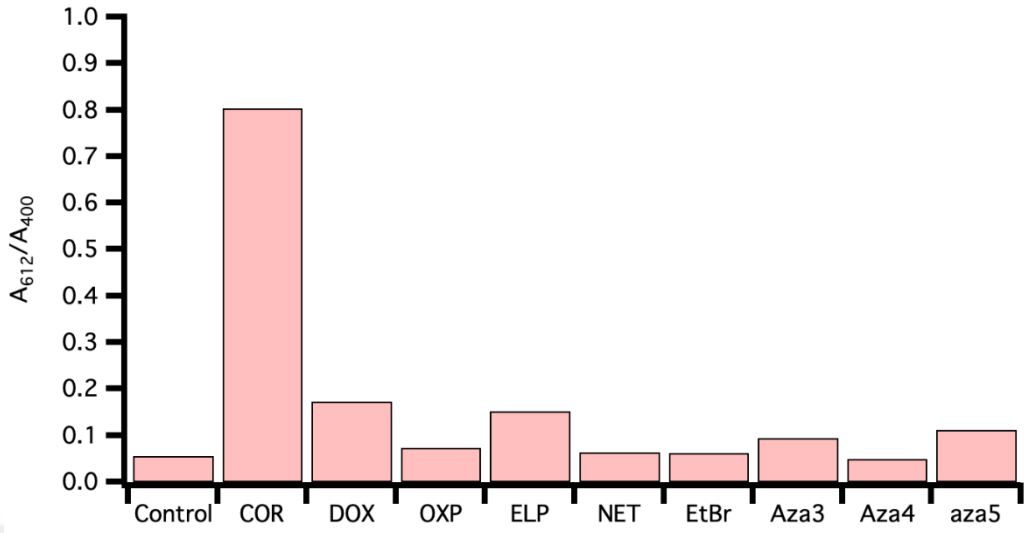

Figure 62. 1st replica - Bar graph of A_{612}/A_{400} for different ligands under optimized conditions (500 µM NaCl and 300 nM ligand).

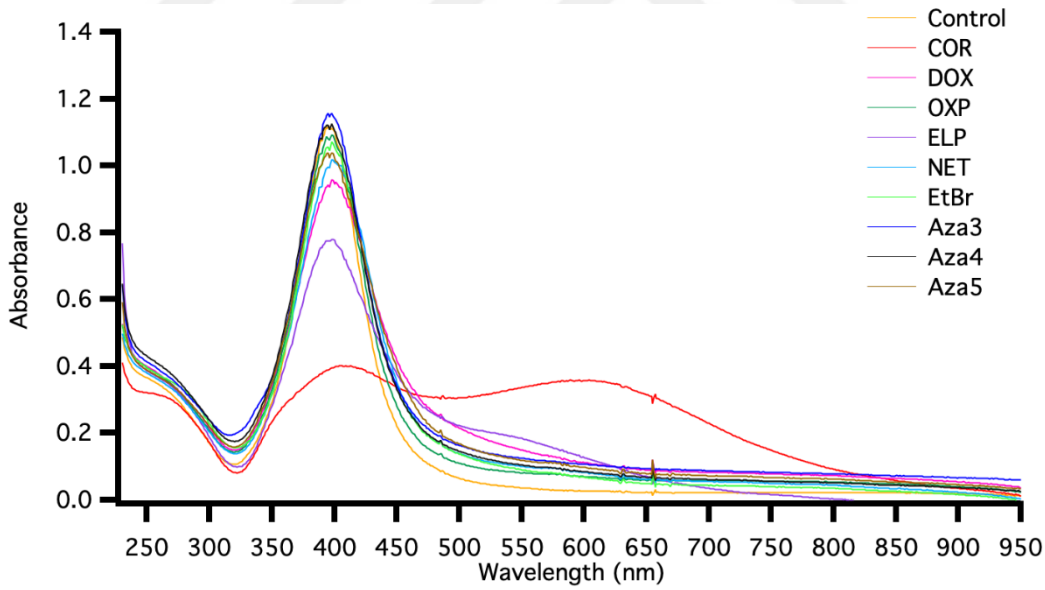

Figure 63. 2nd replica - UV-Vis spectra of AgNPs + NaCl in the absence and presence of different ligands under optimized conditions (500 µM NaCl and 300 nM ligand).

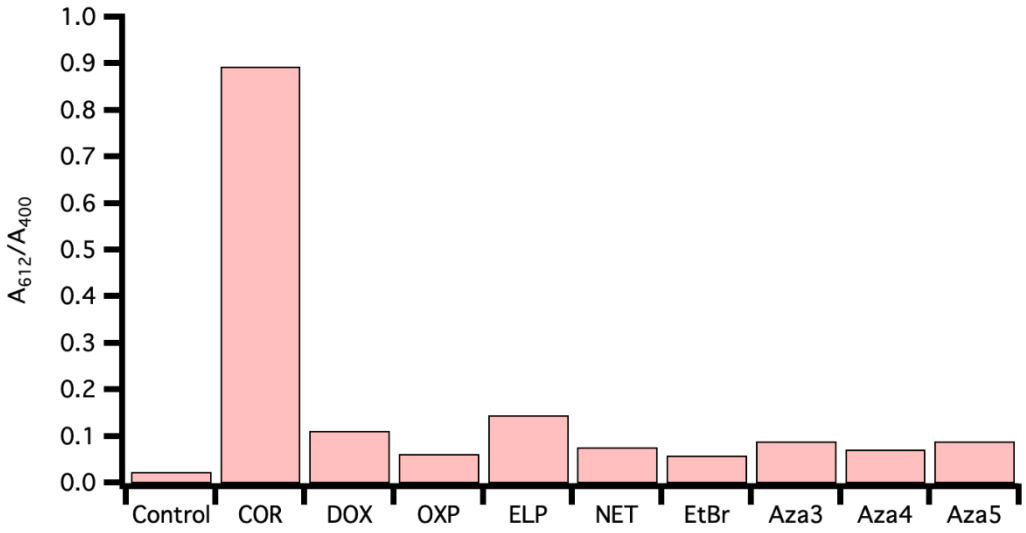

Figure 64. 2nd replica - Bar graph of A_{612}/A_{400} for different ligands under optimized concentrations (500 µM NaCl and 300 nM ligand).

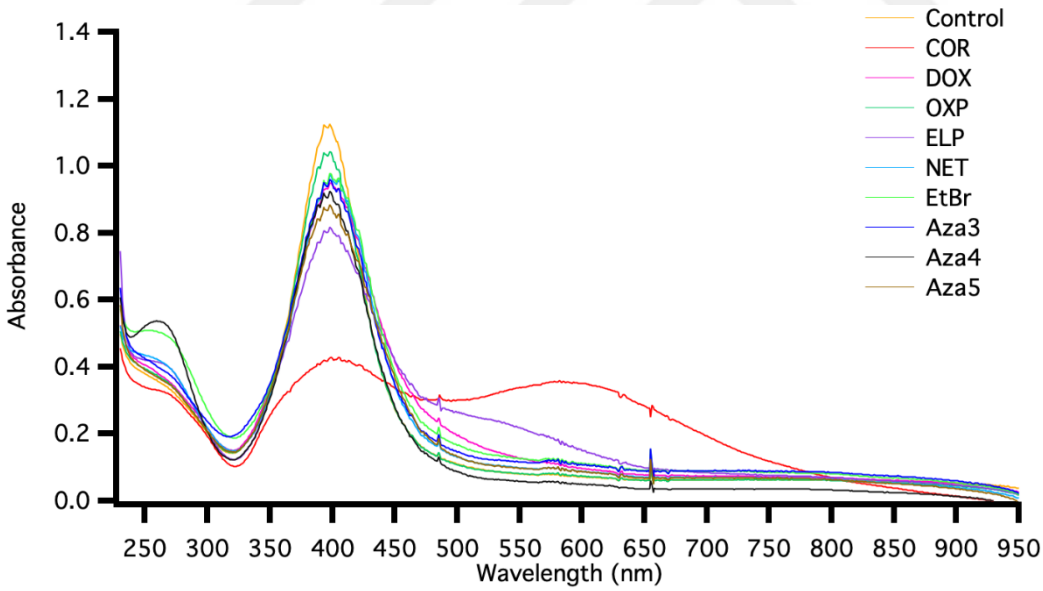

Figure 65. 3rd replica - UV-Vis spectra of AgNPs + NaCl in the absence and presence of different ligands under optimized conditions (500 µM NaCl and 300 nM ligand).

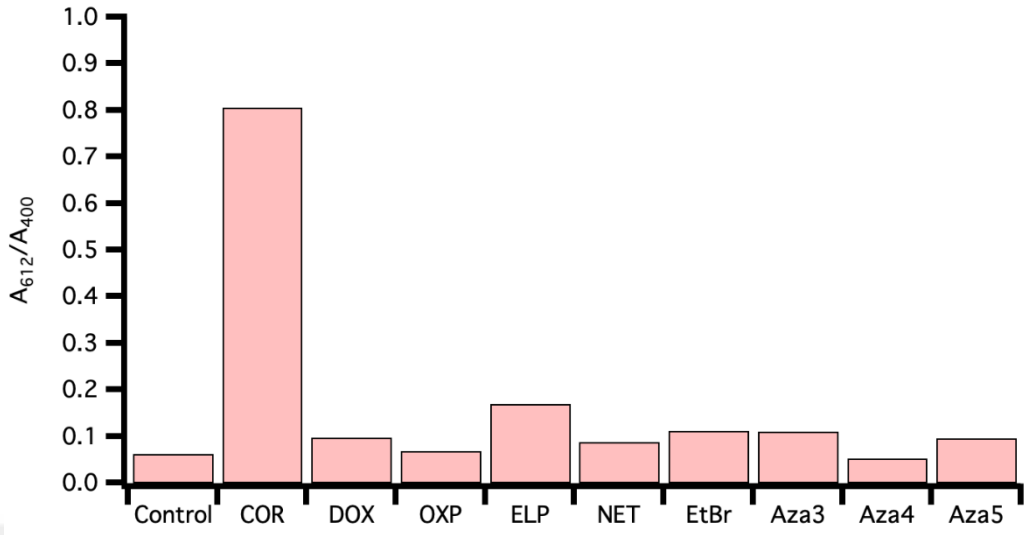

Figure 66. 3rd replica - Bar graph of A_{612}/A_{400} for different ligands under optimized concentrations (500 µM NaCl and 300 nM ligand).

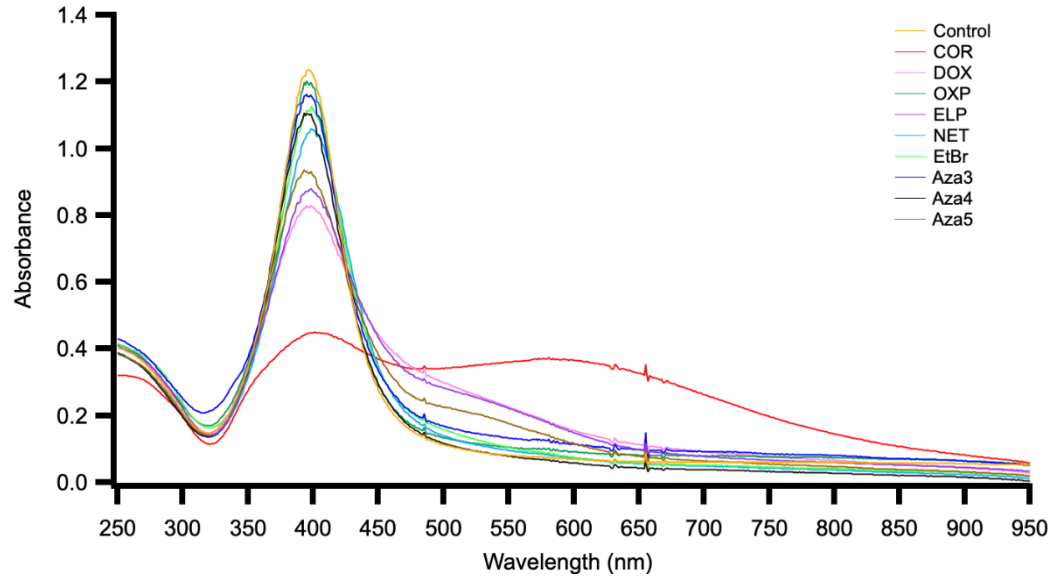

Figure 67. UV-Vis spectra of AgNPs in the absence and presence of different ligands (final concentration of 900 nM, except COR; 300 nM) in the presence of 500 µM NaCl.

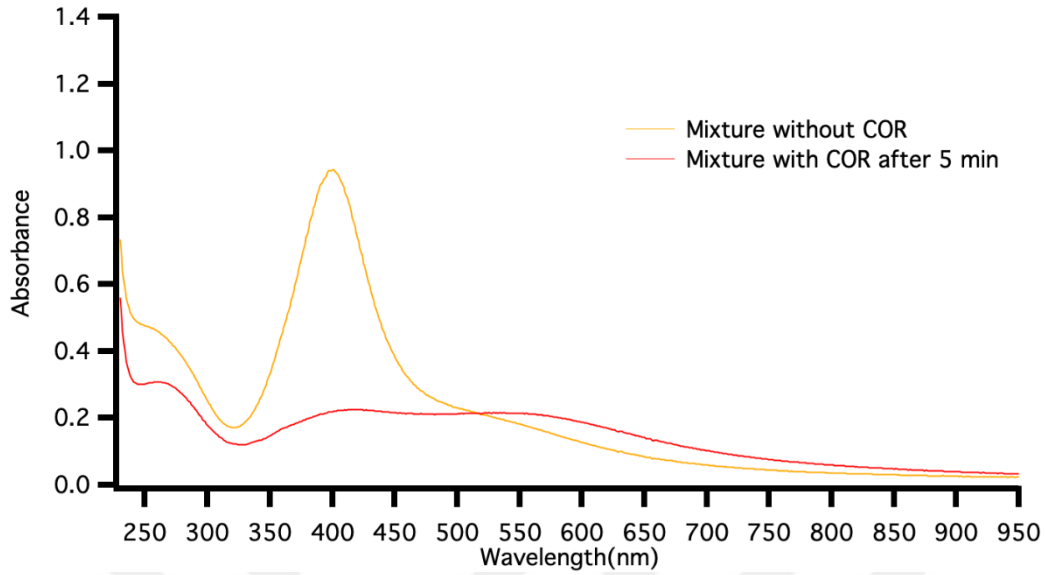

Figure 68. UV-Vis spectra of AgNPs + NaCl + ligand mixture in the absence and presence of COR.

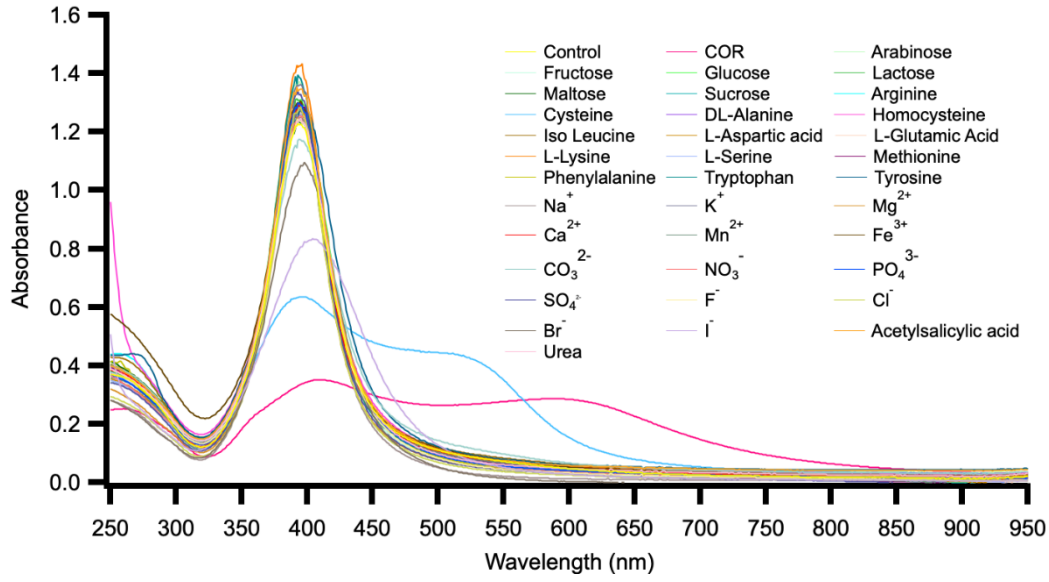

Figure 69. UV-Vis spectra of AgNPs in the absence and presence of common substances (final concentration of the common substances 300 nM, except Fe^{3+} and Tyrosine that are 30 nM) under optimized solution conditions.

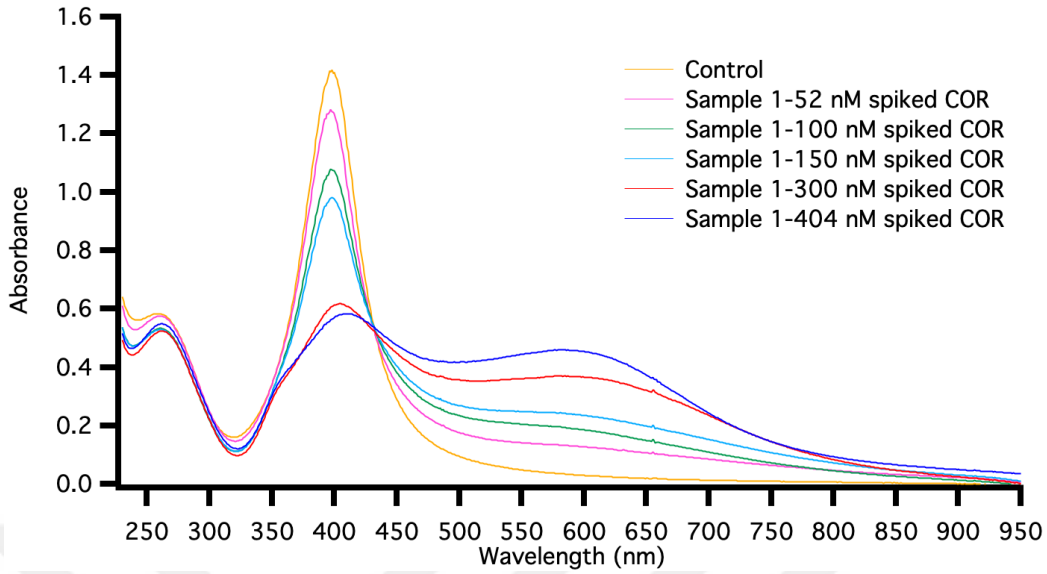

Figure 70. 1st replica – UV-Vis spectra of AgNPs + NaCl spiked with different concentrations of COR, urine sample 1.

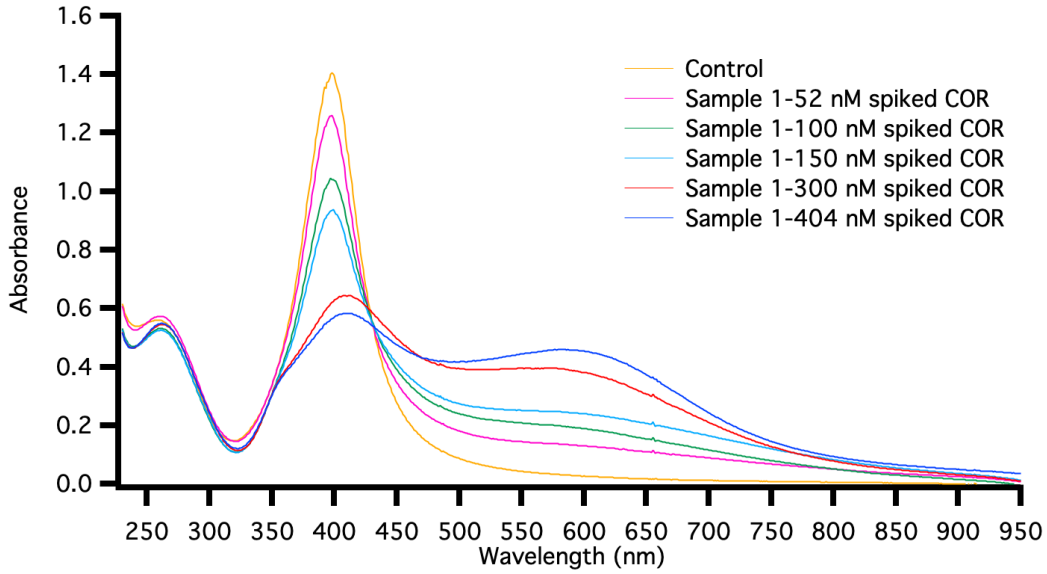

Figure 71. 2nd replica – UV-Vis spectra of AgNPs + NaCl spiked with different concentrations of COR, urine sample 1.

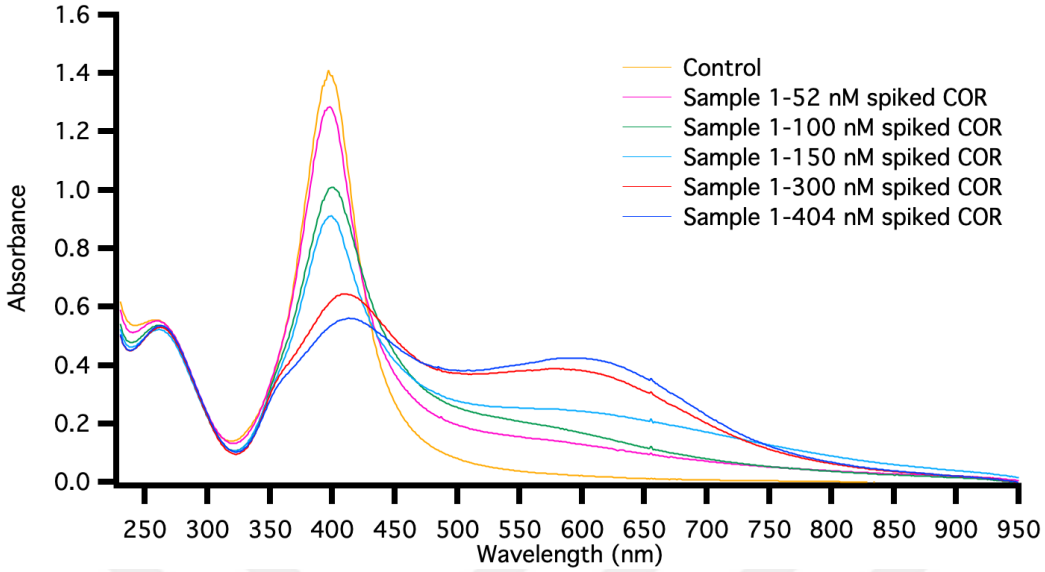

Figure 72. 3rd replica – UV-Vis spectra of AgNPs + NaCl spiked with different concentrations of COR, urine sample 1.

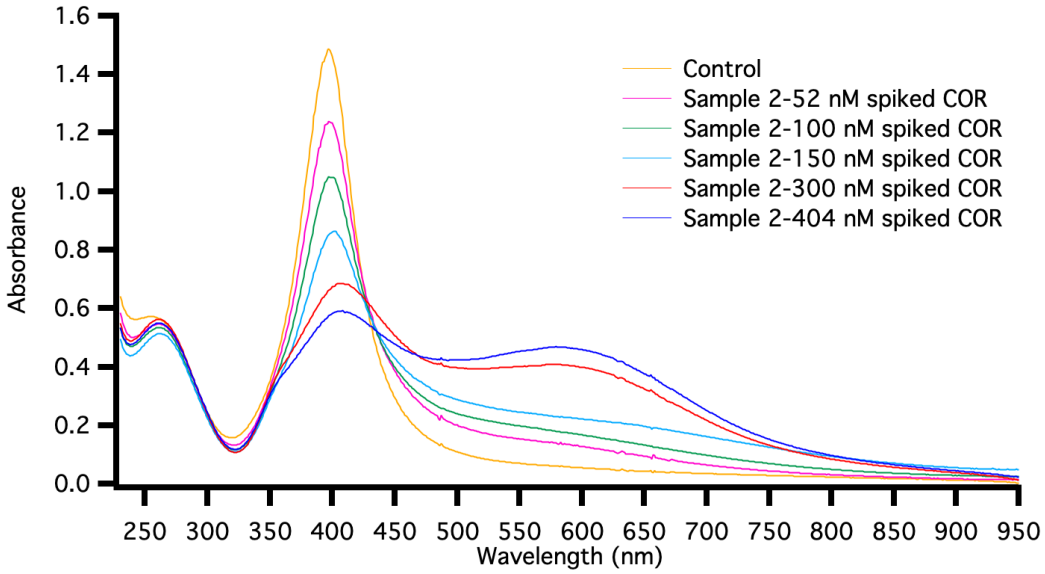

Figure 73. 1st replica – UV-Vis spectra of AgNPs + NaCl spiked with different concentrations of COR, urine sample 2.

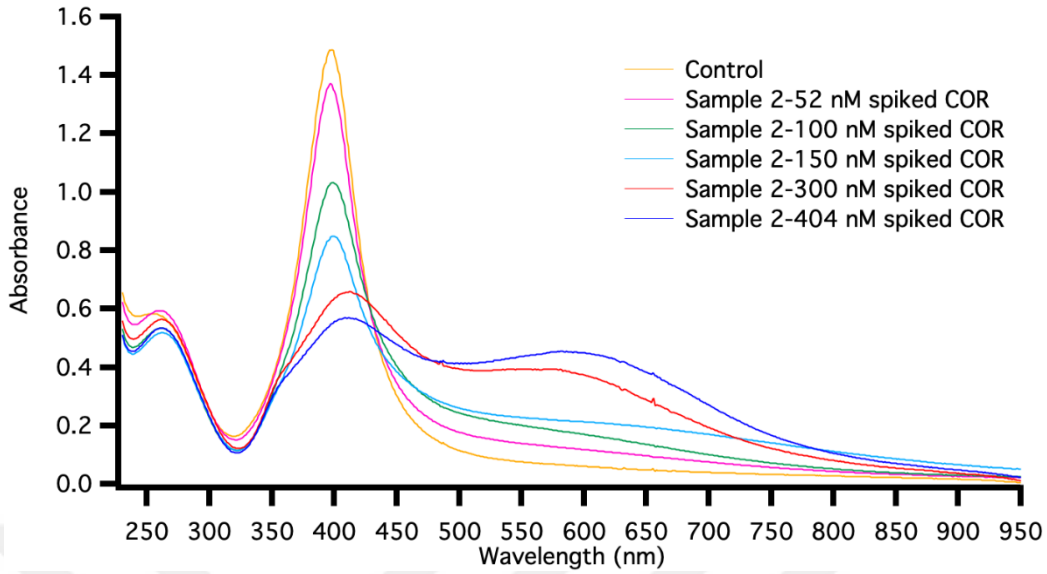

Figure 74. 2nd replica – UV-Vis spectra of AgNPs + NaCl spiked with different concentrations of COR, urine sample 2.

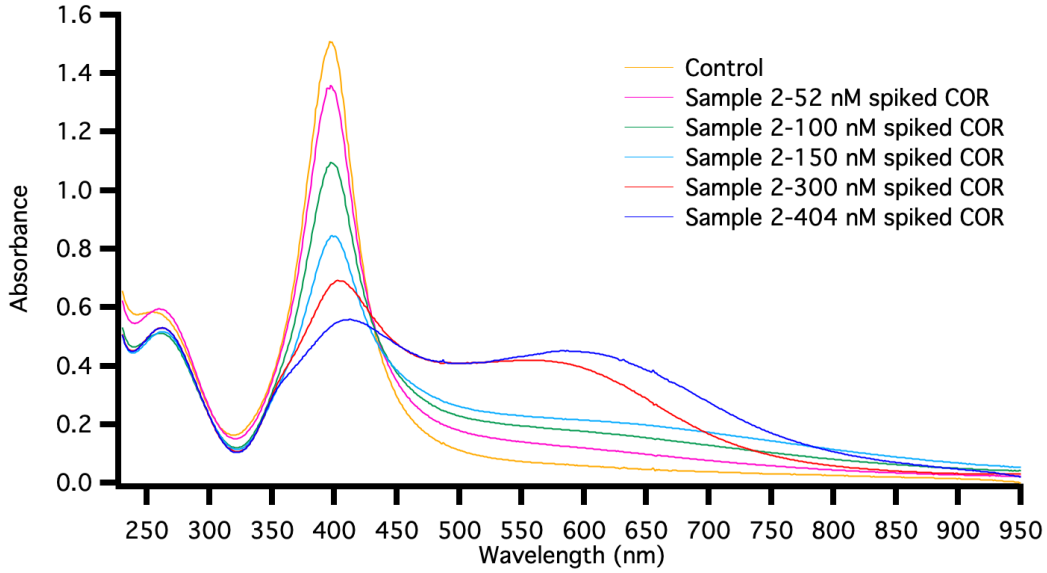

Figure 75. 3rd replica – UV-Vis spectra of AgNPs + NaCl spiked with different concentrations of COR, urine sample 2.

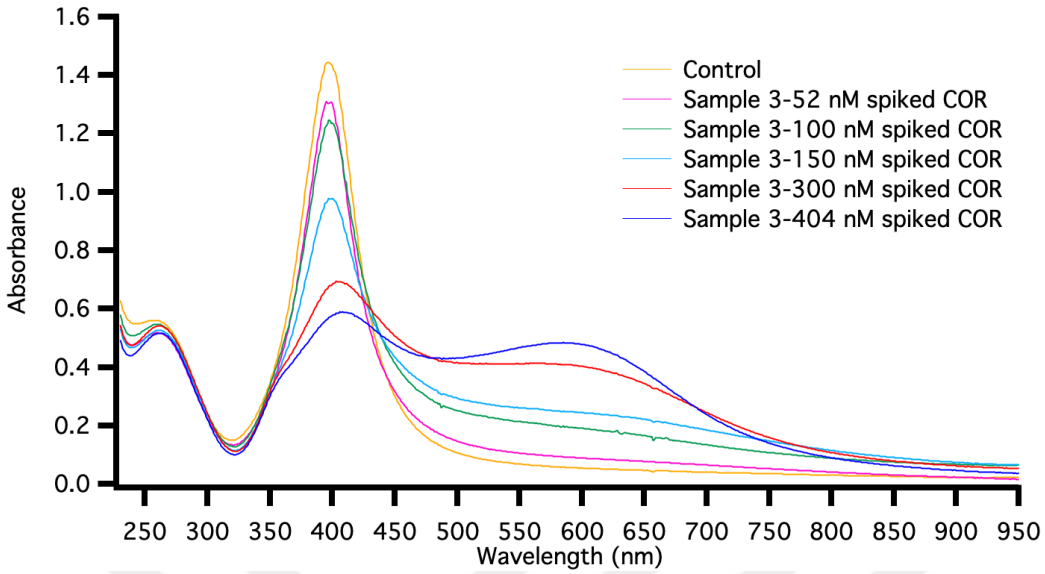

Figure 76. 1st replica – UV-Vis spectra of AgNPs + NaCl spiked with different concentrations of COR, urine sample 3.

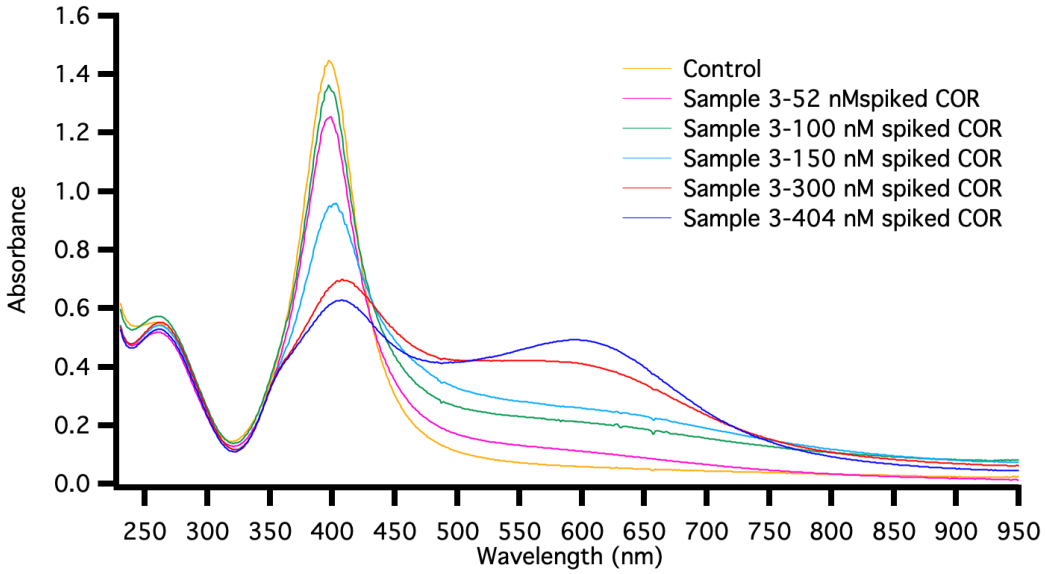

Figure 77. 2nd replica – UV-Vis spectra of AgNPs + NaCl spiked with different concentrations of COR, urine sample 3.

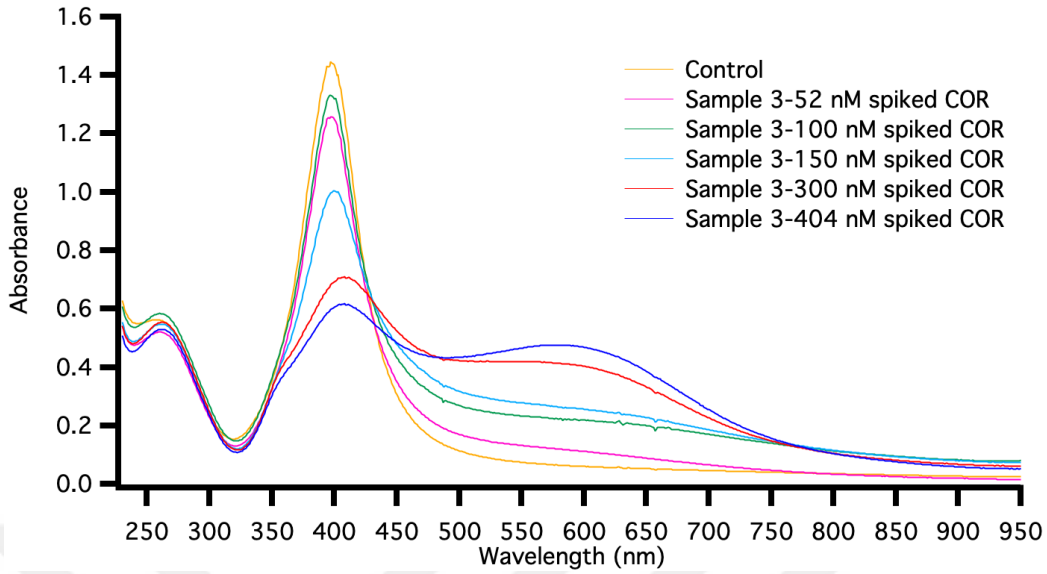

Figure 78. 3rd replica – UV-Vis spectra of AgNPs + NaCl spiked with different concentrations of COR, urine sample 3.

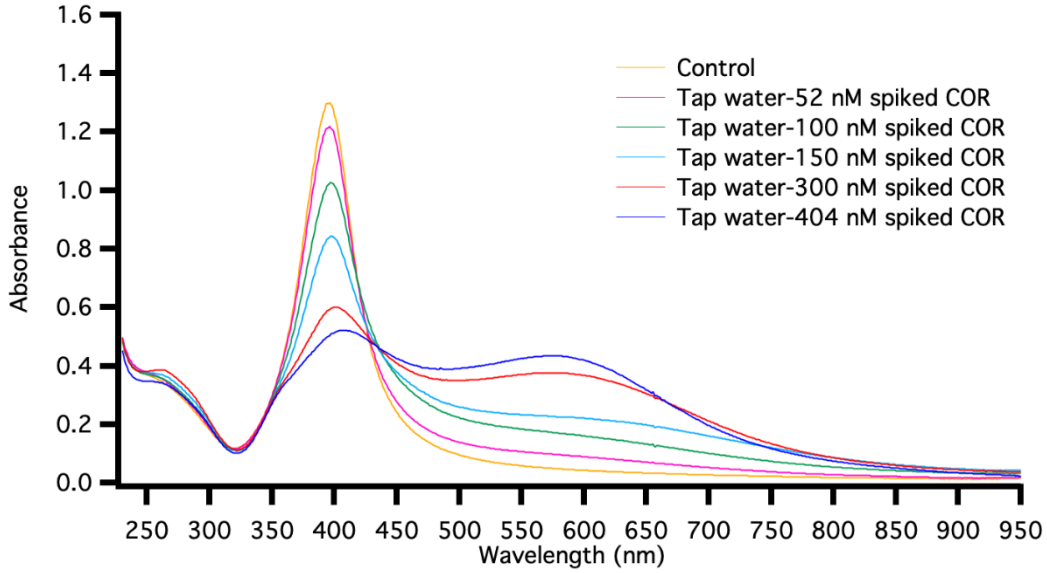

Figure 79. 1st replica – UV-Vis spectra of AgNPs + NaCl spiked with different concentrations of COR, tap water sample.

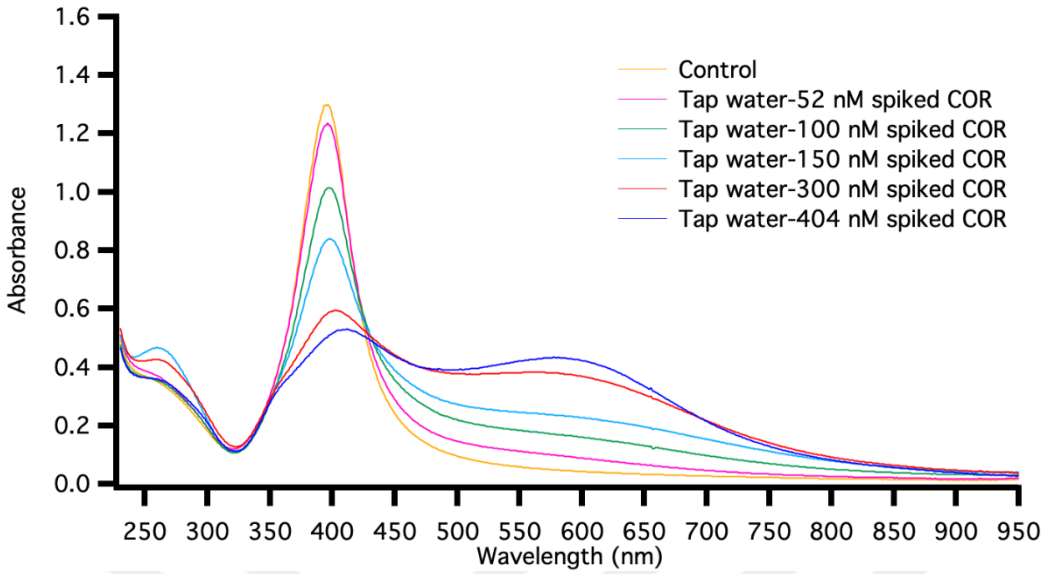

Figure 80. 2nd replica – UV-Vis spectra of AgNPs + NaCl spiked with different concentrations of COR, tap water sample.

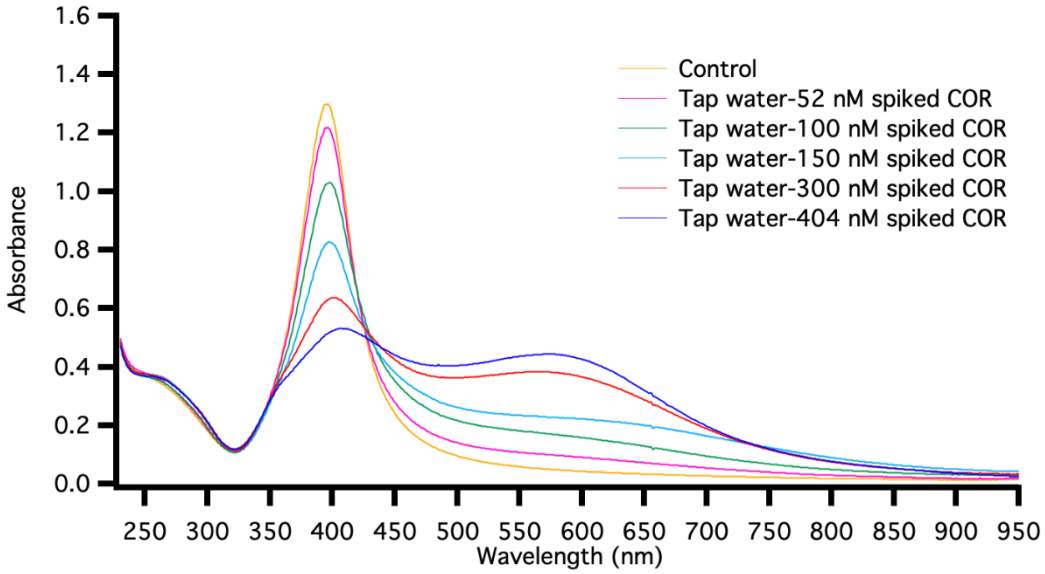

Figure 81. 3rd replica – UV-Vis spectra of AgNPs + NaCl spiked with different concentrations of COR, tap water sample.

C. Fluorometric Detection of Coralyne

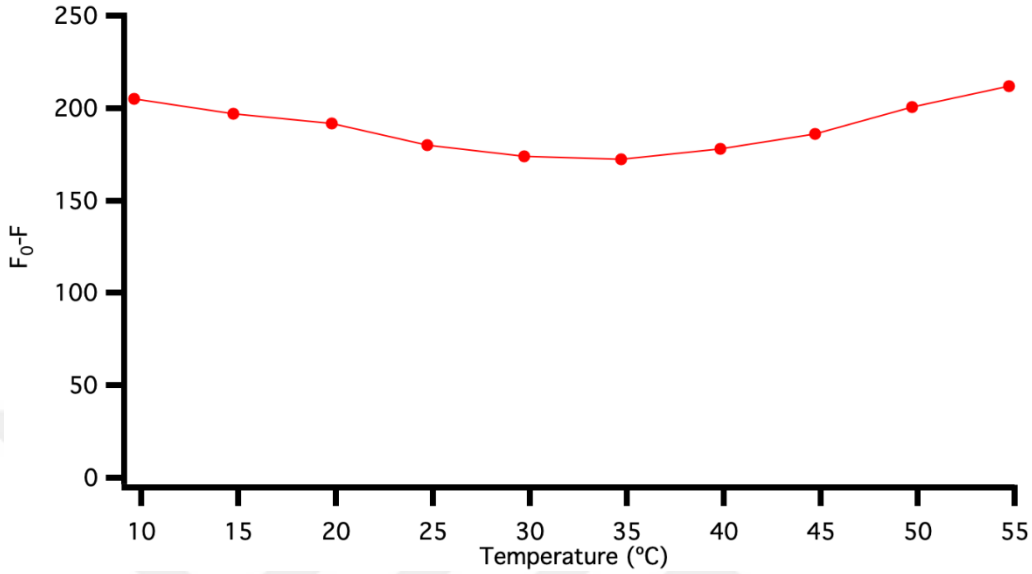

Figure 82. 1st replica - Plot of F_0-F vs. temperature under optimized conditions (1.5 µM dT_{32}, 3.0 µM COU and 100 nM COR).

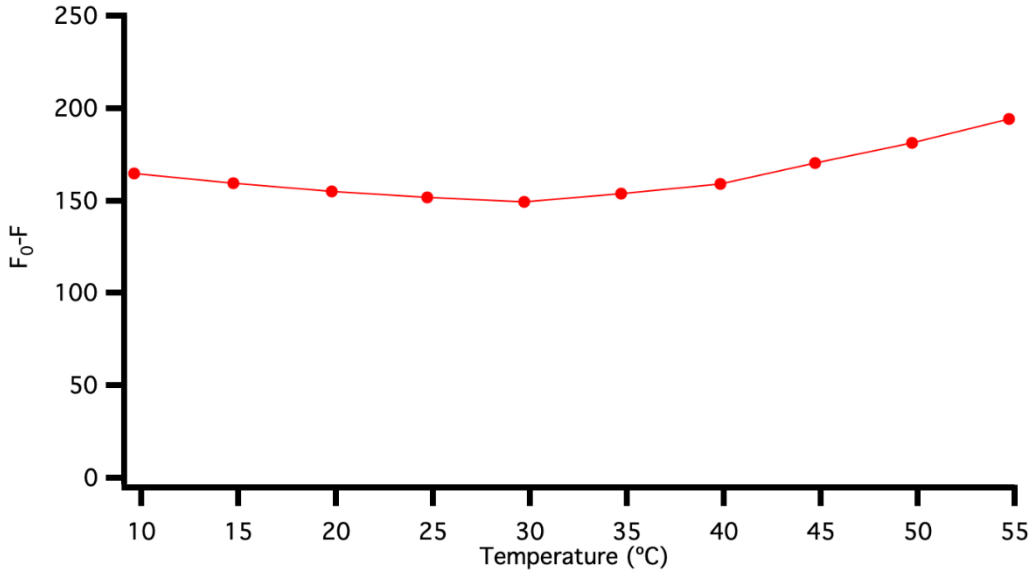

Figure 83. 2nd replica - Plot of F_0-F vs. temperature under optimized conditions (1.5 µM dT_{32}, 3.0 µM COU and 100 nM COR).

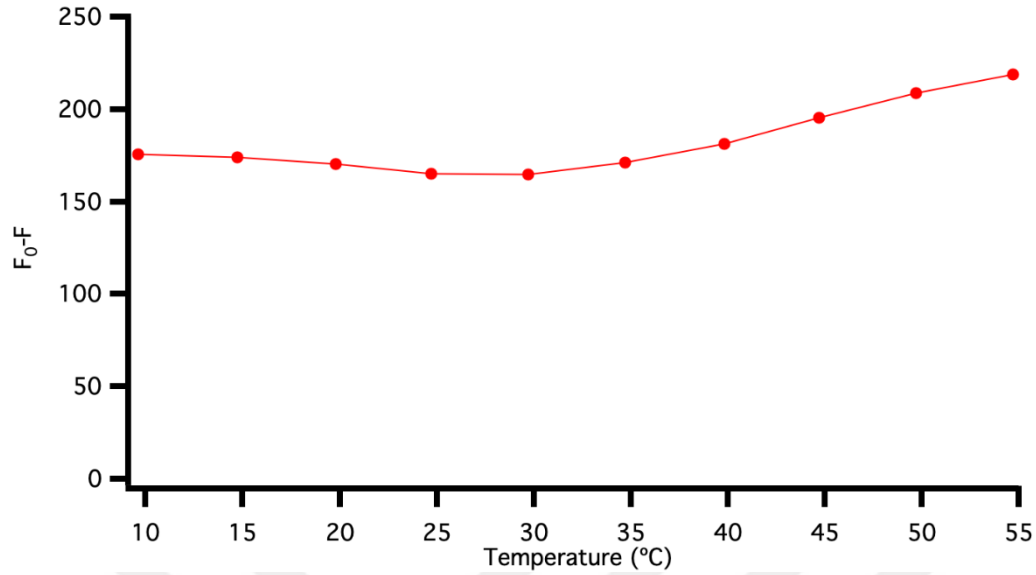

Figure 84. 3rd replica - Plot of F_0-F vs. temperature under optimized conditions (1.5 µM dT_{32}, 3.0 µM COU and 100 nM COR).

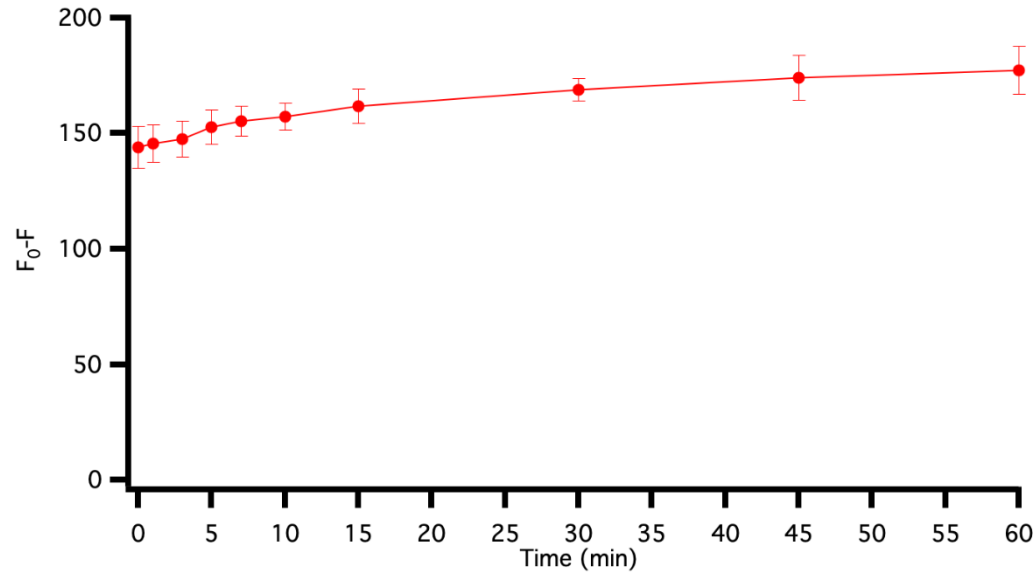

Figure 85.1st replica - Plot of F_0-F vs. time under optimized conditions (1.5 µM dT_{32}, 3.0 µM COU and 100 nM COR).

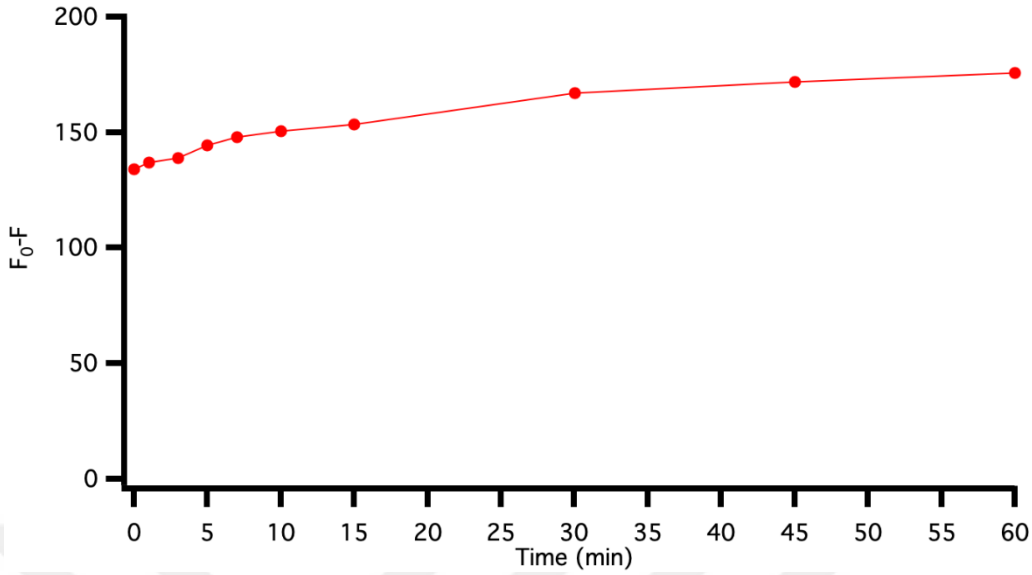

Figure 86. 2nd replica - Plot of F_0-F vs. time under optimized conditions (1.5 µM dT_{32}, 3.0 µM COU and 100 nM COR).

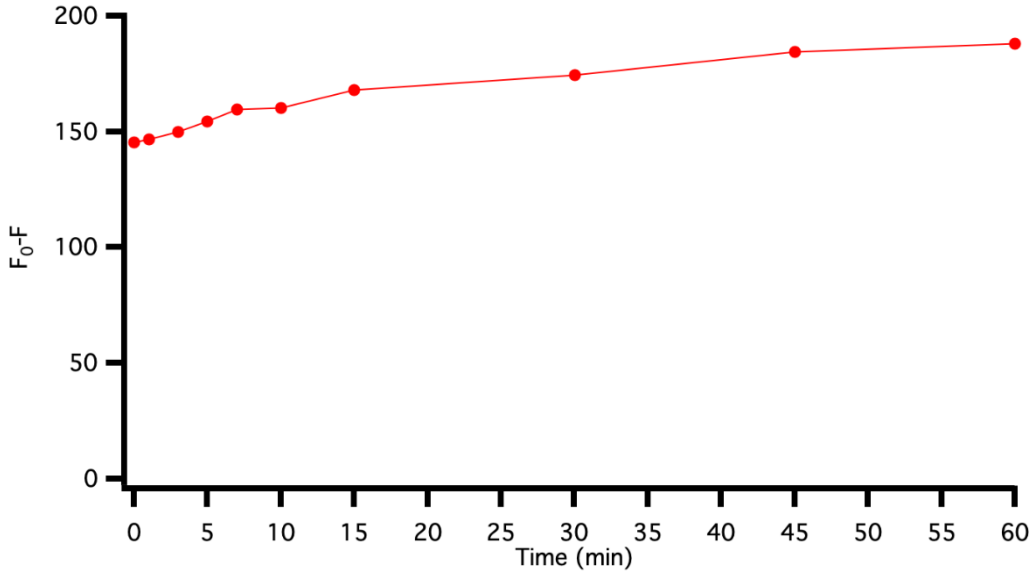

Figure 87. 3rd replica - Plot of F_0-F vs. time under optimized conditions (1.5 µM dT_{32}, 3.0 µM COU and 100 nM COR).

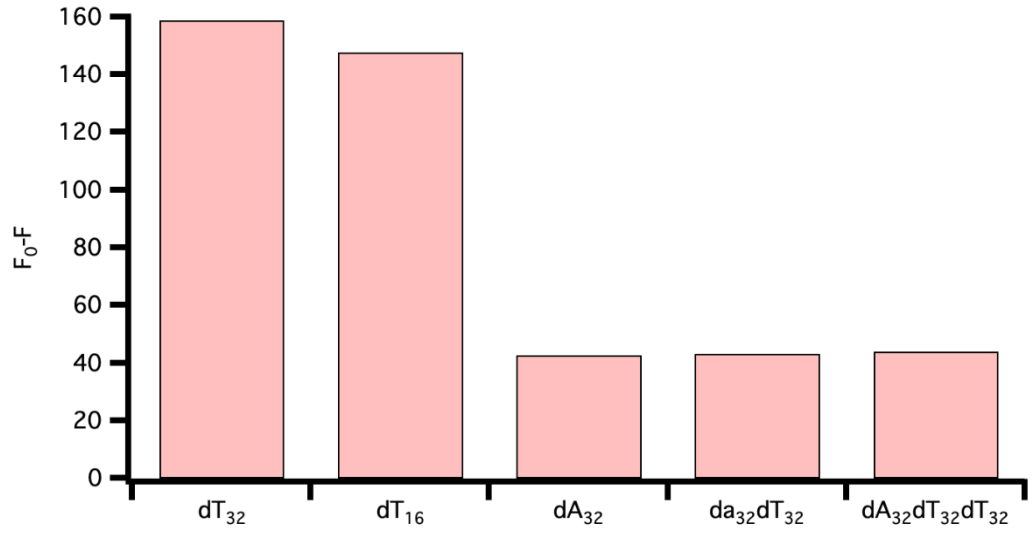

Figure 88. 1st replica - Bar graph of F_0-F for different oligonucleotides under optimized conditions (1.5 µM oligonucleotide, 3.0 µM COU and 100 nM COR).

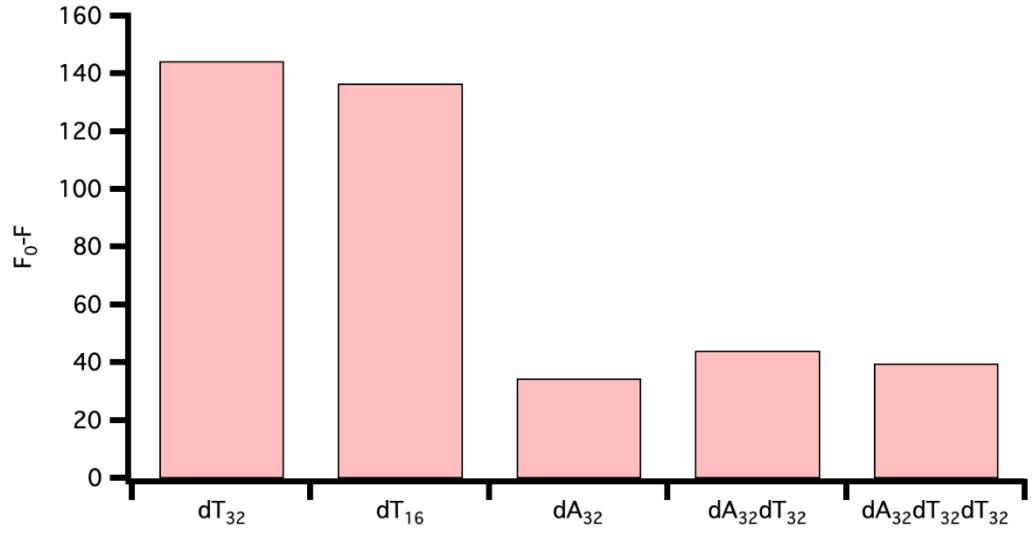

Figure 89. 2nd replica - Bar graph of F_0-F for different oligonucleotides under optimized conditions (1.5 µM oligonucleotide, 3.0 µM COU and 100 nM COR).

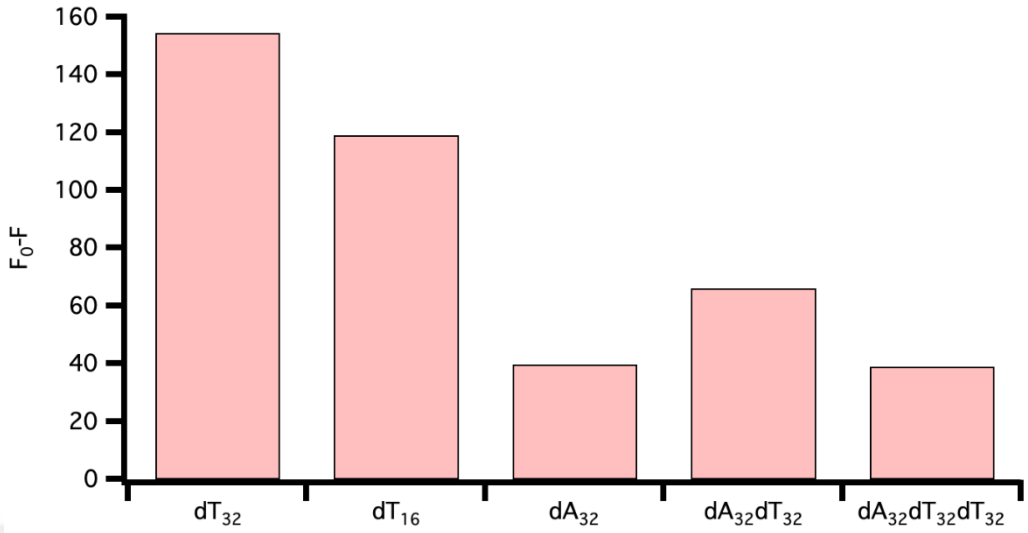

Figure 90. 3rd replica - Bar graph of F_0-F for different oligonucleotides under optimized conditions (1.5 µM oligonucleotide, 3.0 µM COU and 100 nM COR).

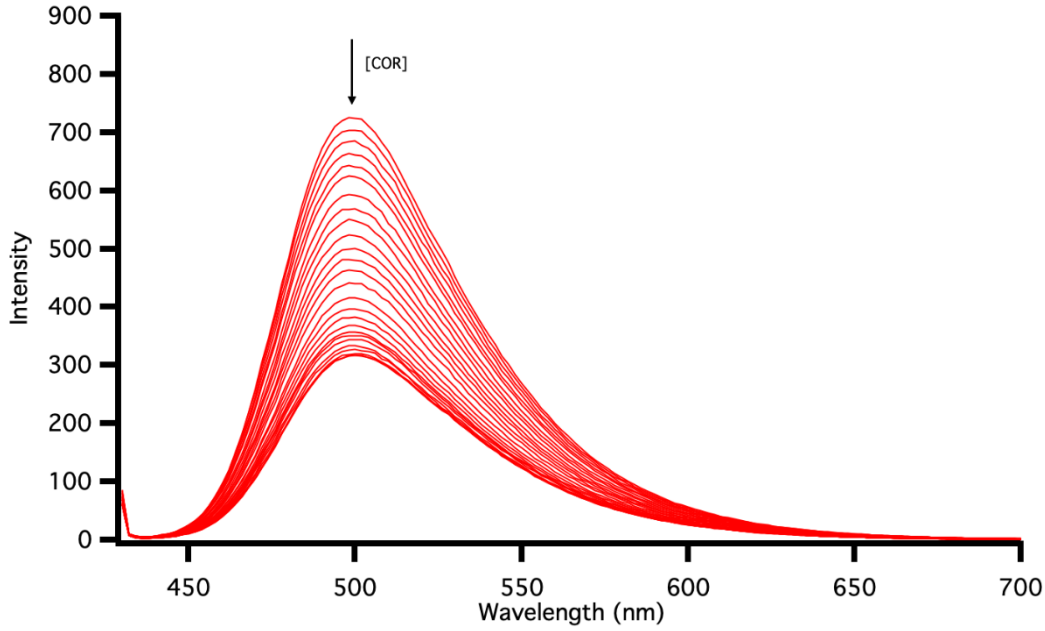

Figure 91. 1st replica - Fluorescence spectra of the titration of 5.0 µM COR to the dT_{32}-AgNPs in the presence of 3.0 µM COU.

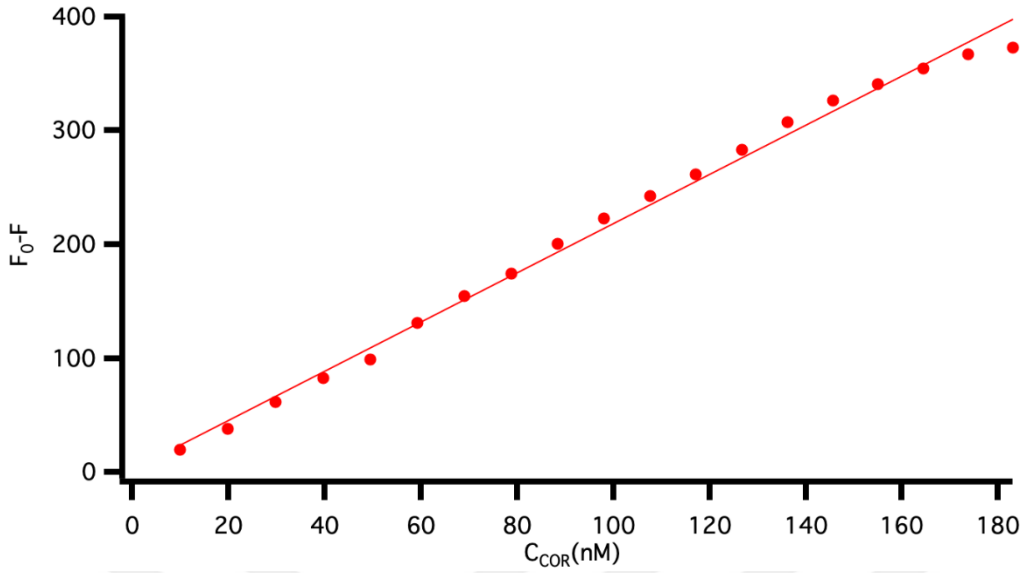

Figure 92. 1st replica - Calibration curve of the titration of 5.0 µM COR to the dT_{32}-AgNPs in the presence of 3.0 µM COU.

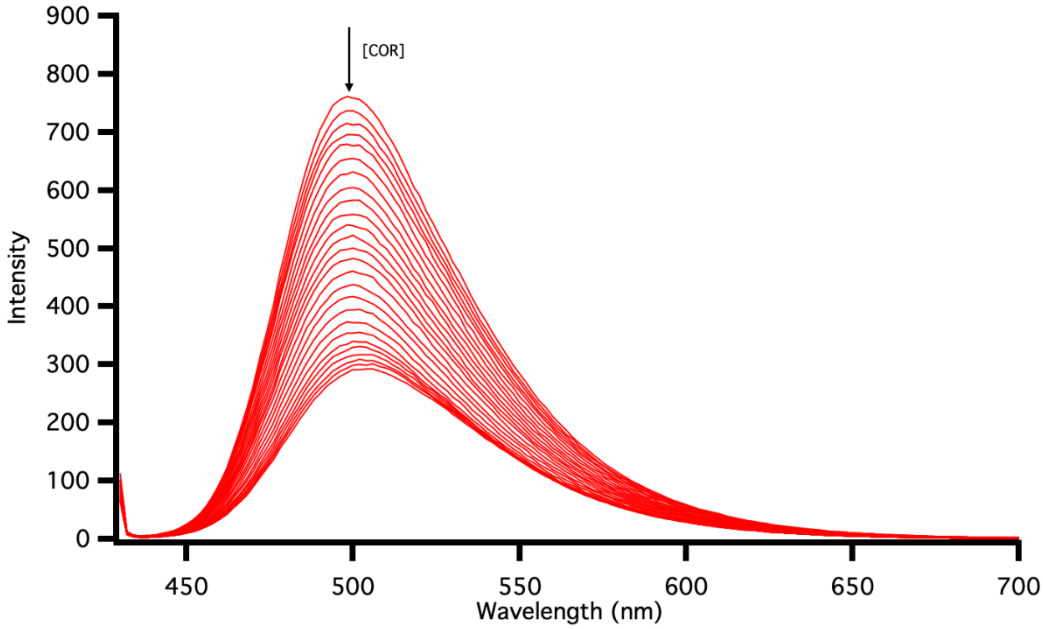

Figure 93. 2nd replica - Fluorescence spectra of the titration of 5.0 µM COR to the dT_{32}-AgNPs in the presence of 3.0 µM COU.

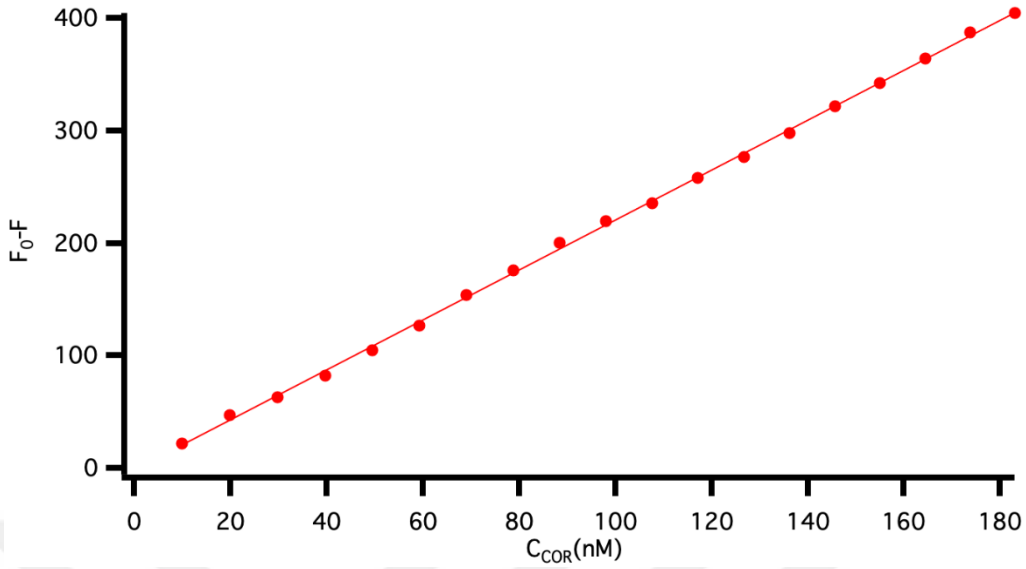

Figure 94. 2nd replica - Calibration curve of the titration of 5.0 µM COR to the dT_{32}-AgNPs in the presence of 3.0 µM COU.

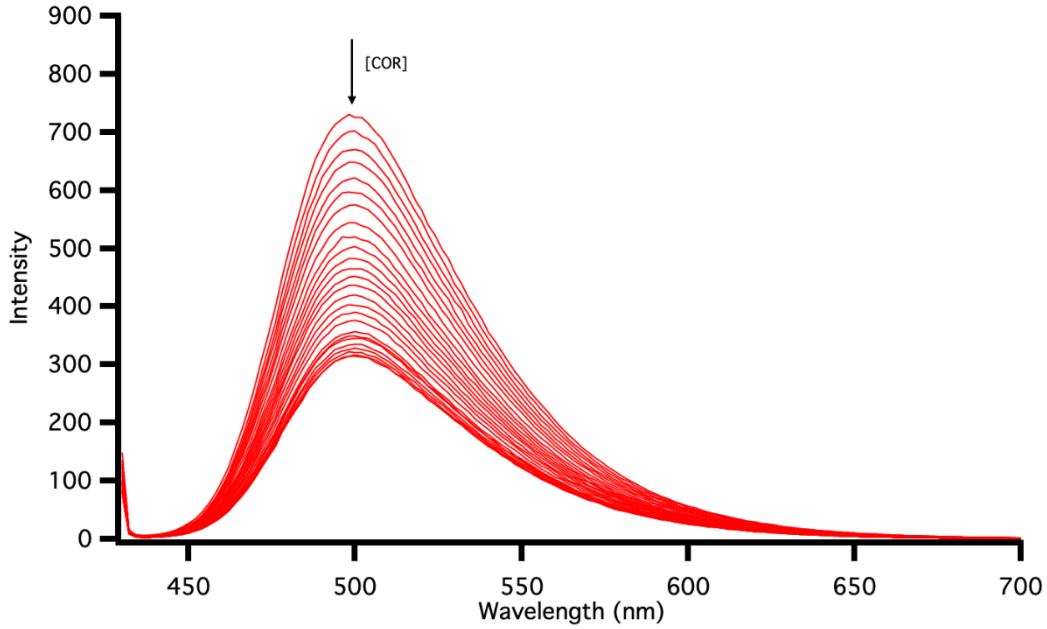

Figure 95. 3rd replica - Fluorescence spectra of the titration of 5.0 µM COR to the dT_{32}-AgNPs in the presence of 3.0 µM COU.

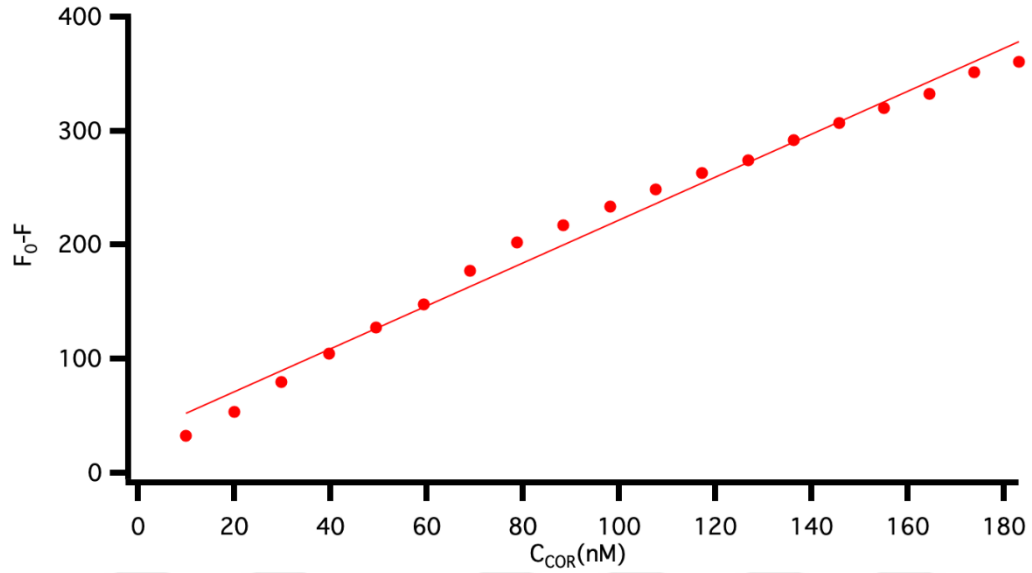

Figure 96. 3rd replica - Calibration curve of the titration of 5.0 µM COR to the dT_{32}-AgNPs in the presence of 3.0 µM COU.

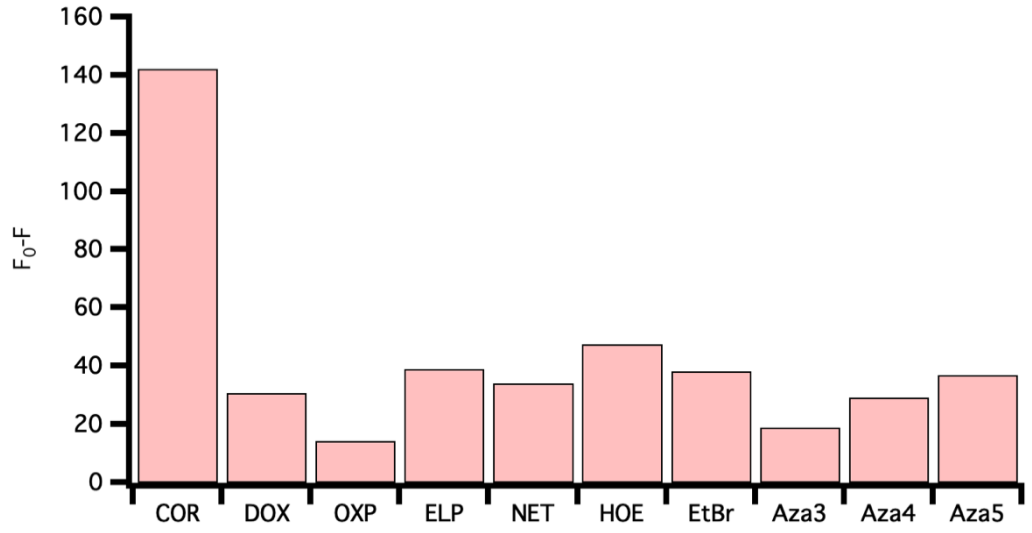

Figure 97. 1st replica - Bar graph of F_0-F for different ligands under optimized conditions (1.5 µM dT_{32}, 3.0 µM COU and 100 nM ligand).

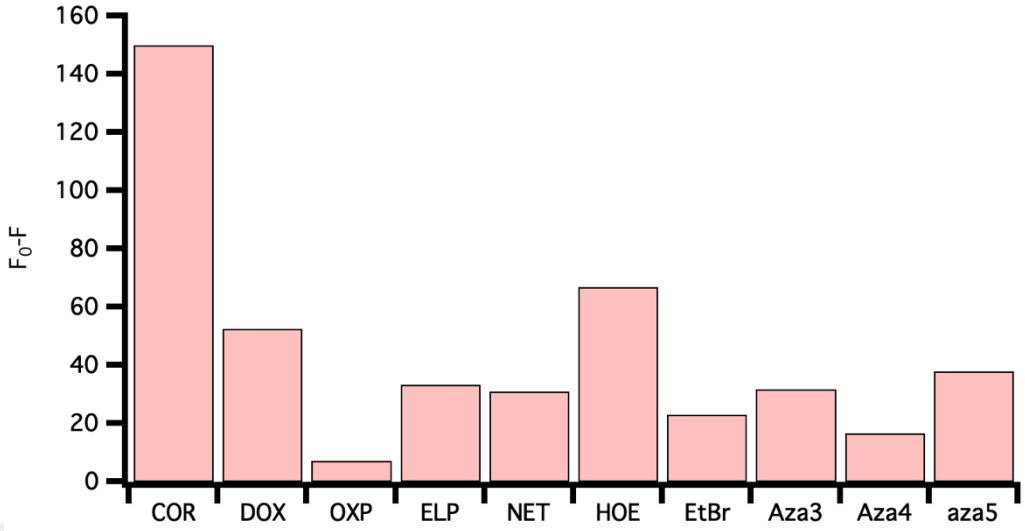

Figure 98. 2nd replica - Bar graph of F_0-F for different ligands under optimized conditions (1.5 µM dT_{32}, 3.0 µM COU and 100 nM ligand).

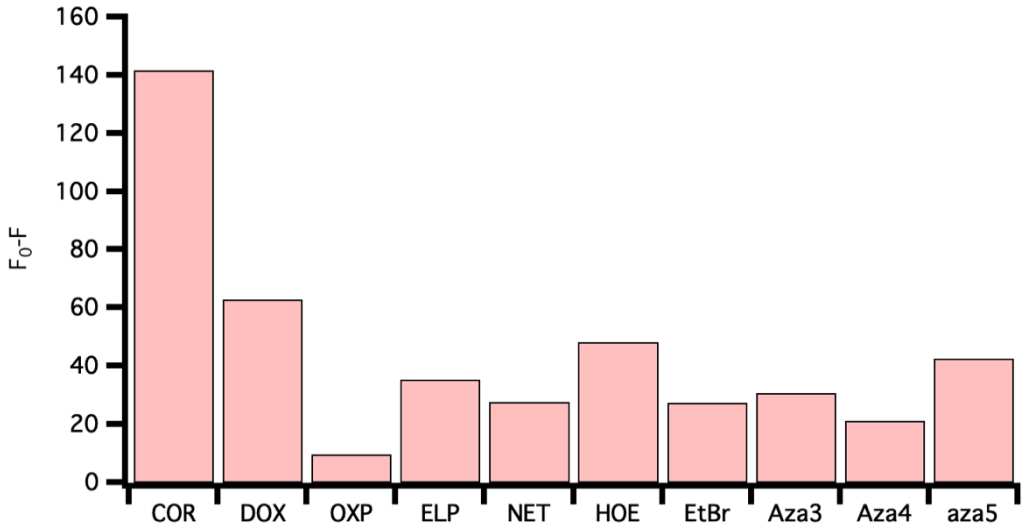

Figure 99. 3rd replica - Bar graph of F_0-F for different ligands under optimized conditions (1.5 µM dT_{32}, 3.0 µM COU and 100 nM ligand).

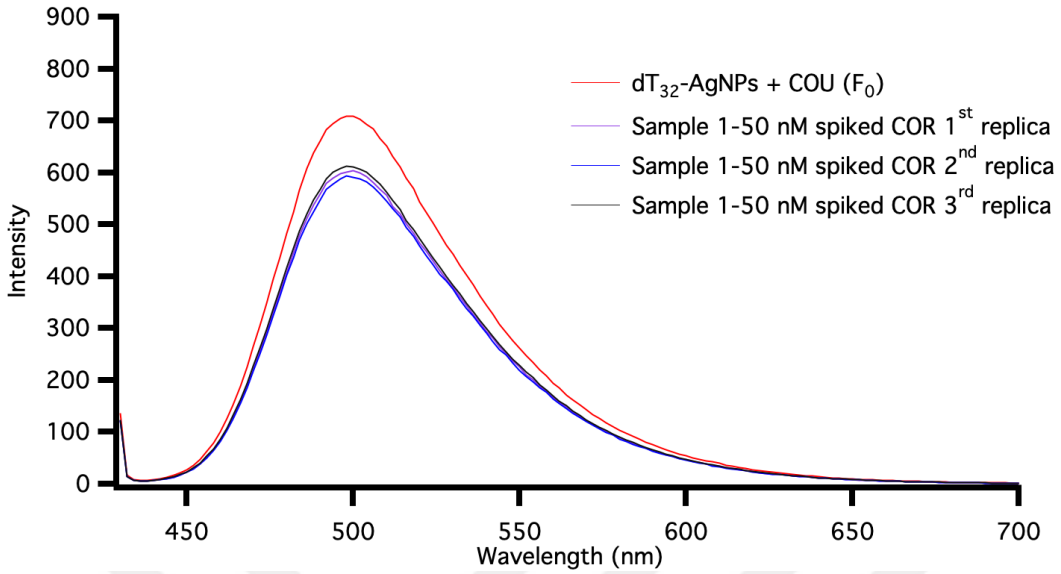

Figure 100. Fluorescence spectra of dT_{32}-AgNPs + COU with 50 nM spiked COR, urine sample 1.

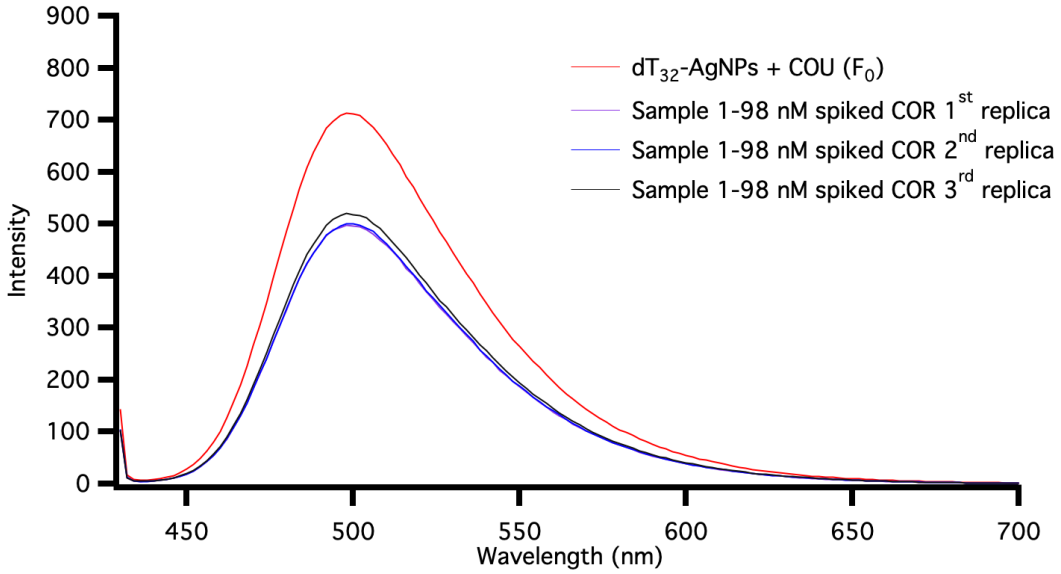

Figure 101. Fluorescence spectra of dT_{32}-AgNPs + COU with 98 nM spiked COR, urine sample 1.

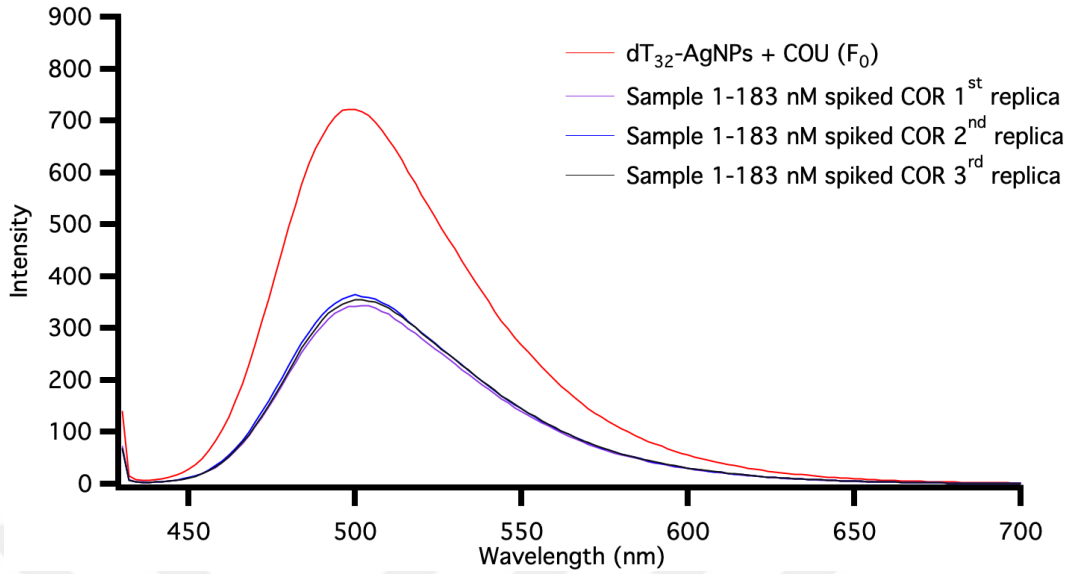

Figure 102. Fluorescence spectra of dT_{32}-AgNPs + COU with 183 nM spiked COR, urine sample 1.

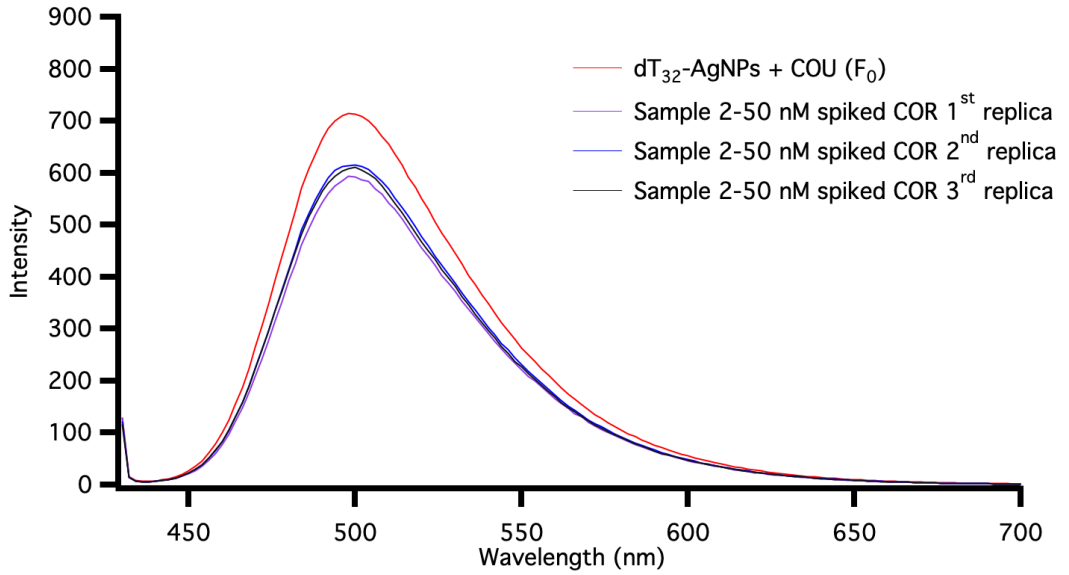

Figure 103. Fluorescence spectra of dT_{32}-AgNPs + COU with 50 nM spiked COR, urine sample 2.

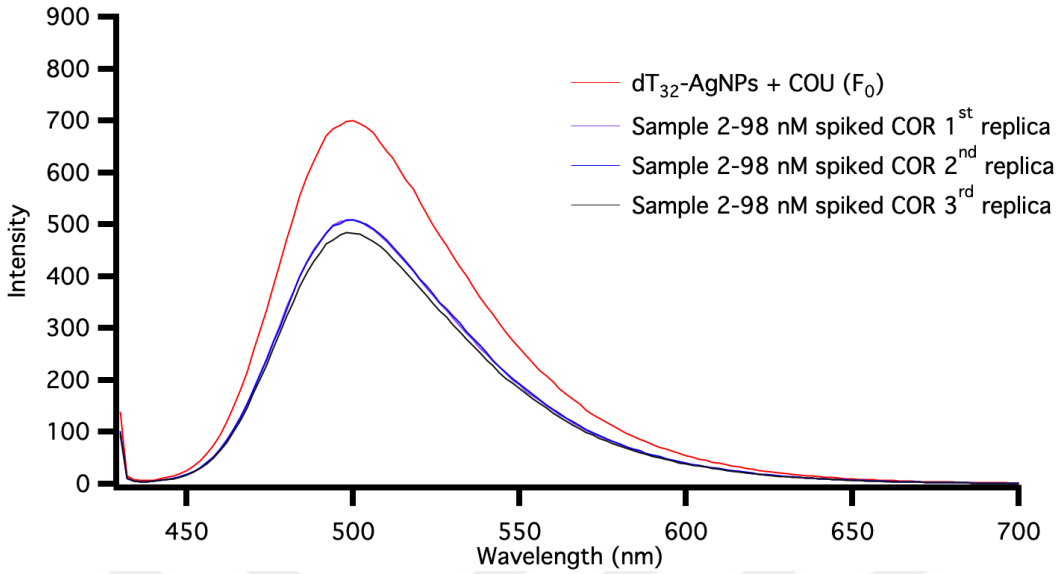

Figure 104. Fluorescence spectra of dT_{32}-AgNPs + COU with 98 nM spiked COR, urine sample 2.

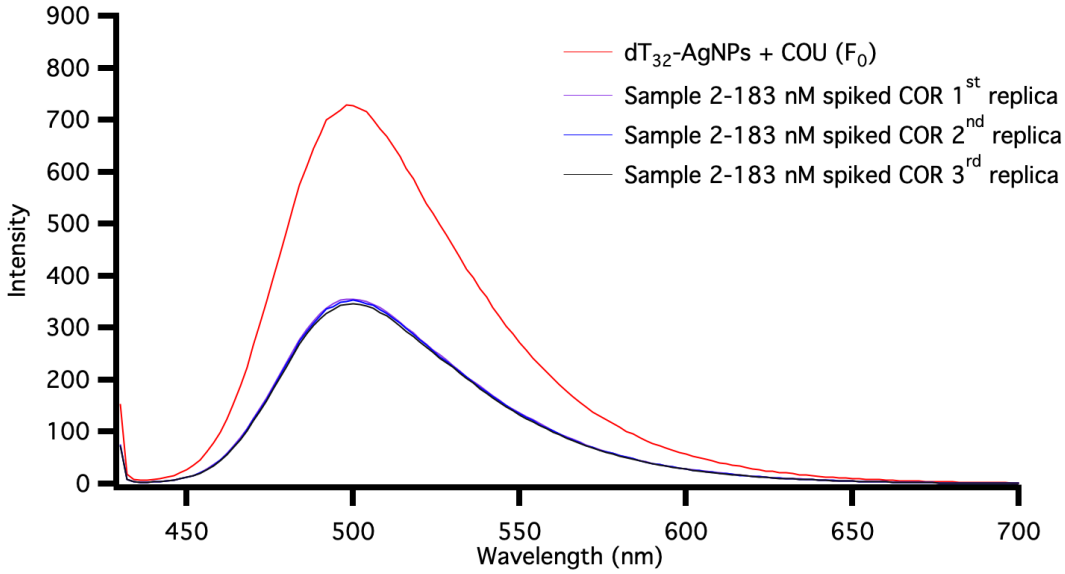

Figure 105. Fluorescence spectra of dT_{32}-AgNPs + COU with 183 nM spiked COR, urine sample 2.

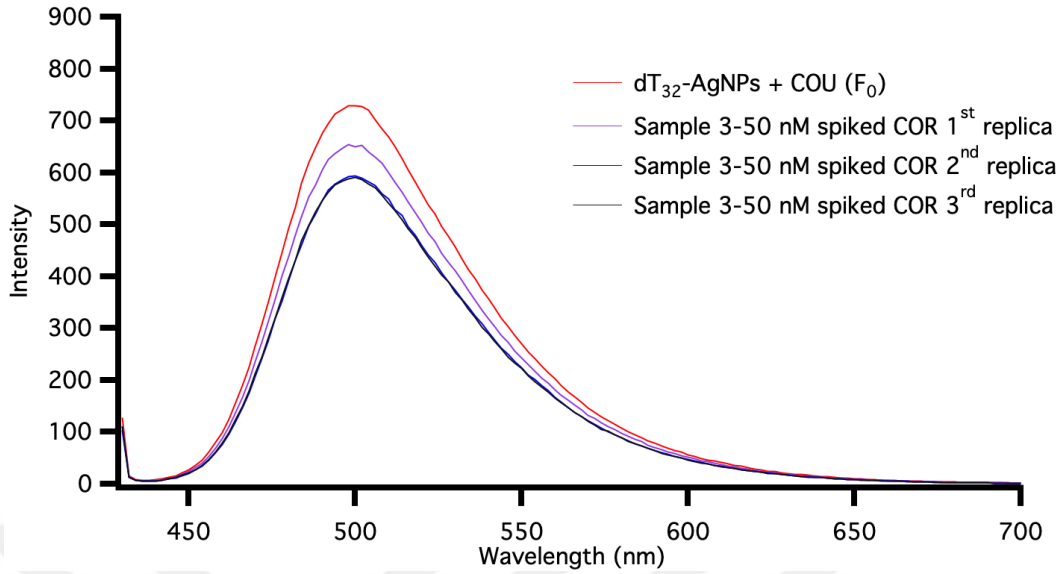

Figure 106. Fluorescence spectra of dT_{32}-AgNPs + COU with 50 nM spiked COR, urine sample 3.

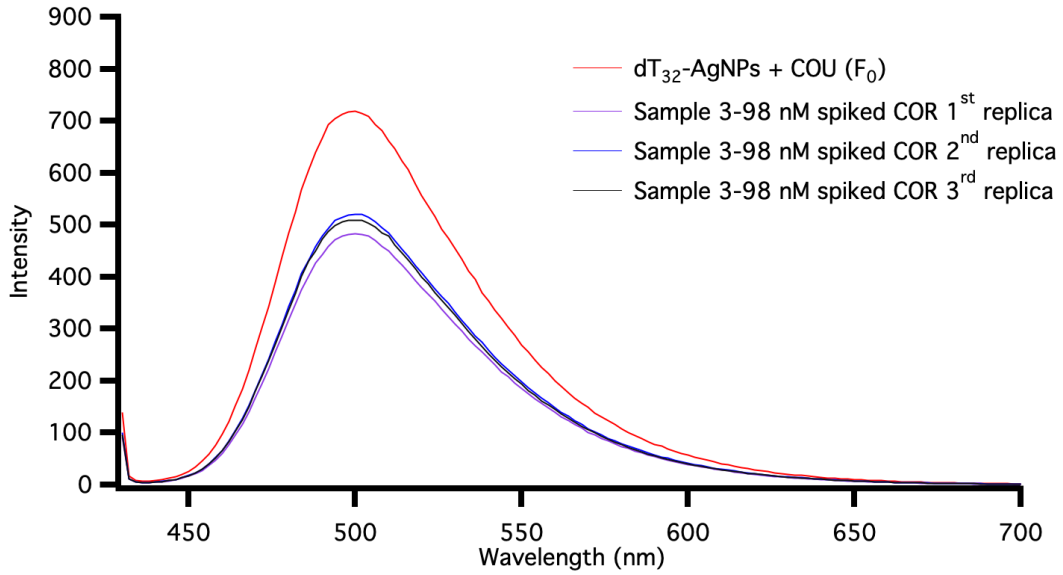

Figure 107. Fluorescence spectra of dT_{32}-AgNPs + COU with 98 nm spiked COR, urine sample 3.

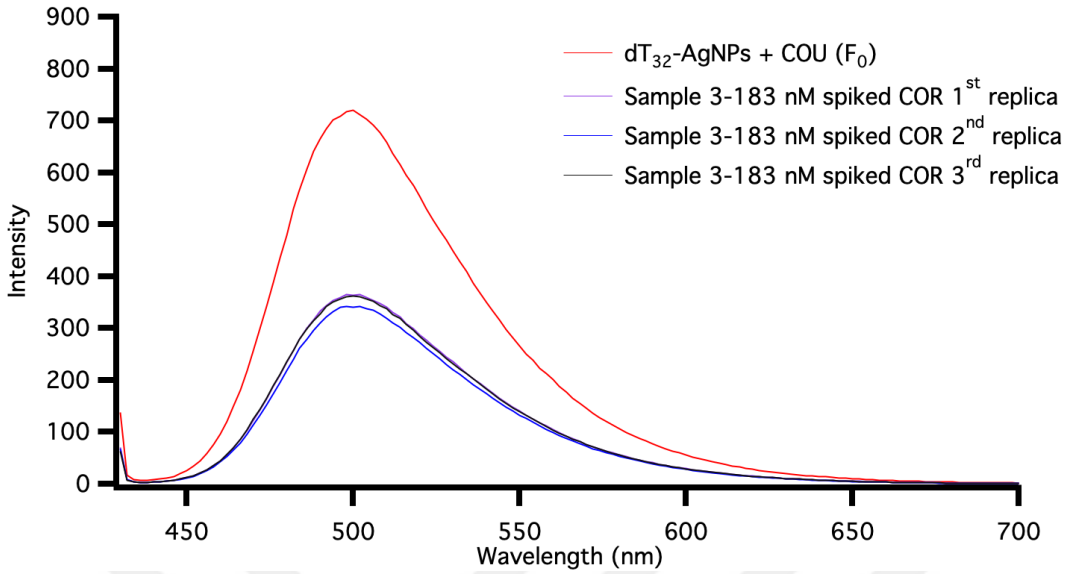

Figure 108. Fluorescence spectra of dT_{32}-AgNPs + COU with 183 nM spiked COR, urine sample 3.